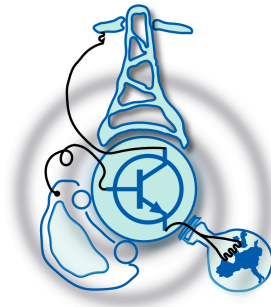# Transient Frequency Drift Compensation on Weak 3-phase AC Microgrids using an Energy Storage System

by

Ángel Navarro Rodríguez

Submitted to the Department of Electrical Engineering, Electronics,
Computers and Systems
in partial fulfillment of the requirements for the degree of

Master of Science in Electrical Energy Conversion and Power Systems

at the

UNIVERSIDAD DE OVIEDO

July 2014

Author . . . .

Certified by. . . . .
Pablo García Fernández
Dr. Associate Professor
Thesis Supervisor

Transient Frequency Drift Compensation on Weak 3-phase AC Microgrids using an Energy Storage System

by

Ángel Navarro Rodríguez

Abstract

Micro-grids are without any doubt the future of electrical grids, advocating for a sustainable and efficient exploitation of the energy sources and the integration of renewable energies. However, these grids are by nature weak grids, exhibiting a low inertia and high impedance which makes them prone to contingencies that compromised the grid quality and stability. The scope of this master thesis is to cover one of these contingencies consisting on the transient frequency drift that occurs when changes in the active power takes place. The low inertia of the generators that compose a micro-grid could cause a fluctuation in their rotor speed, which is directly related to the grid frequency due to the applied transient torque. Thus, the present Thesis is focused on the study of a solution based on Energy Storage System (ESS) for transient frequency drift compensation in micro-grids. Such study covers the design and implementation of a power topology and different control alternatives in both, simulations and in an experimental setup, demonstrating the validity of the proposed system.

Thesis Supervisor: Pablo García Fernández
Title: Dr. Associate Professor

Acknowledgments

First of all, I would like to thank the most important person in my life, my partner, María, who has accompanied me during these two hard years, supporting me, and sharing my best but also my worst moments, making easier to overcome the hardest times during this Master course. So much so, that I dedicate this work to her.

I am extremely grateful to my parents for the effort and dedication they have given me as well as their comprehension of my decisions and acts, allowing me to follow the paths I have chosen along my life. I will never forget the opportunities they have enabled for me, and I will always take into account that my academic progress would not have been possible without their support.

I would like to express also my gratitude to my Thesis supervisor, the Professor Pablo García, for giving me a vote of confidence, recognizing my efforts and interests, offering me the opportunity to work with him, improving my skills and supporting as well as helping me during my Master's Thesis.

I acknowledge the research group LEMUR, as well as all the personnel that forms it, and the Department of Electrical Engineering, Electronics, Computers and Systems, for making possible the development of this Master's Thesis.

Finally, for all the knowledge I have acquired during this two years of Master course, I want to thank all the professors that has participate in this enriching experience, recognizing their hard work and interest to transmit us, as far as possible, their experience and knowledge.

Contents

List of Figures

List of Tables

Chapter 1

Thesis Introduction

1.1 Introduction

The increasing concern about environmental issues leads to the search of solutions for global heating and the greenhouse effect in all fields of science. The energy field plays an important role in the solution, being the renewable energies the preferred choice of energy generation as an alternative to the main cause of environment pollution, the fossil fuels. Thus, the emergence of renewable generation together with the improvements in power electronics and the development in power topologies has led to new kind of power system concepts, pursuing efficiency and sustainability, differing from the conventional grid based on large transmission lines and central power plants. These concepts are known as distributed generation and micro-grid, being the last one able to operate in islanding mode, autonomously from the transmission grid. The integration of distributed generation sources cooperating with other sources in the grid and the existence of dynamic loads can cause an important power quality degradation in this kind of power grid characterized by presenting a low grid inertia that converts them into weak grids, susceptible to transient instability and contingencies.

The new tendencies on energy management and generation, that tend to sustainable and intelligent electricity systems, headed by the concepts of micro-grid, smart-grid and micro-generation, are becoming a reality, enabling the decentralized generation where the user may be able to both, consume and supply energy.

In weak grids, as micro-grids, where the active power is often related to the rotating speed of low inertia generators, the different elements presented in the grid as power generators and loads may cause frequency variations on voltage, being that effect more noticeable during transients on active power given by the connection and disconnection of these grid elements. In such a case, several low inertia generators will supply the grid, being able to withstand with steady state load conditions but, in some cases, being likely to suffer instabilities when significant dynamic active loads are abruptly connected or disconnected. This effect can be mitigated by using a solution capable of injecting power to the grid with a much faster dynamic response than the grid generator. With the rapid development of the power semiconductors technology that has taken place during the recent decades, the solution comes on the heels of grid connected electronic power converters assisted by an Energy Storage System (ESS) thanks to the faster dynamics of these converters compare with conventional generation systems.

Although these kind of systems are already being used in transmission lines as FACTS in order to improve the power flow capabilities with the name of STAT-COM(Static Compensator) with ESS and have being recently introduced in distribution systems with the name of D-STATCOM acting as energy storage in order to improve the offer and demand sharing, there are not too many examples in literature about this kind of power topology, or other solution, being used for transient frequency stability improvement in weak grids. It is true that in the recent years, the use of this topology has been introduced as a solution for integration of wind generators or wind farms in the distribution grid, improving their capabilities and avoiding to compromise the grid quality, including the frequency drift compensation during transients. However, this applications are very limited as the power converter is design for a determined generation system, being not able to operate as an independent system as it needs all the information about the generator it is associated to, involving both mechanical and electrical parameters, or even the information from the grid operator, in order to operate properly.

Thus, the idea of an autonomous ESS capable of compensating the frequency drift

during active power transients in the micro-grid, using only the electrical parameters of the grid in the system placement, is proposed. Thereby, the proposed system could be used independently or associated with a significant load in the grid that can compromise its stability, in which case the electrical information attached to that load can be also available for the control algorithm.

1.2 Objectives

The Master's Thesis proposal is focused on the study and development of a solution for transient frequency drift compensation under changes on the active power load in a micro-grid. The proposed solution will be based on an autonomous system constituted by a 3-phase Grid shunt connected Voltage Source Inverter (VSI as the AC/DC converter) coupled to an Energy Storage System (ESS) formed by a battery, or a dc-link supplied by an uncontrolled rectifier, acting as the energy storage device and a bidirectional boost converter in interleaved configuration(DC/DC), coupled to the AC/DC inverter. Thus, with the proper control system, the proposed topology will be able to interchange, in both directions, active power between the micro-grid and the ESS with faster dynamics than the grid generator. This power exchange managed by the appropriate control algorithm, designed for disturbance rejection, can improved the frequency stability during transients. Thus, the aim of this Thesis is the implementation and testing of the proposed system. Both, the feasibility of the proposed topology as well as the control algorithms will be evaluated in a laboratory experimental setup.

In order to carry out the proposed study, the following objectives are stablish:

- **State of the art study**: As a starting point, the literature related to the topic under study will be reviewed. This will include the actual solutions presented for frequency compensation, examples on the common use of the proposed power topology, the benefits on the use of interleaved DC/DC converters, the different control algorithms for disturbance rejection and the advanced methods for grid frequency estimation based on the measurements of electrical parameters.

- **System design**: A simple micro-grid model will be proposed for the study of the system that will be later used in the experimental setup. Thus, as a first validation, the proposed system will be simulated based on the parameters of the devices of the experimental setup. Both, the power topology including the two converters (DC/DC and DC/AC converters), as well as the control associated to each one for power exchange between the battery and the grid will be simulated. Finally, some control algorithms for frequency drift compensation will be proposed and simulated. The selected platform used for the simulation stage is Matlab/Simulink.

- **Experimental implementation**: Once the micro-grid model and the proposed system has been analysed in simulation, the system will be implemented physically in the laboratory of the group LEMUR (Laboratory of Enhanced Micro-grids Unbalanced Research), in the University of Oviedo. For that purpose, commercial IGBT converters will be used to model the power stage of the proposed system while the control of the two converters will be implemented in the Texas Instrument Control Card TMS320F28335. The micro-grid generator will consist on two Permanent Magnet Synchronous Machines (PMSMs) coupled to each other, one acting as generator and the other as prime mover. Concerning to the energy storage device, due to the unavailability of a real Litium-ion battery, a simple battery emulator will be construct based on a rectifier, fed by an autotransformer, and a breaking system being able to consume and deliver energy, allowing the bidirectional power flow in the power stage. As final aim, the system implemented experimentally should be able to compensate the transient frequency drifts.

It is worth noting that, the modelled micro-grid and power topology will become a useful platform for the future development of control algorithms not only for frequency control but also for the study of other solutions for other contingencies within a microgrid.

20

1.3 Opportunities

Different opportunities are presented on the topic covered in this master Thesis. They can be summarized as follows:

- Micro-grids are becoming the alternative of future electrical grid. However, it is still an emerging concept, which means that several issues are still to be solved as an stable alternative for its proper implementation as large scale. Thus, the mitigation of contingencies that compromise the power quality presents a wide range of opportunities in this grid. Transient frequency drift compensation is one of this promising research lines.

- Concerning the solutions for frequency compensation, although some power topologies has been imported from transmission line applications, there are still opportunities in the design of power converters or topologies that improve the performance of the actual ones. Thus, in this Thesis the study of a dual phase interleaved DC/DC topology is carried out for the implementation of the ESS, analysing its properties and remarking their potential advantages in this kind of systems.

- Regarding the precise topic on control strategies for transient frequency compensation, it has been realized that there are still few studies on that field. Although active power compensation using ESS has been already applied to distribution grid, these systems are usually use to compensate during both steady state and transients, participating in the primary control of the grid. This implies a lack of specific methods for disturbance rejection and transient compensation, opening a possible line of research. Thus, a study in the possible control that limit the operation of the ESS system to transient compensation will be carried out, proposing and analysing different methods, including algorithms for the detection of such transients.

- Frequency estimation is one of the main concerns in the control of transient frequency variations. In order to estimate it from electrical parameters, for

instance the grid voltages, several methods have been presented in the past, and there are still several studies covering this topic. The opportunities in this field, with regard to the study in this Thesis, relies on the analysis and evaluation of the existing methods and the selection of the proper solution.

- Finally, it is worth mentioning that improvements on control may be obtained by the use of system information. Thus, the study on advanced techniques that allows the estimation of electrical or mechanical parameters, as the grid impedance or the grid inertia, precise special attention for future developments and research.

1.4   Thesis structure

The Thesis document will gather to the maximum extent possible the carried out study covering all the accomplished stages to fulfil the proposed objectives in section 1.2. The Thesis document is organized as follows, matching with the followed methodology.

- *Chapter 2* presents the state of the art on the topic of this Thesis covering the power topology used in the proposed system, its applications, with special attention paid to frequency drift compensation. Also the grid frequency estimation and disturbance rejection topics are covered.

- *Chapter 3* describe the proposed system, that will be later implemented, covering the basics of operation of the two power converter topologies used in the proposed system and their control schemes. Also, the micro-grid model is presented. Finally, the different studied control strategies used for frequency drift compensation are proposed.

- *Chapter 4* shows the operation of the proposed system in simulation, covering the behaviour of each power converter, the interaction between them, and its performance as a solution for frequency drift compensation.

- *Chapter 5* describes the experimental setup and presents the operation of the experimental implemented system. The experimental results are showed and commented based on the previous conclusions reached during the theoretical and simulation stages.

- *Chapter 6* conclude with the analysis of the carried out tasks as well as the obtained results, and the discussion of future work on the topic of this Thesis.

Chapter 2

State of the Art

In the scope of the proposed study, different research lines should be considered due to the integration of the different concepts and technologies that the proposed system involves. Thus, the review on topics related to power systems, electrical energy conversion and control will be given. The developed state of the art can be summarized in the following points:

- Development and integration of power converters for the improvement of power quality in micro-grids.

- Proposed power topology origin and applications covering the concept of STAT-COM with ESS.

- Specific carried out studies in frequency compensation.

- ESS converter.

- Grid frequency estimation.

- Control techniques for disturbance rejection.

2.1   Power quality in micro-grids

The weakness and stability problems associated to a micro-grid has been considered since the apparition of this grid concept, setting up the emergence of several lines

of research. Among them, investigations at both grid management level, concerning control algorithms for the stability of the electricity supply and power flow in the micro-grid, and device level, focused on the grid contingencies suppression [26, 40, 25]. In the scope of this Thesis the concern is focused on the device level researches, particularly those involving the development and integration of power converters for the power quality improvement.

Studies for different types of contingencies have been carried out with the aim of mitigation of unbalances, harmonics, frequency variations, and the power quality improvement [14, 15, 43, 1, 2]. The literature revels that the particular case of frequency drift compensation during transients has not been exploited in depth for its application in micro-grids, justifying the topic selected for this Thesis.

2.2 The proposed power topology

The power topology for the proposed system in this Thesis is characterized for being able to exchange power, bidirectionally, from a DC energy storage device, in this case a battery or dc-link supplied by an uncontroller rectifier, to a 3-phase AC grid. This topology is referred in the literature as STATCOM with ESS, and has the conceptual scheme on Figure 2-1 where the inverter will be coupled to the ESS through a DC link [4]. Although the basic concept was proposed, the type of ESS and inverter topology vary depending on the application.
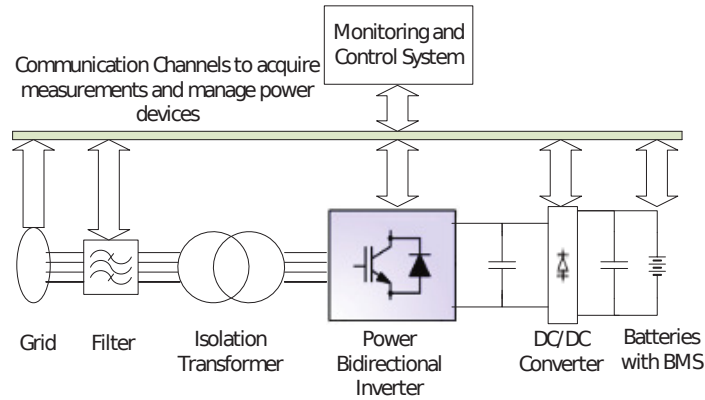
Figure 2-1: STATCOM with ESS concept [13].

Thus, three main storage systems for STATCOM with ESS can be found based on batteries, super-capacitors, flywheels and superconductors [21, 8, 27, 3, 48, 44, 46, 50]. The first two consist on DC sources requiring for a bidirectional DC/DC converter which will interface the storage device with the DC link capacitor, while in the other cases, an AC/DC inverter will acts as interface.

Concerning the grid side inverter (STATCOM) different topologies has been proposed [10], being the two level 3-phase IGBT inverter the preferred one in low-medium voltage applications due to its simplicity, effectiveness and cost.

The proposed system in this Thesis will make use of the two level 3-phase IGBT inverter with a battery or dc-link supplied by an uncontroller rectifier, called according to literature as STATCOM with Battery Energy Storage (BESS). Figure 2-2 shows a representative schematic used as base for the power topology proposed in this Thesis with the difference of the energy storage device that will be substituted by a battery, and the DC/DC converter topology which will be improved to an interleaved configuration.
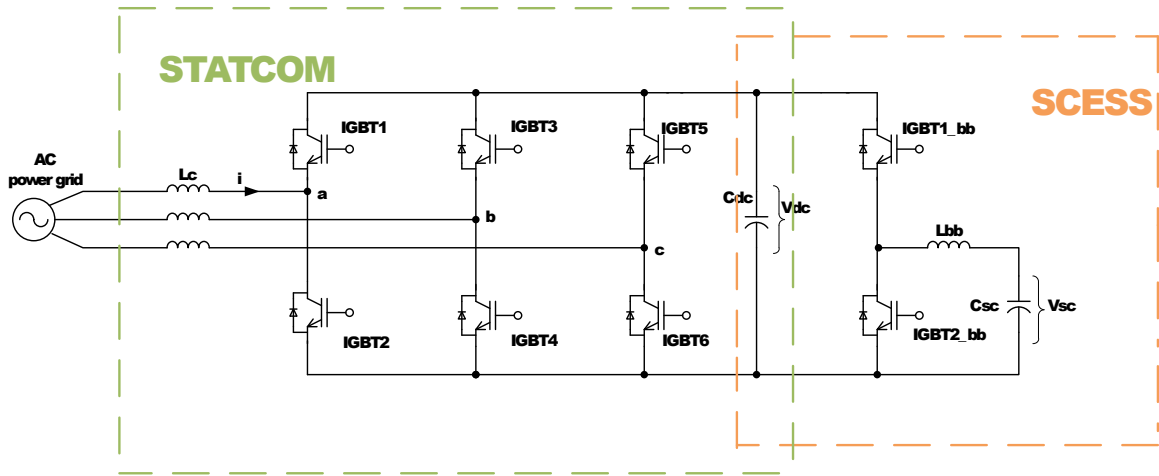
Figure 2-2: Power circuit diagram of a STATCOM with SuperCapacitor Energy Storage [2].

Regarding the applications of such a topology, it is already being used in transmission lines as improvement for Flexible AC Transmission Systems(FACTS) in order to enhance the power flow capabilities in the grid [27, 4, 6, 20, 48]. Recently, it has been introduced in distribution networks [46], acting as energy storage and as

a solution for integration of intermittent renewable energy power plants, mainly related to the wind power generation being associated to a wind turbine or wind farm [3, 7, 21, 29, 38, 41, 50]. It is also being introduced in micro-grids for power quality improvement [13, 8]. However, although there are some examples of STATCOM with ESS for primary frequency control [19, 39], in the particular application of transient frequency drift compensation in micro-grids, few examples can be find in the literature [1].

2.3 Specific studies in frequency compensation for micro-grids

Two studies focused on the particular topic of this Thesis can be highlighted, one using batteries and the other based on super-capacitor systems. The first one covers the use of an inverter with battery energy storage for frequency support in micro-grids participating in the primary frequency control [39]. The second one, more related to the scope of this thesis, carries out the study of a power topology for the precise application of transient frequency compensation in a micro-grid presenting the capability of these kind of systems for such application [1, 2]. Although these two studies establish a starting point for this line of research, there is still much to do on this field, specially regarding the control strategies to enhance the micro-grid stability.

2.4 The energy storage system

Several ESS for power applications have been presented in the literature based on different storage devices [34]. In the scope of this Thesis, the ESS will consist on a battery or dc-link supplied by an uncontrolled rectifier, emulating a Litium-ion battery and a bidirectional DC/DC boost converter.

First, the use of Litium-ion batteries for the design of the proposed system is justified by the emerging concept of *Second Life Batteries* consisting on the second usage of batteries discarded for their use in electrical vehicles, integrating them in

ESSs for the improvement of power quality in micro-grids [18, 28].

Regarding the power converter, the bidirectional DC/DC boost converter was introduced in traction applications [9], presenting the desired bidirectional flow capabilities. This concept has evolved and the apparition of the concept of interleaving has lead to converters that improve the current ripple, reducing the stress in the battery and extending its life [17, 31, 16]. Among the options, 2-phase ,3-phase and 4-phase interleaved topologies can be found. The converter proposed in [16] present a dual phase interleaved as shown in Figure 2-3 for high power applications that will serve as a model for the system implemented in this Thesis.
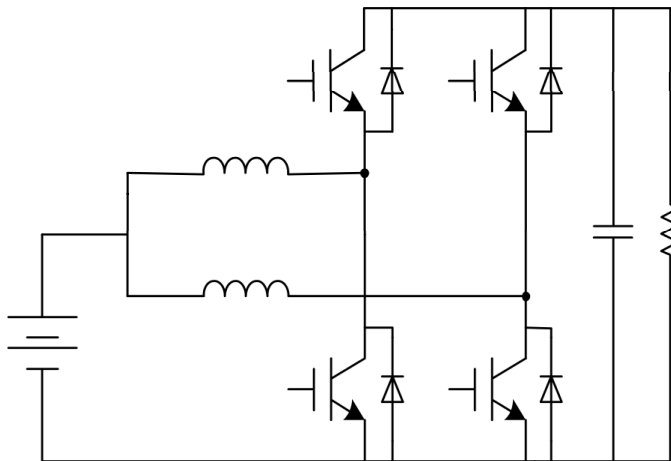
Figure 2-3: Dual phase interleaved DC/DC bidirectional boost converter [16].

2.5   Grid frequency estimation

Although the main aim of the Thesis is not focused on the study of alternatives for frequency estimation and grid synchronization, this two concepts become a major concern as far as the frequency drift compensation will be done by a control based on the feedback of the grid electrical parameters, being the grid frequency the most important parameter. The use of Phase Locked Loop (PLL) based on dq synchronous reference frame is one of the most simple and extended methods in grid connected applications to track the grid angle, using only the grid voltage measurements, allowing the synchronization with the grid and so, the proper control on active and reactive

29

power exchange [11]. However, this technique is very sensitive to grid unbalances and harmonic distortion, leading to the development of enhance PLL methods [22, 42, 36]. Nevertheless, these improved PLL techniques, are focused on angle tracking, being the frequency estimation ofter noiser and thus potentially affecting the focus of this thesis. Thus, the use of a technique known as Frequency Locked Loop is proposed as a possible solution [35].

2.6 Control Techniques for Transient frequency drift compensation

The control algorithm for transient frequency drift compensation should present a very specific characteristic, it only should compensate active power during transients, being inactive during steady state operation when the power should be supplied only by the grid generator. Considering that, conventional Proportional Integral regulator (PI) can not be seen as possible solution due to its steady state compensation properties. Thus, a control that offers proper transient disturbance rejection should be selected. The available options go from PD regulators, including feedback differentiation [45, 30, 30, 23], to Disturbance Input Decoupling (DID) methods based on both, grid electrical parameters measurement and grid parameter estimation through disturbance observers [33, 32, 37, 24]. The second option appears to be the more advantageous solution for the study of an autonomous frequency drift compensator system since observers as Luenberger's observer may allow not only to estimate electrical parameters in the grid reducing the needs for sensors but also to estimate the physical behaviour of the system without the need of external information [12].

Chapter 3

Power System Modelling and Control Design

This Chapter covers the model of the proposed system in the Thesis. The Power Stage used for the proposed frequency compensation solution will be presented and its operation will be described. The basics of operation for the DC/DC and AC/DC converters will be explained including their associated control topologies for current and DC link voltage and the complete system control will be defined as well as its integration in the micro-grid. Finally, the studied control alternatives for frequency drift compensation are presented.

3.1 Modelling the Power Stage and its Dynamic Control Topology

3.1.1 System description

The proposed solution is illustrated in Figure 3-1, and will be able to exchange active power between the grid and the battery.

As shown in the figure, the system will be composed by two converters coupled by a DC link capacitor:
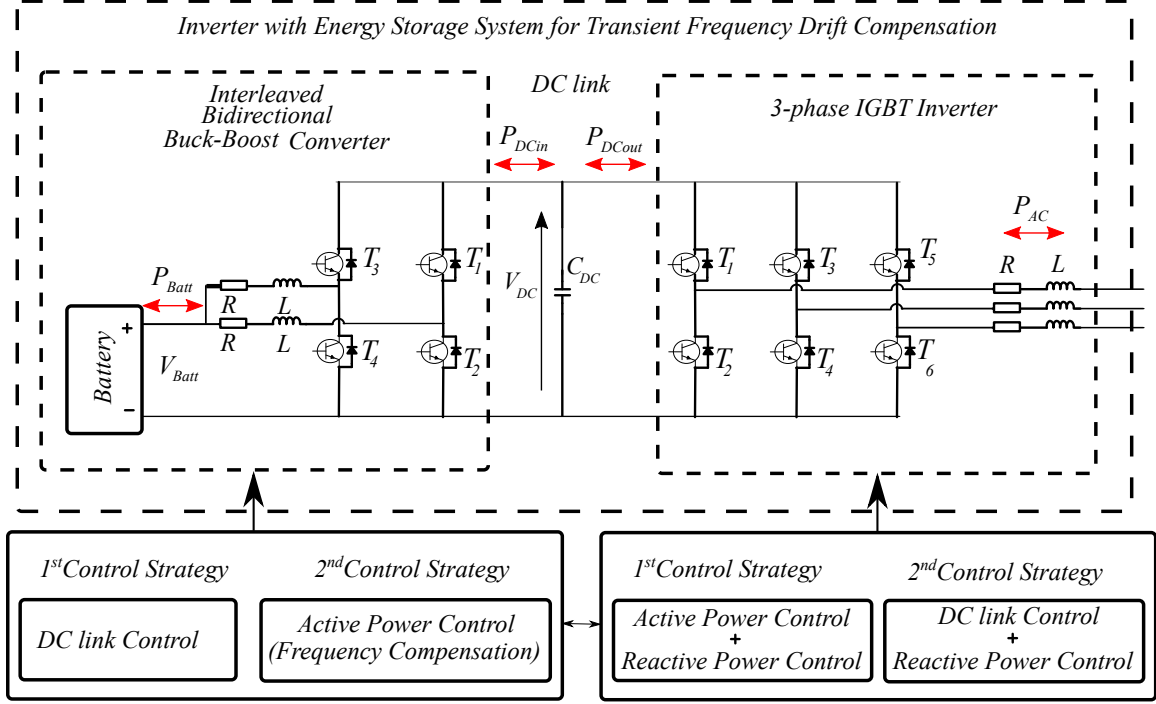
Figure 3-1: Proposed system topology for transient frequency drift compensation.

- **DC/DC converter**: the DC/DC converter will consist on a bidirectional boost converter implemented in a two branch IGBT interleaved topology and two boost inductors each one corresponding to one of the branches in the low voltage input. The ESS will be connected to the low voltage side, while the high voltage output will be connected to the DC link.

- **AC/DC converter**: the AC/DC converter will consist on a two level 3-phase Inverter composed by 6 IGBTs and 3 boost inductors (RL filter) connected to the AC side of the converter. It is connected to the DC/DC converter through the DC link while the AC side will be the grid connection point.

Regarding the power flow control on the proposed system, two alternatives are considered:

- **First Control Strategy**: In this configuration, the DC link voltage V_{DC} is controlled by the DC/DC converter which maintains it in a fixed voltage value higher than the battery voltage. The AC/DC converter will control therefore

the injection/consumption of active and reactive power to/from the grid. In this case, the active power command will be determined by the control associated to the frequency compensation while the reactive power capabilities will not be exploited in this Thesis, setting its command to 0 Var in every moment.

Then, considering no losses, it is fulfilled that $P_{Batt} = P_{DCin} = P_{DCout} = P_{AC}$ in steady state, and the power will flow as explained below:

1. The frequency controller will generate an active power command to inject/consume power from the grid.

2. The AC/DC inverter will inject/consume the commanded active power. Such active power will be provided as a first instance by the energy stored in the DC link capacitor, flowing from P_{DCout} to P_{AC}, which will discharge or charge the capacitor decreasing or increasing the DC link voltage.

3. However, the DC/DC converter aim is to maintain fixed the DC link voltage, and for such a purpose it should inject/consume power from the battery to the DC link in order to reach the steady state condition $P_{Batt} = P_{DCin} = P_{DCout} = P_{AC}$.

- **Second Control Strategy**: If considered a real system where de DC link capacitor is not ideal and present losses due to parasitic elements, with the first configuration the ESS is supplying those loses continuously which means a long term degradation of the storage device. In the second strategy the DC link voltage V_{DC} is controlled by the AC/DC inverter while the power injection/consumption control will lies on the DC/DC converter, which instead of controlling DC link will inject the commanded power given by the frequency compensator controller. Then the inverter uses its active power capabilities to maintain the DC link constant. Thus, in this case the losses presented in the DC link are supplied from the grid instead of the battery, improving its life. The power flow in the system will be similar to the first method.

For both control methods, feed-forward of the power command can be used in the

converter that controls the V_{DC} in order to improve the dynamics in the DC link.

Notice that in order to carry out the control, Pulse Width Modulation (PWM) is used in both converters.

3.1.2 The battery interface: Interleaved Boost DC/DC converter

Figure 3-2 shows the schematic of the proposed interleaved bidirectional boost DC/DC converter. This topology allows the bidirectional flow of currents from the battery to the DC link, and vice-versa with the advantage of reduced current ripple at the battery terminals compare to conventional bidirectional DC/DC converters. This is given by the modulation and control pattern used in this kind of converters that makes possible the cancellation of current ripple between the two boost inductance branches.
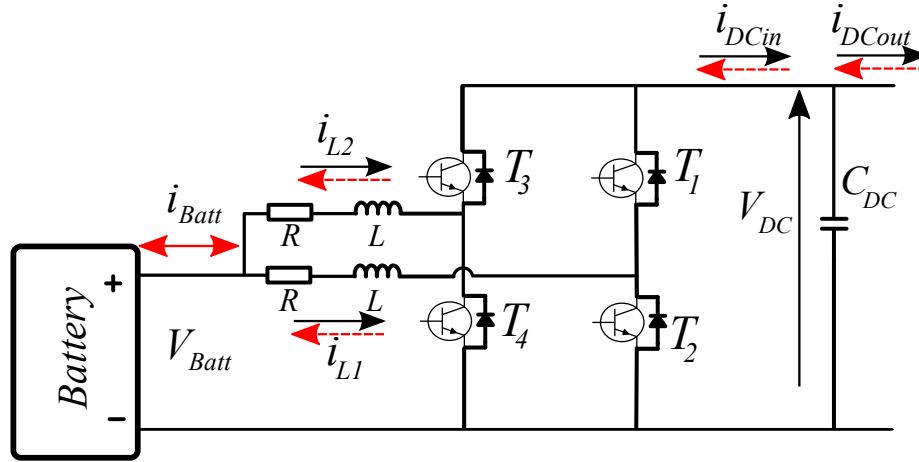
Figure 3-2: Schematic diagram of the dual phase interleaved bidirectional DC/DC boost converter.

As shown in figure, the relation in (3.1) is given.

$$i_{Batt} = i_{L1} + i_{L2} \tag{3.1}$$

Due to the square nature of the voltage applied to the inductors owing to the PWM, the currents present inevitably a ripple. In the case of a conventional DC/DC

converter, this ripple is unavoidable and will depend on the inductance. However, in the case of interleaved, where the total current injected/consumed by the ESS is shared by the to branches, conducing the same average current in a period, the ripple can be cancelled by applying opposite voltage to each inductor within each switching period, i.e. applying 180° degrees phase shift between the PWMs driving the two branches of the converter.

Leaving aside the advantages of interleaved, this kind of converter is just a particular case of bidirectional DC/DC converter and its basics of operation are the same apart from the modulation pattern and the current command, that should be shared by the two branches in the interleaved. Thus, in order to facilitate the comprehension of this converter, its basics of operation and control scheme are explain in detail using the conventional single branch bidirectional converter.

Boost operation: Power supply mode

Figure 3-3 shows the current flow during operation in boost mode. Since the current flows through the inductor towards the load (DC link), the top switch will not affect the operation as the current will always flow through its respective diode. Then, the output will depend just on the bottom switch. During the first part of the switching period, the bottom switch is on, creating a closed circuit composed by the inductance (L), the resistance (R) and the battery, then, the power is provided to the output by the DC link capacitor (C_{DC}), discharging it. In the second part of the period, the bottom switch is off, thus, the inductor current flows through the diode towards the load and the DC link capacitor, charging also this last one (current i_{CDC})[9].
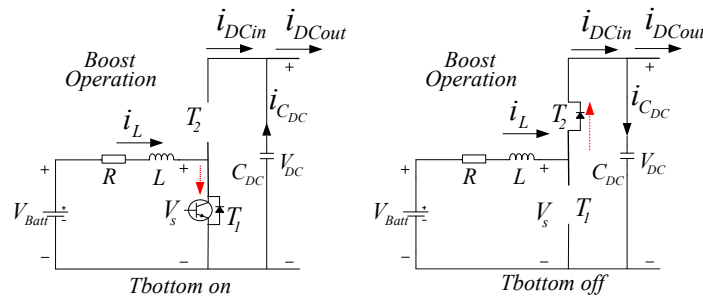
Figure 3-3: Bidirectional boost in boost converter operation.

35

Consider the top switch to be called as T_2 and bottom switch as T_1. When T_1 is closed, as seen before, the voltage at the inductor $V_{RL} = V_{Batt}$, and when it is off, $V_{RL} = V_{Batt} - V_{DC}$. Then, as the current through the inductance should be constant at the end of the switching period, and considering $I \cdot L = \int V$ the expression in (3.2) will be fulfilled [5].

$$\int_0^{DT} V_{Batt} \ dt + \int_{DT}^{(1-D)T} V_{Batt} - V_{DC} \ dt = 0 \tag{3.2}$$

Solving this equation, the expression of the boost converter in steady state is obtained (3.3).

$$V_{DC} = \frac{V_{Batt}}{1 - D} \tag{3.3}$$

Buck operation: consuming active power

During regenerative braking, the current comes from the output, i.e., the machine, which acts as a generator, towards the battery. Figure 3-4 illustrates the buck operation of the converter. In this case, the top switch determine the behaviour instead of the bottom one. Then, while the top switch is conducting the current flows through the inductance from the output to the battery, charging also thee DC link. In case the top switch is off, as there is energy stored in the inductance, the current i_L flows towards the battery charging it, while the current coming from the machine charges the DC link capacitor[9].
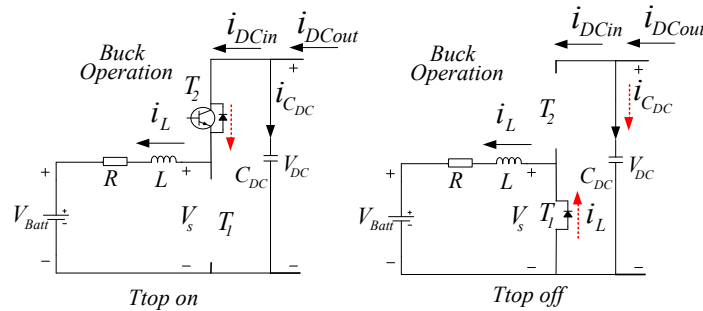
Figure 3-4: Bidirectional boost in buck converter operation. Powers flows towards the battery.

In this case, when T_2 is on, $V_{RL} = V_{DC} - V_{Batt}$, while if T_2 is off, $V_{RL} = -V_{Batt}$. Then, applying the same procedure than before (3.4), the expression of buck mode in steady state is obtained (3.4), where $D_2 = 1 - D$ [5].

$$\int_0^{D_2T} V_{Batt} \ dt + \int_{D_2T}^{(1-D_2)T} V_{Batt} - V_{DC} \ dt = 0 \tag{3.4}$$

$$Vdc = D_2 V_{Batt} \tag{3.5}$$

Bidirectional boost control basics

Once the main characteristics of the bidirectional boost has been described, the control basics must be fixed. Using state space averaged method [47], the below expressions are met in the converter (3.6)(3.7)(3.8) [47].

$$L\frac{di_L}{dt} + i_L R_L = V_{RL} = V_{Batt} - V_s \tag{3.6}$$

$$C_{DC}\frac{dV_{DC}}{dt} = i_{DCin} - i_{DCout} = i_{CDC} \tag{3.7}$$

$$V_{Batt} i_L = V_{DC} i_{DCin} \tag{3.8}$$

Where V_s is the gate to source voltage of the transistor T_1, V_{RL} is the voltage at R_L and L, i_{DCin} is the output of the boost before the DC link and i_{DCout} the input to the load, in this case the inverter and motor.

Then, with these equations, a current control loop can be developed for i_L. As the control should be done by the duty cycle D, the relation between the magnitudes in the boost with D is needed. Starting from (3.6), considering that V_s will change in a period, the average value in such period is obtained as in (3.9), depending on V_{DC} and D.

$$V_s = (1 - D)V_{DC} \tag{3.9}$$

Then, $V_{Batt} - (1 - D)V_{DC} = V_{RL}$ will allow to calculate the duty in the control loop as in (3.10).

$$D = \frac{V_{RL} - V_{Batt}}{V_{DC}} + 1 \tag{3.10}$$

The system transfer function of the system, represented in (3.6), which correspond to a first order system, can be compensated with a PI regulator, compensating the system $\frac{1}{Ls+R_L}$ by applying zero pole cancellation, being its output the voltage at the inductor V_{RL}, obtaining the necessary duty cycle D by applying the non linear equation in (3.10) dependent on measured parameters and the PI output.

For the case of interleaved converter, two equal control loops should be used, and therefore, two duty cycles will be obtained, one for each branch. Such duty cycles will be inputs to two phase-shifted PWM.

Bidirectional boost control scheme

At the beginning of these Section two control alternatives were proposed concerning the DC link voltage control. Figures 3-5 and 3-6 shows the interleaved DC/DC converter proposed control schemes for the two alternatives. In both cases a cascade control should be implemented.
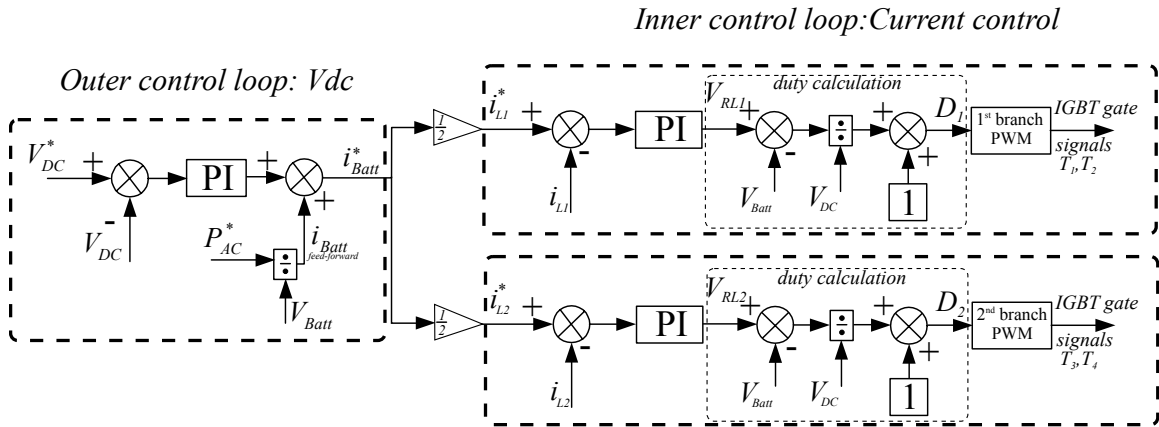
Figure 3-5: Control scheme for the interleaved DC/DC converter using the first proposed control strategy.

In the case the V_{DC} is controlled by the DC/DC converter, the outer loop will
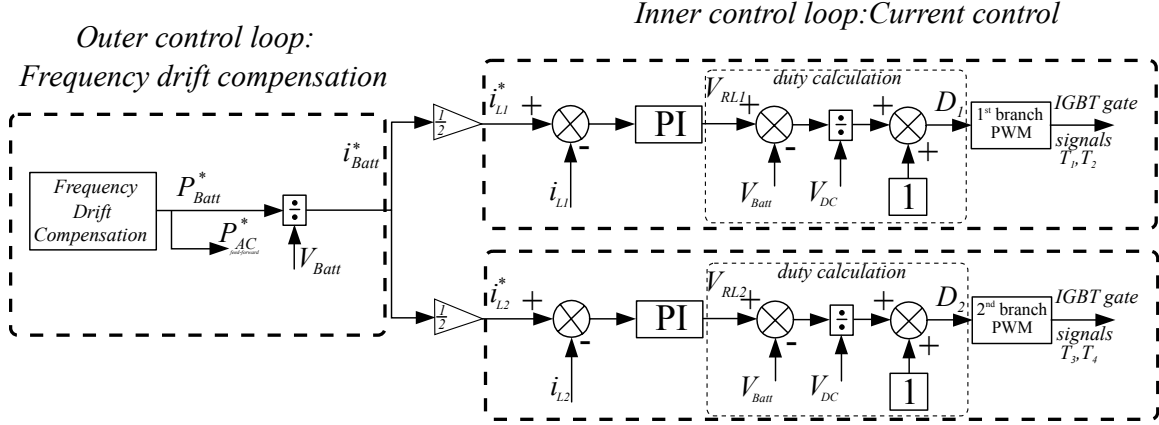
Figure 3-6: Control scheme for the interleaved DC/DC converter using the second proposed control strategy.

consist on a PI regulator for controlling the V_{DC} by compensating the system given by (3.7), being the output of such a regulator the current command for the inner control loop. The tuning of the outer PI will be designed to provide good dynamic behaviour and proper disturbance rejection.

For the second control scheme, the outer loop will be devoted to the frequency compensation controller. This will provide the active power command that should be scaled by the battery voltage in order to obtain the current command for inner control loop.

Notice that in both cases the current command is divided by two in order to share the current between the two interleaved branches.

3.1.3   The grid side converter: two level 3-phase IGBT inverter

The grid side connected converter will consist on a two-level 3-phase AC voltage source converter(VSC). Figure 3-7 shows the schematic diagram including its associated RL filters (boost inductors) and the connection to the DC link. This topology is characterized for being able to present at each of its AC-side terminals two voltage levels $\frac{V_{DC}}{2}$ or $\frac{-V_{DC}}{2}$ [49].

Each of its three legs, composed by two IGBT, is associated to a grid phase. The
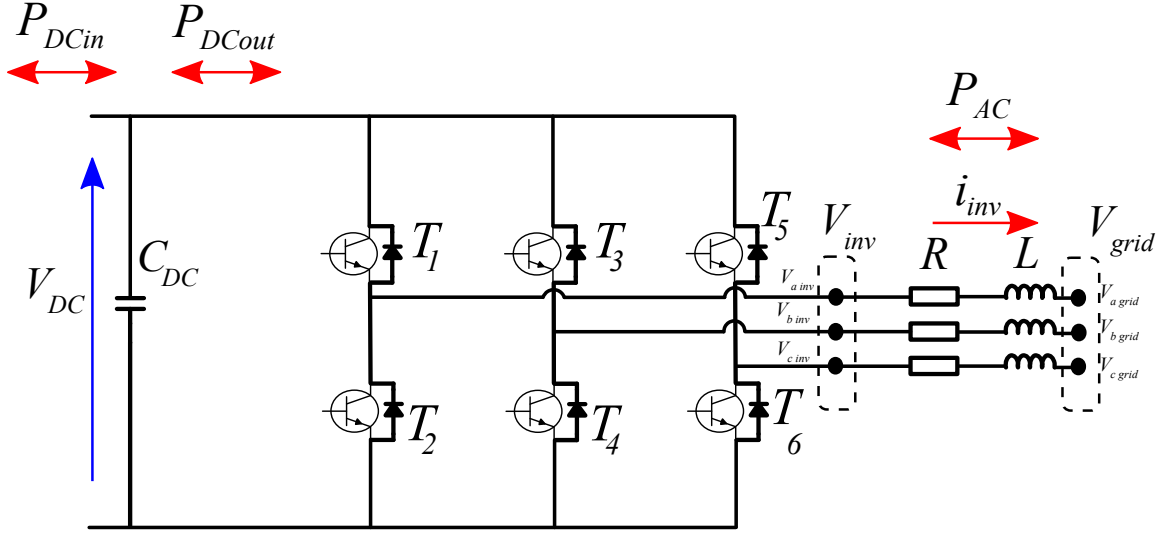
Figure 3-7: Schematic diagram of the two level 3-phase IGBT inverter.

IGBTs in the same leg are operated in complementary mode so that two IGBTs in the same leg are never conducting (ON state) at the same time in order to avoid short circuits. Moreover, in real implementation, as the switching elements are not set to OFF state immediately, a dead-time is introduced between the ON state of the two IGBTs.

The IBGTs are driven through a gate signal given by a 3-phase PWM modulation consisting on the comparison of 3 sinusoidal voltage references, with the desired fundamental frequency, normally the grid frequency, and phase-shifted by 120° between them, with a triangular waveform whose frequency is equal to the switching frequency f_{sw} being this much higher than the fundamental one. Thus, the output voltage of each phase will present a square waveform of frequency equal to f_{sw} whose pulse width , or duty cycle, will vary with the fundamental frequency presenting therefore the commanded 3-phase sinusoidal voltage at that fundamental frequency. Then, although the output voltage is a square waveform, the currents flowing through the boost inductors present a filtered form approximated to a fundamental frequency sinusoidal waveform. Nevertheless, this topology may inject high frequency components distorting the grid, thus, in same applications passive filters as LC or LCL filters are used instead of a single RL branch. These ones filter both voltage and current

40

but also complicate the control scheme.

Regarding the control, this topology will be able to inject/consume current to/from the grid as a function of the relation between grid voltage and the fundamental voltage commanded to the inverter. Since inverter voltage is assumed to be controlled directly in open loop by the PWM modulation, the control topology adopted generally for this kind of converters consist on a current close loop controller scheme based on the compensation of the system composed by the RL branch.

In order to carry out the current control different alternatives exist, being the most extended the close loop control in dq synchronous reference frame, also known as vector control. The basics of this control is explained below covering from the reference frame transformation to the final control scheme.

Equivalent electrical system in 3-phase reference frame

Figure 3-8 shows the equivalent system for one of the phases. Similar to the process carried out in the DC/DC converter design, the system can be represented by the expression in (3.11) and its equivalent in Laplace transformation in (3.12), where V_{inv} is the voltage in one of the phases of the inverter and V_{grid} the voltage in the corresponding phase of the grid.
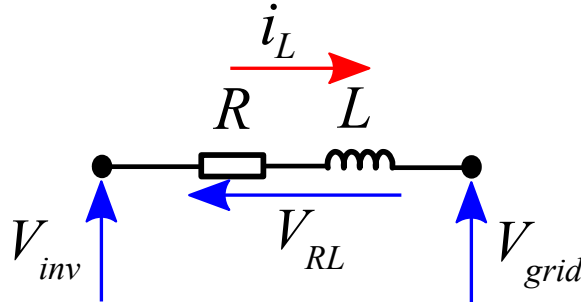
Figure 3-8: Equivalent electrical system for one of the phases in the 3-phase inverter.

$$L\frac{di_L(t)}{dt} + i_L(t)R = V_{RL}(t) = V_{inv}(t) - V_{grid}(t) \qquad (3.11)$$

$$Lsi_L(s) + i_L(s)R_L = V_{inv}(s) - V_{grid}(s) \qquad (3.12)$$

Although it is straight forward to think on implementing the control using a PI for each of the phases as was done in the DC/DC converter, in this case, the sinusoidal nature of the currents and voltages does not allow to use PI controllers for achieving zero steady state errors. Thus, other techniques should be considered, being the control in dq reference frame the preferred one as it allows the proper functioning of PI regulators without complicating in excess the control scheme.

Equivalent system in synchronous dq reference frame

The equivalent dq reference frame allows to reduce the 3-phase electrical variables to 2 components of DC nature thanks to the synchronization with the rotational grid angle. For this reference frame, the equivalent system is given in Figure 3-9, where it is worth noting that not only the components L and R appear but also a coupling factor between components should be considered.
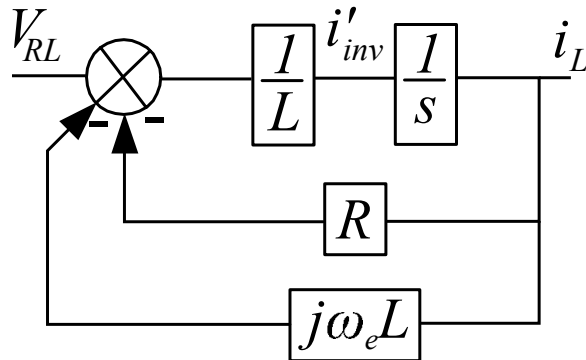
Figure 3-9: Equivalent system diagram of the RL branch in the synchronous reference frame.

If expressed using state space format, the system equation (3.13) is obtained in time domain, where i_d and i_q are the current components through the inductor, ω_e is the fundamental frequency in rad/s and v_d and v_q are in this case the voltage drop in the inductor, i.e. the inverter voltage minus the grid voltage.

$$\frac{d}{dt}\begin{bmatrix} i_d(t) \\ i_q(t) \end{bmatrix} = \begin{bmatrix} -\frac{R}{L} & \omega_e L \\ -\omega_e L & -\frac{R}{L} \end{bmatrix} \begin{bmatrix} i_d(t) \\ i_q(t) \end{bmatrix} + \begin{bmatrix} 1 & 0 \\ 0 & 1 \end{bmatrix} \begin{bmatrix} v_d(t) \\ v_q(t) \end{bmatrix} \tag{3.13}$$

This equation leads to the transfer functions (3.14) and (3.15), where two elements can be appreciated: a first order system and a coupling term.

$$v_d = Lsi_d(s) + i_d(s)R + L\omega_e i_q(s) \tag{3.14}$$

$$v_q = Lsi_q(s) + i_q(s)R - L\omega_e i_d(s) \tag{3.15}$$

This system will compensate for each of the components, using a PI regulator for the first order term and adding a decoupling term in order to remove the cross coupling. The PI regulator will be tuned using the zero pole cancellation method used before in the DC/DC converter.

abc to dq Park's transformation

The Park's transformation consist on a coordinate change from the stationary 3-phase system to a 2 components rotating reference frame. In a balanced system the 3-phase stationary components can be represented as a rotating vector, which speed is the electrical frequency, and the magnitude is given by the peak voltage. Aligning with that vector expressed as a complex number, two orthogonal components can be extracted. Component d will be named to the one aligned to the vector (real component) while q will be used for the orthogonal (imaginary axis).

The transformations from the abc reference frame to dq and dq to abc can be expressed by equations 3.16 and 3.17 respectively.

$$\begin{bmatrix} X_a \\ X_b \\ X_c \end{bmatrix} = \frac{2}{3} \begin{bmatrix} cos\theta & cos\left(\theta - \frac{2\pi}{3}\right) & cos\left(\theta - \frac{4\pi}{3}\right) \\ -sin\theta & -sin\left(\theta - \frac{2\pi}{3}\right) & -sin\left(\theta - \frac{4\pi}{3}\right) \\ \frac{1}{2} & \frac{1}{2} & \frac{1}{2} \end{bmatrix} \begin{bmatrix} X_a \\ X_b \\ X_c \end{bmatrix} \tag{3.16}$$

$$\begin{bmatrix} X_d \\ X_q \\ X_0 \end{bmatrix} = \frac{2}{3} \begin{bmatrix} cos\theta & -sin\theta & \frac{1}{2} \\ cos\left(\theta - \frac{2\pi}{3}\right) & -sin\left(\theta - \frac{2\pi}{3}\right)) & \frac{1}{2} \\ cos\left(\theta - \frac{4\pi}{3}\right) & -sin\left(\theta - \frac{4\pi}{3}\right) & \frac{1}{2} \end{bmatrix} \begin{bmatrix} X_d \\ X_q \\ X_0 \end{bmatrix} \tag{3.17}$$

Where X denotes any of the electrical variable in the system, and X_0 is the homo-polar component that is considered as 0 in a balanced system.

Control scheme in synchronous reference frame

Taking into account all the above considerations about the dynamic model of the system to be compensated, the vector control based scheme for the AC/DC converter is presented in Figure 3-10. In this control model, the voltages and currents variables in the abc reference frame ($[v_{a\ grid}, v_{b\ grid}, v_{c\ grid}], [i_{a\ inv}, i_{b\ inv}, i_{c\ inv}]$) are measured and later transformed to their synchronous reference frame equivalents ($[v_{d\ grid}, v_{q\ grid}],$ $[i_{d\ inv}, i_{q\ inv}]$). The angle needed for such a transformation (θ), will be obtained from the grid voltage measurement using a Phase Lock Loop (PLL). In order to decouple both, the dq components and the grid parameters. Two feed-forward terms are included in each of the dq components current control loops after the PIs. The control output will be given in dq voltage components and will be transformed back to the abc reference frame serving as 3-phase voltage command for the PWM block.
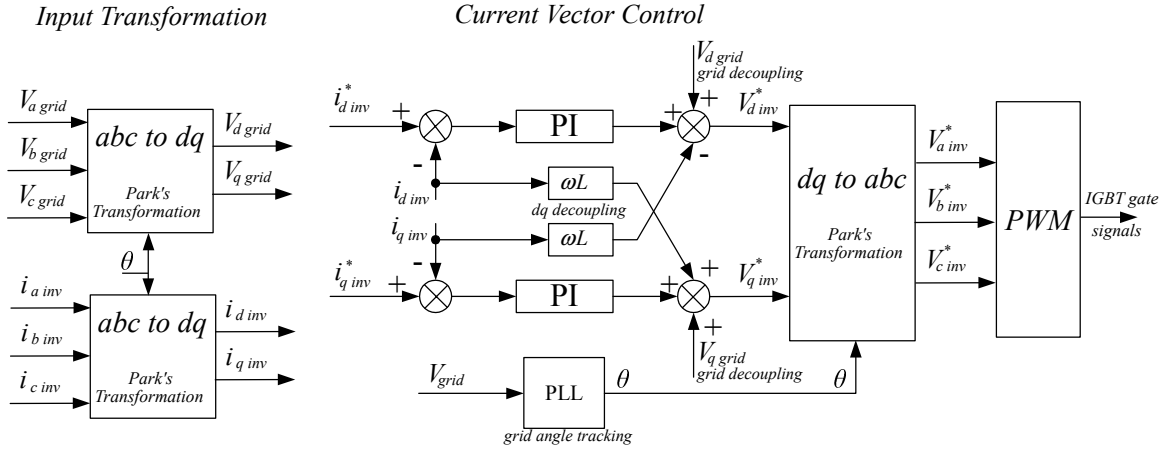
Figure 3-10: Vector current control scheme for the 3-phase inverter.

Concerning the command inputs to the controller, i_q^* current will be set to 0 A, in order to maintain reactive power injection disabled, while i_d^* command will depend on the two control modes presented at the beginning of Section 3.1. In case the V_{DC} is controlled by the DC/DC converter, the current command i_d^* will be imposed by the frequency compensation controller while if the DC link voltage is controlled by

44

the inverter, the current command is set by the V_{DC} control loop. As shown before in the DC/DC converter control scheme, the output of the frequency controller will be a power command. When the frequency control is done in the DC/DC converter the obtained power command will be, assuming no losses, P_{Batt} calculated as (3.18). In the case of frequency control in the inverter control scheme, the command will be the AC power, P_{AC}, which will be equal to P_{Batt} considering no losses, and which expression in the dq reference frame is shown in (3.19).

$$P_{Batt} = V_{Batt} i_{Batt} \tag{3.18}$$

$$P_{AC} = \frac{3}{2} V_{d\ grid} i_{d\ inv} + V_{q\ grid} i_{q\ inv} \tag{3.19}$$

As the dq grid voltage components are obtained synchronizing with the grid angle, $V_{q\ grid}$ is 0, and then the expression can be simplified to (3.20). Thus, the d current reference will be obtain as (3.21)

$$P_{AC} = \frac{3}{2} V_{d\ grid} i_{d\ inv} \tag{3.20}$$

$$i_{d\ inv} = \frac{2}{3} \frac{P_{AC}}{V_{d\ grid}} \tag{3.21}$$

3.1.4   Inverter with Energy Storage System

Once the basics and control of the two involved converters has been established, they should be joint in order to integrate the complete proposed inverter with ESS. Figures 3-11 and 3-12 show the system with the detailed power stage schematic, including the placement of sensors and the control scheme for the two proposed control methods.

As shown, in both proposed strategies a power command feed-forward is presented on the V_DC control loop in order to improve the dynamics in the DC link. This feed-forward terms are based on the ideal relation $P_{Batt} = P_{AC}$, thus, once the system DC link control is on steady state operation (V_DC is the commanded DC link voltage)
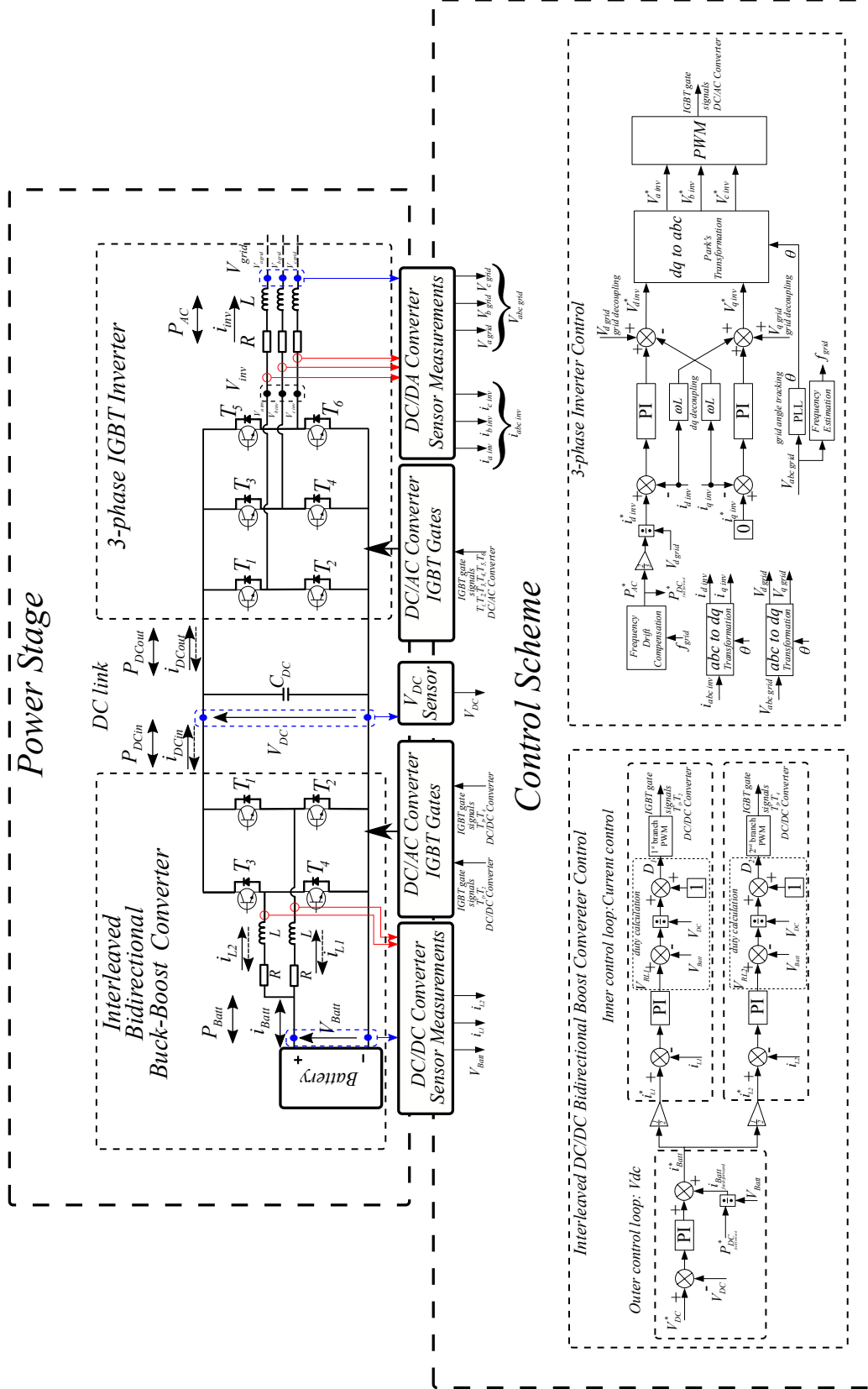
Figure 3-11: Proposed system diagram: power stage and control scheme for the transient frequency compensation system. First proposed control strategy.
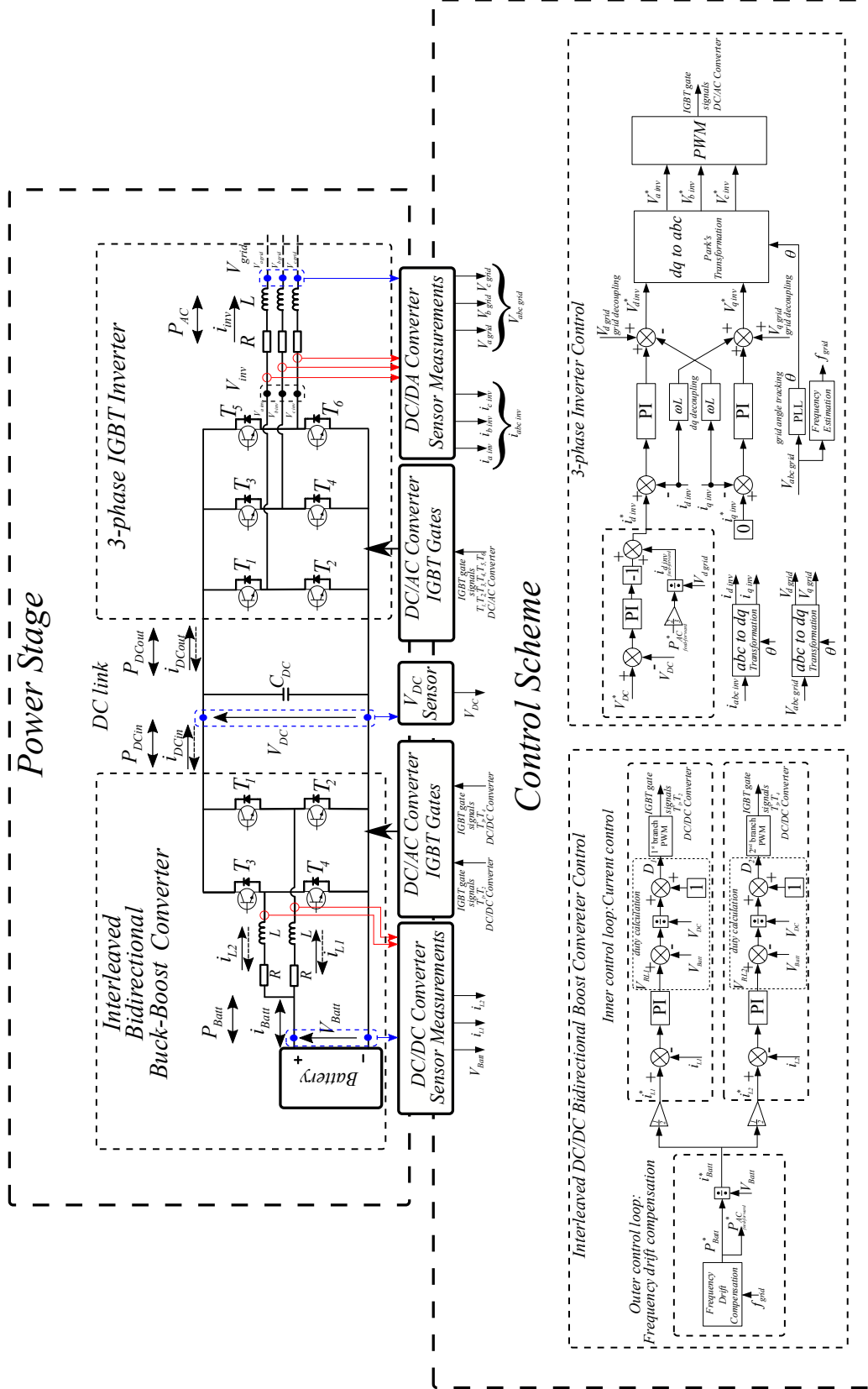
Figure 3-12: Proposed system diagram: power stage and control scheme for the transient frequency compensation system. Second proposed control strategy.

the DC link controller will only compensate losses and small disturbances, while relevant disturbances caused by load changes will affect minimally.

3.1.5 Implementation concerns in real control systems: Digital PI controllers

Real time implementation of control systems for power devices is usually done on Digital Signal Controllers (DSC) or Digital Signal Processors (DSP). This means that the implementation should be done on discrete digital domain. Thus, the Proportional Integral (PI) regulators proposed in the system control scheme should be defined for the digital implementation. In order to do that, the PI transfer function in continuous domain, denoted in (3.22) where U is the controller action and E is the input error, should be obtained in the discrete domain using the Z transformation.

$$\frac{U(s)}{E(s)} = TF_{PI} = K_p(1 + \frac{1}{T_i s}) \tag{3.22}$$

Using the Tustin method for the discretization, a transfer function of the form shown in (3.23) is obtained.

$$\frac{U(z)}{E(z)} = \frac{b_0 z + b_1}{a_0 z - 1} \tag{3.23}$$

Dividing the expression by z, the resulting equation is that shown in (3.24).

$$\frac{U}{E} = \frac{b_0 + b_1 z^{-1}}{a_0 - a_1 z^{-1}} \tag{3.24}$$

Substituting the factor z^{-1} in (3.25) by the corresponding previous sample of U and E, and clearing U and E, the equation results in (3.26).

$$U(a_0 - a_1 z^{-1}) = E(b_0 + b_1 z^{-1}) \tag{3.25}$$

$$U[k]a_0 - U[k-1]a_1 = E[k]b_0 + E[k-1]b_1 \tag{3.26}$$

Then, the expression which should be implemented in digital controller is the one shown in (3.27), where U[k] and E[k] are the present values while E[k-1] and U[k-1] are the values obtained in previous sample. As a_0 and a_1 are 1, they can be skipped from the equation.

$$U[k] = E[k]b_0 + E[k-1]b_1 + U[k-1] \tag{3.27}$$

Concerning the PI parameters b_0 and b_1, they are dependent on the proportional and integral gains of the PI as well as the sample period, following the relation shown in (3.28) and (3.29).

$$b0 = K_p \frac{1}{F_s 2 T_i} + 1 \tag{3.28}$$

$$b1 = K_p \frac{1}{F_s 2 T_i} - 1 \tag{3.29}$$

Due to the fact the output voltage of the converter is physically limited depending on the DC-link value, an anti wind-up technique is required. In this thesis, anti wind-up is implemented based on back-calculation, which consists on uploading the variable E[k-1] with the limited PI output as shown in (3.30).

$$E[k-1] = (U[k] - E[k]b_0 - U[k-1]a_1)b_1 \tag{3.30}$$

3.2 System integration in the micro-grid

Once the proposed system has been modelled, it should be integrated in a micro-grid. Figure 3-13 represent the network setup used as model for the testing of the system. It consists on a simple 1 node micro-grid composed by a synchronous generator acting as the weak grid, a pure active 3-phase load and the proposed inverter with the ESS. Both, the load and the system under study will be able to connect and disconnect from the weak grid while the generator which will be governed by a speed controller will supply the network with a 3-phase voltage having a frequency proportional to its

rotor mechanical speed.

Concerning the power flow in the system, the load will be able to consume power, the generator will inject power, while the inverter with ESS will be able to both inject or consume power, thus, it can assist the generator during transients due to load connections and disconnections.
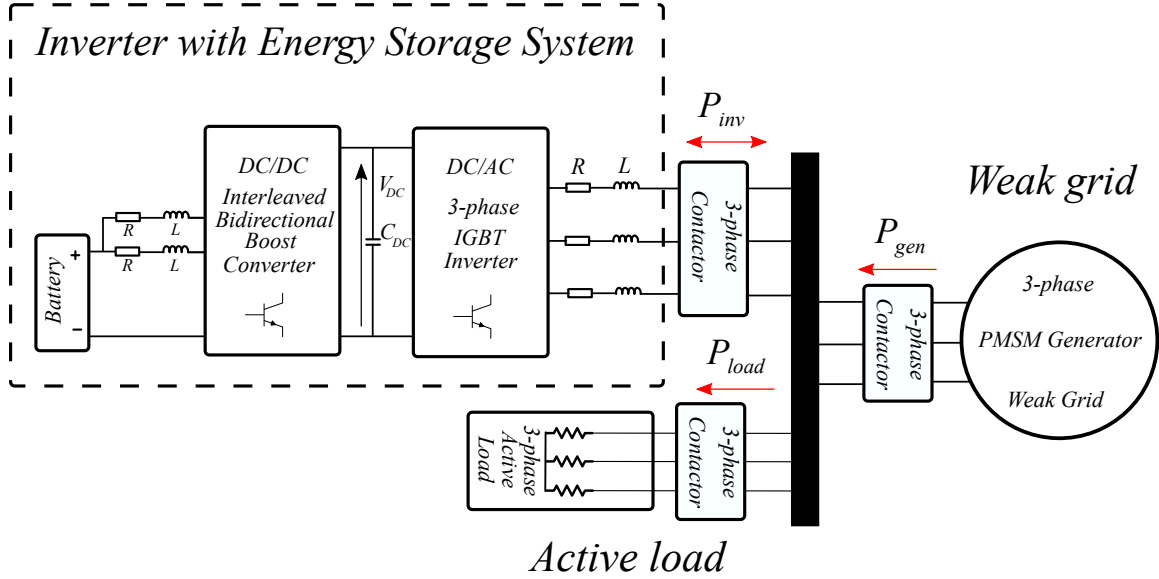
Figure 3-13: Integration of the system under study in a proposed micro-grid model.

This simple setup allows to evaluate the frequency stability provided by the generator and the performance of the proposed solution for transient frequency drift compensation.

3.3 Control Strategies for Grid Frequency Disturbance Compensation

As introduced before in this document (Chapter 1), micro-grids are often govern by low inertia synchronous generators. Such generators not only present low mechanical inertia but also are characterized for a high output impedance compared with conventional transmission level power plants. These characteristics convert the micro-grid in what is known as weak-grid, which may mean instabilities in both voltage magnitude

and frequency, specially during transients. The scope of this study is focused in the second contingency.

As the mechanical characteristics of the generator are coupled to its electrical ones, any change or disturbance in the electrical grid will be reflected in its mechanical system. Thus, in the case an electrical active load is suddenly connected to the grid, it will represent an equivalent torque load at the generator's shaft. This will slow down the rotor shaft speed momentarily before it return back to its commanded speed. In case the generator presents a low mechanical inertia this effect will be specially noticeable and will cause a transient frequency drift in the 3-phase voltage signal due to the coupling between electrical and mechanical speed.

Similar effect occurs when a load is disconnected. In such a case, the rotor speed will increased above the commanded speed momentarily before returning back to its operating speed, which will cause also a transient in the grid frequency.

Then, summarizing, a step on active load, either connection or disconnection, will cause a transient in grid frequency. This effect is illustrated in Figure 3-14 where the frequency under the connection and disconnection of a resistive load is shown.

This transient can be smoothed by using the proposed inverter with ESS for injecting or consuming active power during such a transient event, so that the generator is helped to maintain or to return back to its commanded speed avoiding deep frequency drops or peaks. On the other hand, during steady state operation, the inverter with ESS should be idle, i.e. it should not inject neither consume active power unless the battery needs to be charged. Then, the power load should be shared only during transients. This is a limitation imposed not only by the pursued aim of transient compensation system but also by the limitations of the energy storage device, as the ESS should be used as least as possible in order to reduce its cycles and extend its life.

It is worth noting that another problem is presented related with the steady state grid frequency. In micro-grids, generator's commanded frequency is set by a primary control based on Power-frequency droop. Thus, the grid steady state frequency will vary depending on the grid operator commands, and therefore, the controller in the
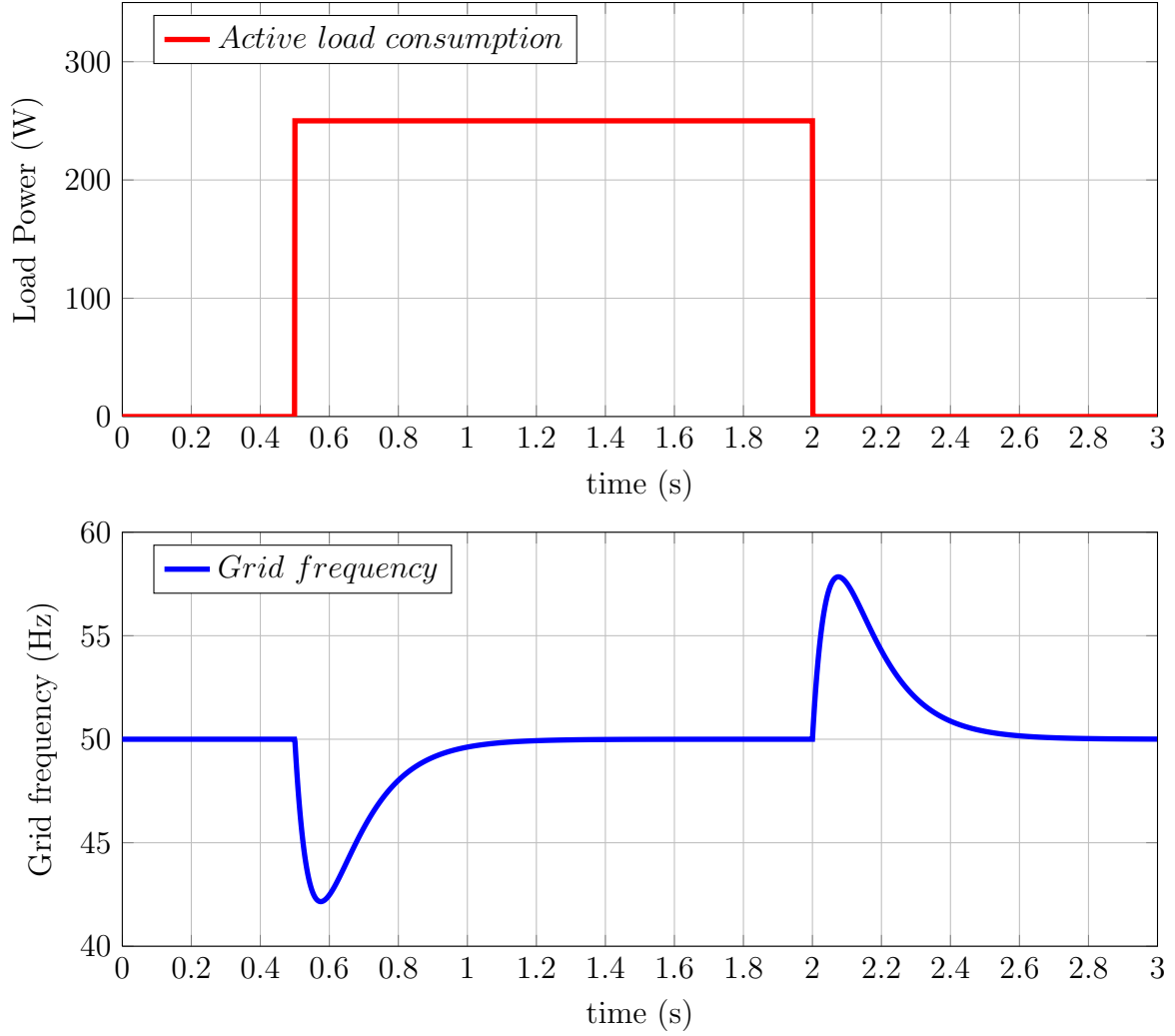
Figure 3-14: Illustration of the transient frequency drift effect when an active load is connected to the weak-grid.

proposed inverter with ESS for frequency compensation may need that commanded frequency in order to operate correctly. In the best case, that frequency command will be given as a parameter from the grid operator or the generator, however, in the worst case, the inverter with ESS will act autonomously and will need to estimate that frequency.

In this Section, some control methods are proposed for the objective of frequency compensation during transients as well as strategies for steady state frequency estimation.

3.3.1 Weak grid identification: using the system information for Frequency Disturbance Rejection

Although the majority of the proposed control strategies will be based on a grid frequency feedback control, it is necessary to identify the generator electro-mechanical system in order to know which kind of system should be faced by the controller of the inverter with ESS. Thus, the different controllers can be tuned based on the estimation of such a system. Moreover, the identification of the system will become a mandatory task when parameter estimation and advanced control methods are used in future development on this topic.

Figure 3-15 shows the equivalent system of a synchronous generator coupled to a governor which controls the shaft speed. The governor in this case is out of the Thesis scope, it is just necessary to considered that the synchronous generator speed is imposed by an external source that could be for example a diesel motor or a wind turbine. Then, for the generator system, the input is power established by the torque and shaft speed while the output is the grid voltage which is created by its back electromotive force (back emf).
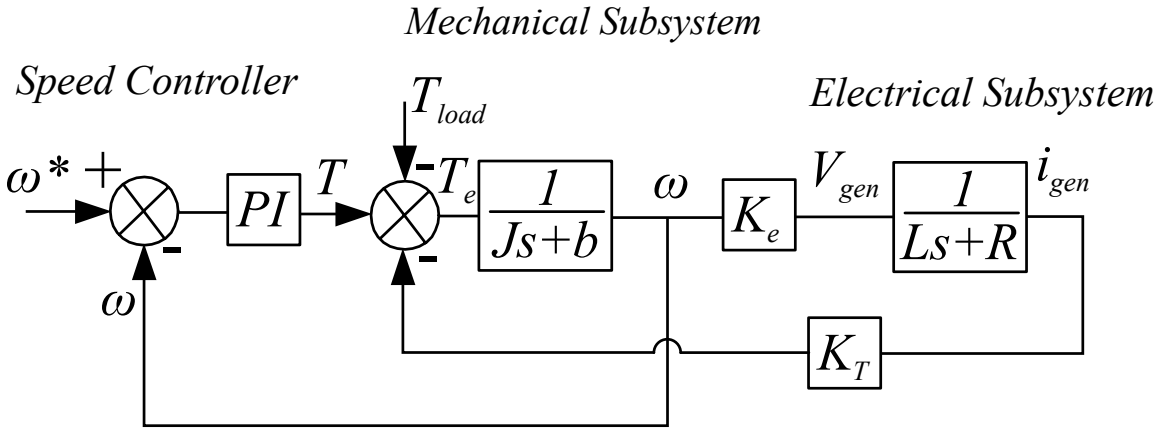
Figure 3-15: Equivalent system diagram of a PM synchronous generator.

The inverter with ESS should compensate the disturbance transfer function present in this electromechanical system. Thus, as stated before the Torque load (T_{load}) will be the input of such a transfer function while the output will be the rotor speed which is directly proportional to the electrical frequency with the relation on (3.31), wher

ω_e is the grid frequency in rad/s, ω_m is the mechanical rotor speed and P is the pole pairs of the generator.

$$\omega_e = \omega_m P \tag{3.31}$$

Concerning the input disturbance, the load step will be given in electrical active power being the relation with the electromotive torque of the machine expressed in (3.32) considering no losses in the machine.

$$P_{electrical\ load} = P_{mechanical\ load} = \omega_m T_{load} \tag{3.32}$$

Thus, the system to be compensated will be defined by the transfer function $\frac{\omega_e}{T_{load}}$ shown in (3.33) where the electrical dynamics are neglected considering L = 0 in the electrical subsystem.

$$\frac{\omega_e}{T_{load}} = \frac{\frac{1}{J}s}{s^2 + \frac{K_p+b}{J}s + \frac{K_i}{J}} \tag{3.33}$$

Although the theoretical system will defer from the real behaviour of the generator it could be very approximated as shown in Figure 3-16, where the real frequency response of the system is shown compared with the response of approximated models. One of the approximation is based on mathematical model approach while the other one corresponds to the approximation using the simplified theoretical transfer function presented in (3.33), showing both of them excellent performance. Although the mathematical model approach provides with a better response, its system transfer function also present higher order increasing the analysis complexity.

3.3.2 Transient frequency drift compensation control alternatives

Knowing the system to be compensated and the characteristics needed in the frequency compensation solution, five control methods will be evaluated based on close loop control.
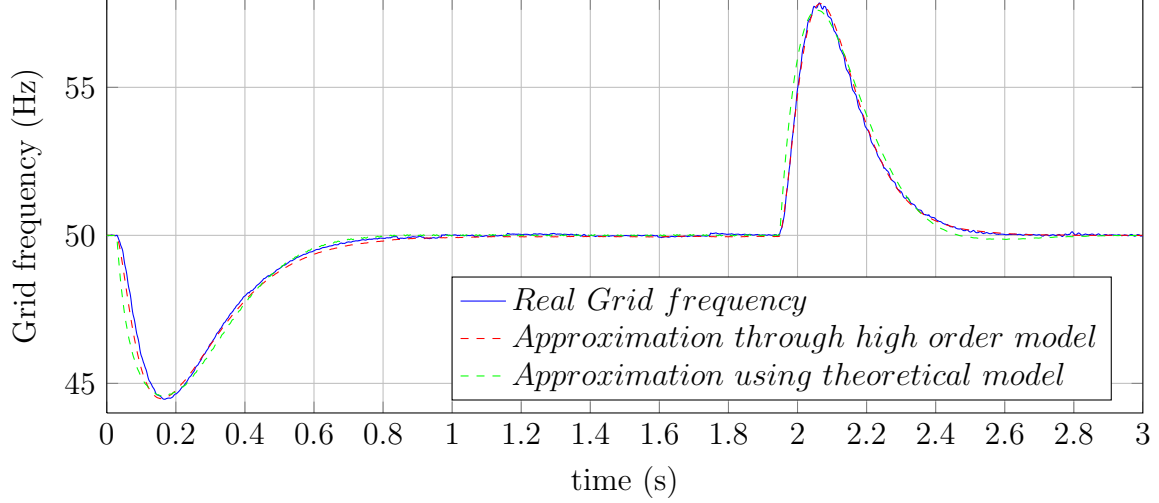
Figure 3-16: Weak-grid system identification using approximated models.

Frequency/Power Droop control based strategy

The first proposed strategy is represented in Figure 3-17. It consist on a classical close loop proportional droop controller. The estimated grid frequency will be subtracted to a grid frequency reference which will be considered up to this point as the steady state frequency of the generator at that moment.
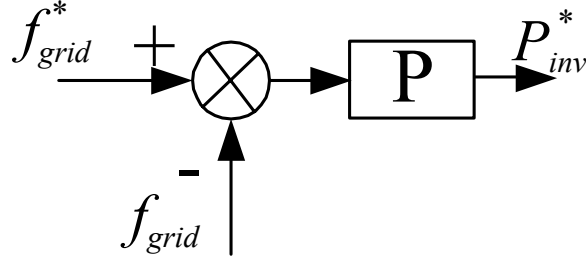
Figure 3-17: Droop based control method using a proportional regulator.

Its major advantage relies on the simplicity of implementation and tuning. It provides the weak grid with a smoothed transients reducing the drops and peaks of frequency. However, it presents some critical disadvantages. Although the peaks on frequency are reduced, the settling time of the transient increases proportionally to its gain, i.e. the better the smoothing the longer the settling time. Moreover, it can present steady state errors on frequency compared with the reference and, as it is still a droop based control, it may inject power during steady state, sharing the load as

any other generator in the grid.

PI regulator control based strategy

The second proposal is illustrated in Figure 3-18 and it consists on a conventional PI regulator. Although it provides very good dynamic response, allowing to smooth the frequency drift and the settling time considerably, it should be discarded from the solutions due to its steady state response. Even if the transient is well compensated, it remains injecting power during steady state and then is is unacceptable for the system under study.

$$f_{grid}^* \xrightarrow{+} \bigotimes \rightarrow \boxed{\text{PI}} \rightarrow P_{inv}^*$$

$$f_{grid}$$
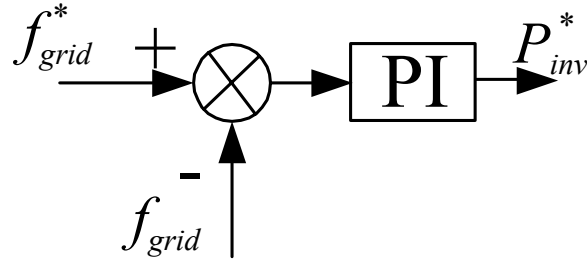
Figure 3-18: PI regulator control method.

PD regulator control based strategy

A solution to improve the performance of the P regulator is shown in 3-19. The Proportional Differential (PD) regulator allows to better detect the disturbance due to its derivative component. Thus, the derivative component provides a similar response to the proportional controller but with reduced settling time. As it still has a proportional component, even the derivative component does not actuate during steady state, this solution may present a steady state error and inject power during steady state depending on the gain of such a proportional. Also the effects of derivatives when a noise or step signal is used should be considered. Thus, in case the frequency command is subject to fast changes, the derivative may even worsen the performance.
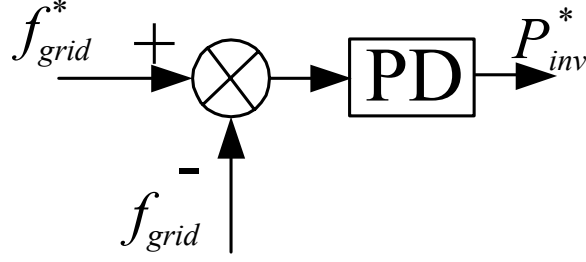
Figure 3-19: Proportional Differential (PD) regulator control method.

P-D/PDF regulator using feedback differentiator

Figure 3-20 shows an alternative to the conventional PD. It is referred in literature as PI-D or PDF (Pseudo-derivative feedback) controller [45, 30, 30, 23]. In this control scheme, the derivative controller is located on the feedback path while the proportional controller remains in the original place. This allows to use derivative controller avoiding the overrun problem due to rapid command changes. As this is likely to happen as frequency command will vary constantly as a function of a operator droop control. Moreover, in case the steady state frequency needs to be estimated, as exposed at the beginning of this Section, the frequency command could be a noise signal. All the above converts this method in the preferred up to this point.
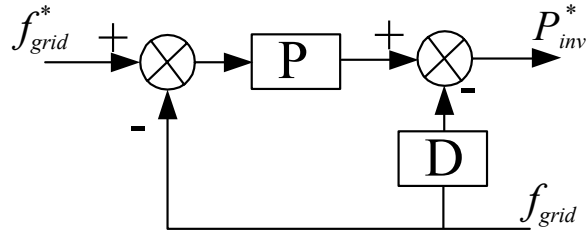
Figure 3-20: Pseudo derivative feedback PD regulator control method.

PD regulator with Disturbance Input Decoupling

As presented first in this document (Chapters 1 and 3) the solution under study could be associated to a significant load or set of loads in order avoid its effects on the grid. If this is the case, current sensors may be available to read the current flowing towards the load. Then, such measurements can be used in the control scheme to calculate

the power load step delivered to the grid. As shown in Figure 3-21, the load current can be used to perform what is known as Disturbance Input Decoupling DID.
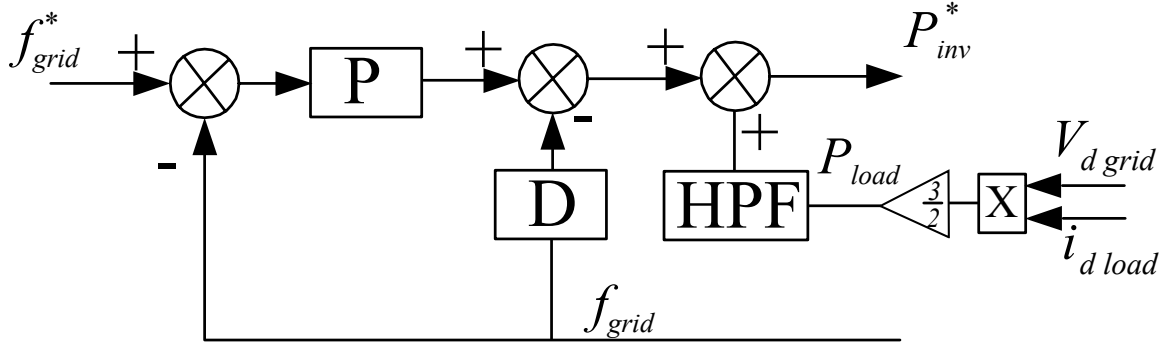
Figure 3-21: Disturbance Input Decoupling based control method with PD regulator.

As fas as the disturbance is known, the control action could be calculated based on it, so much so, that ideally, considering the fast response of the electronic converters, the frequency drift could be reduced completely by making the power injected with the inverter equal to the power consumed by the load. However, this solution is not suitable as power should only be injected during steady state and the system under steady does not acts as a power supply. Then, a solution to use the information of the system is to perform a High Pass Filter, or a derivative, on the calculated power load P_{load}. This method, with the combination of the PDF regulator can offer a faster and smoother response compared to the others, being the preferred solution provided that power load is available either by using sensors or any other method[1].

3.3.3   Comparison of the different techniques

Several techniques have been presented for frequency compensation offering each one advantages and drawbacks. Table 3.1 compares these methods highlighting their main features.

After the analysis of the different alternatives has been performed, there are still two main problems to be covered. The first one relies on the fact that the possible

---

[1]"Although is out of the scope of this thesis, one of the lines for the suggested future development and opportunities on the topic points to the use of observers in order to estimate grid parameters, being one of those parameters the steps of power in the grid"

Table 3.1: Summary of the different proposed control techniques for transient frequency drift compensation

Strategy	Advantages	Disadvantages
P Controller	• Easy concept and implementation • Smooths the transient	• Longer settling time • Steady state error • Possible power sharing in steady state
PI Controller	• Effective fast response • Transient Smooth	• Steady state power sharing • Discarded as an option
PD Controller	• Good Transient compensation • Good disturbance rejection • Fast response	• Possible Steady state error • Possible Steady state error • Overrun due to step command change and noise
PDF Controller	• Good Transient compensation • Good disturbance rejection • Fast response • immunity to command changes	• Possible Steady state error • More complex concept and implementation
DID strategy	• Improved Transient compensation • Improved disturbance rejection • Fast response • immunity to command changes	• Possible Steady state error • More complex concept and implementation • Extra sensors or complex techniques

steady state error of the controllers can lead to the injection of power during the steady state. Moreover, the proposed methods operates constantly and, thus, they will actuate even for a minimum variation in the frequency although such a variation does not compromise the grid quality. Therefore, a technique for detecting major transients would be desired.

The second problem is the selection of the frequency command in the presented controllers. In case the frequency command is not available neither from the grid operator nor the generator, the actual operating steady state frequency should be estimated somehow, and this should be done constantly as it can change at any time.

3.3.4 Advanced techniques on transient frequency detection

Transient detection becomes an important concern in the study of transient frequency drift compensation, solving two issues, the elimination of compensation during steady state and the detection of grid frequency steady state value that should be used as a command for the frequency compensation control. Although the first approach can consist on the use of a frequency threshold as presented in [2], this method is only valid if the steady state grid frequency commanded by the grid operator is known. Therefore, two alternative ideas are proposed for its used in future development. They have been implemented offline using the real frequency signal obtained in experimental

setup.

The first one consist on the use of a second order filter that provides a signal with 0 value during steady state, changing when a transients occurs. This signal may present positive and negative values, then, its absolute value can be obtained to reach a positive signal with a zero crossing. Finally, the zero crossing can be eliminated by a low pass filter, obtaining a positive signal that can be compared to a threshold and set a transient window. Figure 3-22 illustrates the idea using real experimental signals offline.
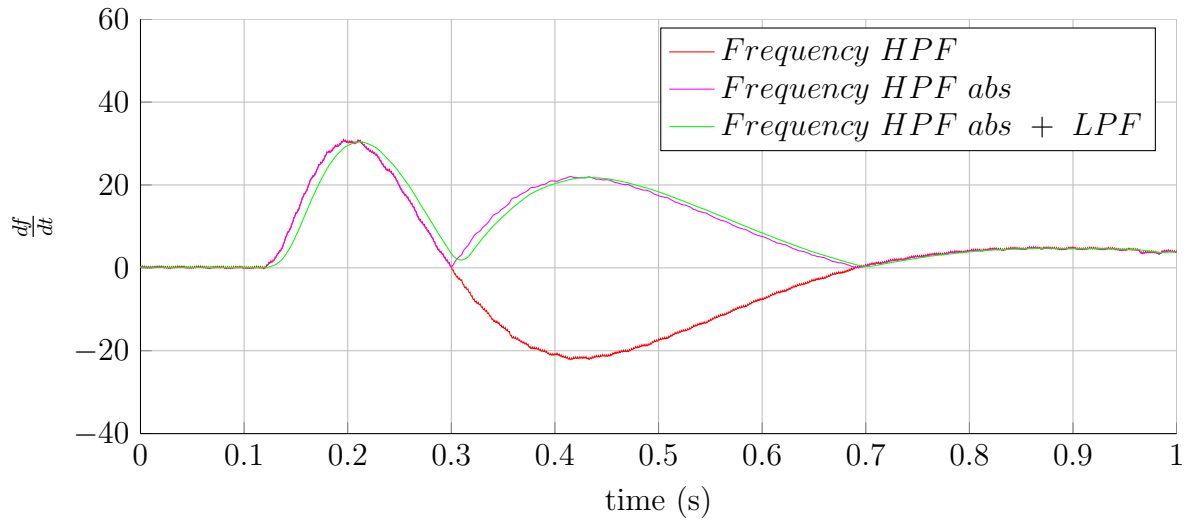
Figure 3-22: Transient detection method based on High Pass Filter.

The second method is based on the use of a signal obtained by a correlation method for comparing it with the threshold. Even the concept seems to be more complex, it also provides a simpler tuning compare with the first method. The procedure consist on applying a correlation between the frequency signal and any signal with zero average, for instance a sine wave with period equal to the one used for correlation. Equation (3.34) shows the operation to obtain the correlated signal that will be used for its comparison with a threshold. The performance of this method is shown in Figure 3-23.

$$u(t) = \left(\int_0^T x(t)f(t)dt \right)^2 \tag{3.34}$$

60

In these two methods, when the transient window is activated, the last read frequency value is taken as reference and the compensator starts actuating.
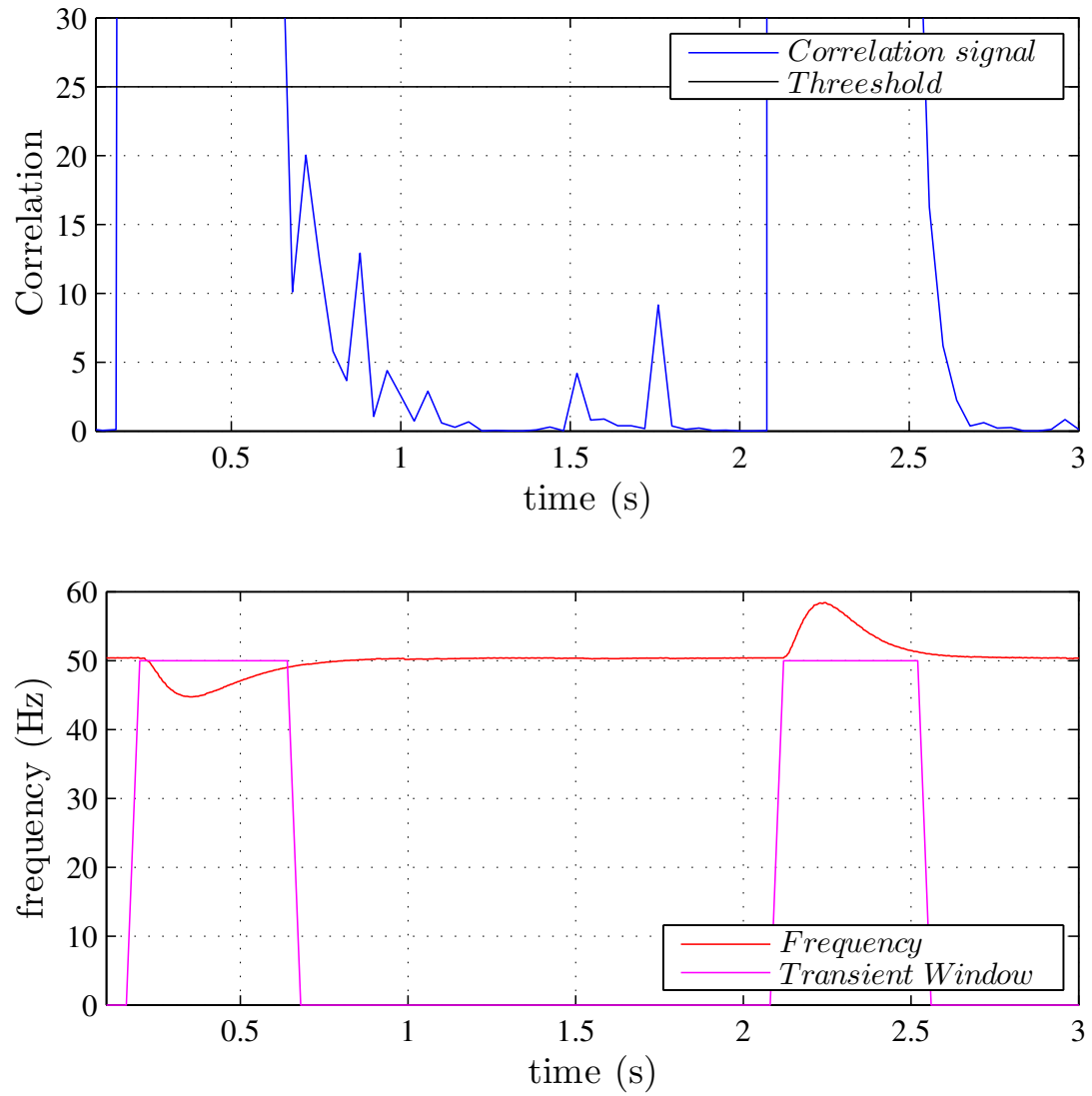
Figure 3-23: Transient detection method based on zero average signal correlation.

Chapter 4

Simulation of the Proposed System: Validating the Power Stage and Control Models

The proposed system will be validated both in simulation and in a lab prototype. As first approach, the system will be modelled in Matlab/Simulink using the Sim-PowerSystems tool set. For such a purpose, a scheme similar to the one presented in Chapter 3 Section 3.2 will be used, which will be taken later also as a model for the experimental setup. Thus, the simulation will try to reproduce as far as possible the conditions that will be given in the experimental setup, adapting therefore the parameters and the dimensioning of the system to match this constraint.

In this Chapter, the simulation results will be presented showing the expected performance of the proposed system. The results will include the operation of the inverter with ESS and the response of the proposed controllers for frequency drift compensation. The simulation will be validated using the complete power model and the simplified system based on the generator model studied in Section 3.3.1. Tables B.1, B.3, B.2 in Appendix B, collects the relevant control and physical system parameters. The same parameters has been used in both stages simulation and experimental prototype in order to obtain a proper design of the system.

4.1 Interleaved Boost DC/DC Converter Simulation

As an improved topology solution compared to other ESS used in the topic of this study [1, 2], it is worth to point out the benefits of the interleaved converter for the ESS interface. Figure 4-1 shows the the current through each one of the boost inductors in the interleaved compared to the current at the battery terminals, having the last one a noticeable reduced ripple.

4.2 Grid Side Inverter Simulation

For the simulated system, the two control strategies proposed for the inverter with ESS have been implemented. Thus, the main features to point out in the grid side inverter are the control of the DC link and the injection of active current. The DC link performance will be shown later with the operation of the whole system. The power injection capabilities are shown in Figure 4-2, where the current control performance is shown during the compensation of a transient in load, for both dq components, as well as in Figure 4-3, where the actual variables of the system showing the phase A of current and grid voltage are compared with the $i_{d\ inv}$ current. As shown, one of the requirements for active power injection is the current being perfectly synchronized with the grid voltage.

4.3 Simulation of the weak grid behaviour

The weak grid will be modelled as a PM machine acting as a generator. Its performance in simulation is shown in Figure 4-4 where the grid frequency and voltage is shown for the connection and disconnection of an active load. Although the focused of this study is the transient that appears in frequency, the weak grids are not only characterized by a low inertia but also by a high electrical impedance that cause variations in the voltage when the delivered power changes. This explains why even
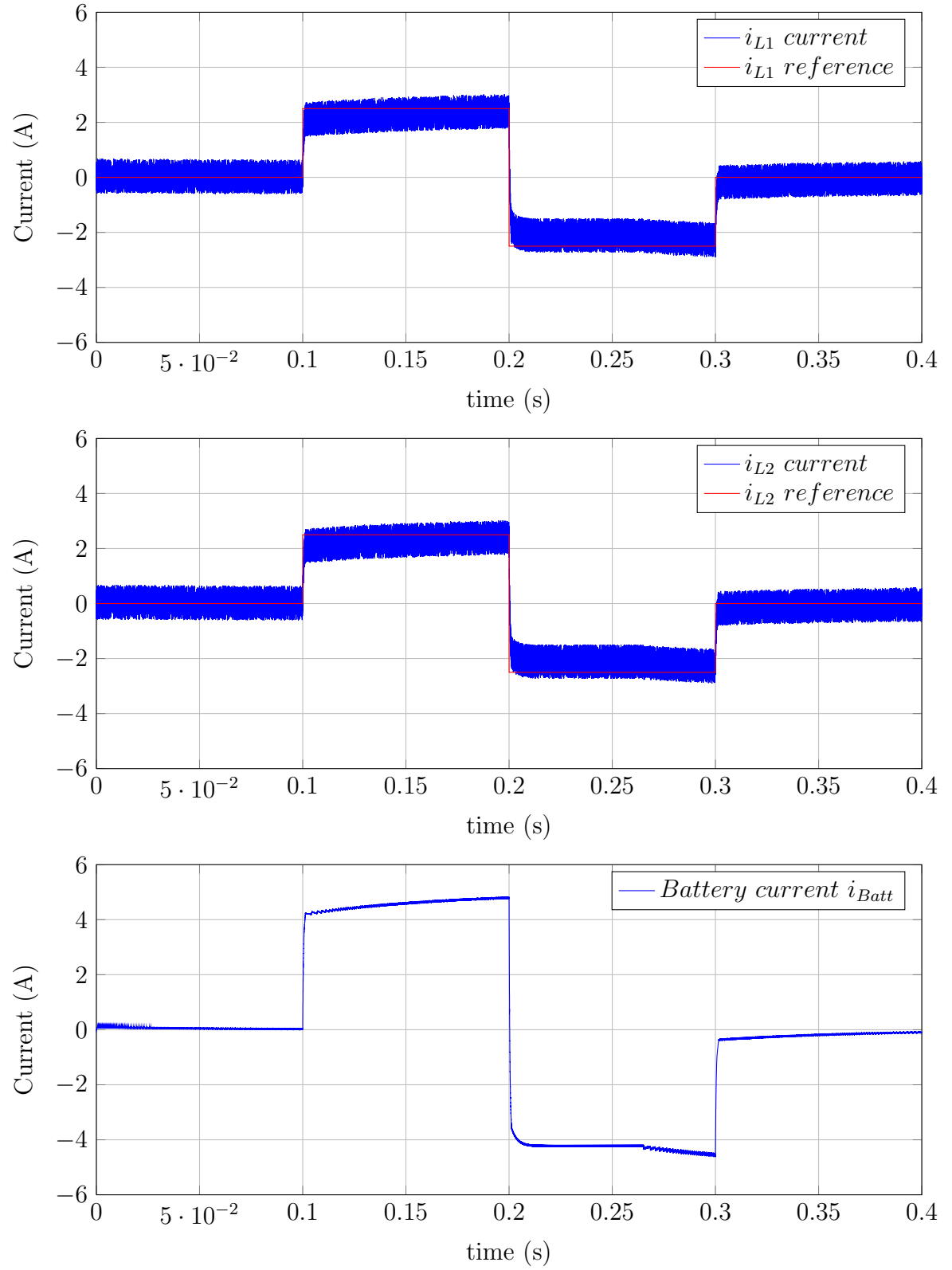
Figure 4-1: Interleaved DC/DC bidirectional boost converter currents and current seen by the battery in simulation stage.
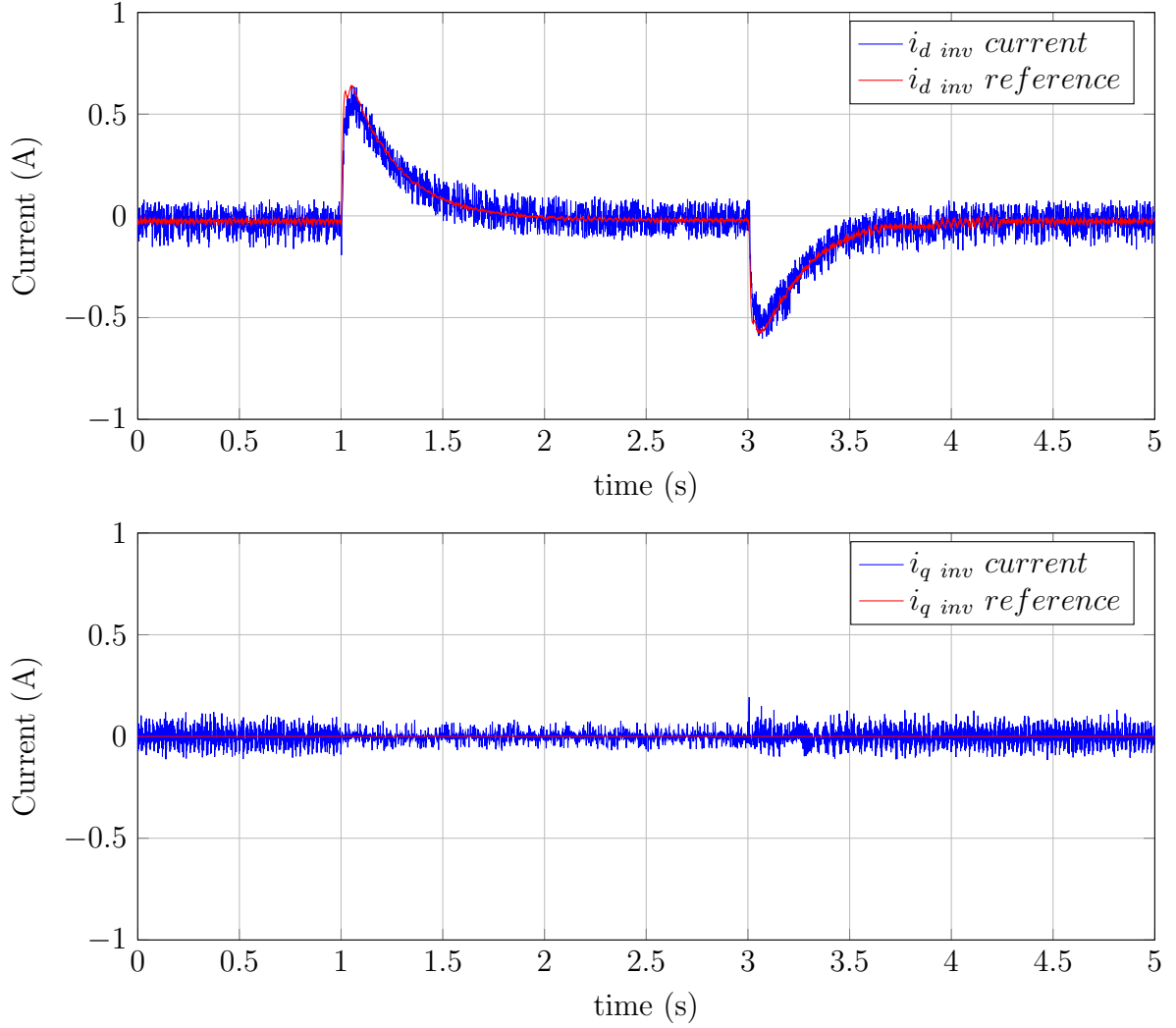
Figure 4-2: Inverter current control performance in simulation stage. Synchronous reference frame variables.

when a pure resistive load is connected, it does not present exactly an step on power as it depends on the voltage, that is varying.

4.4 Frequency Disturbance Rejection models in simplified simulation

In order to simplify the design and tuning stage of the different control architectures for frequency compensation, a first approach of their behaviour is achieved by using
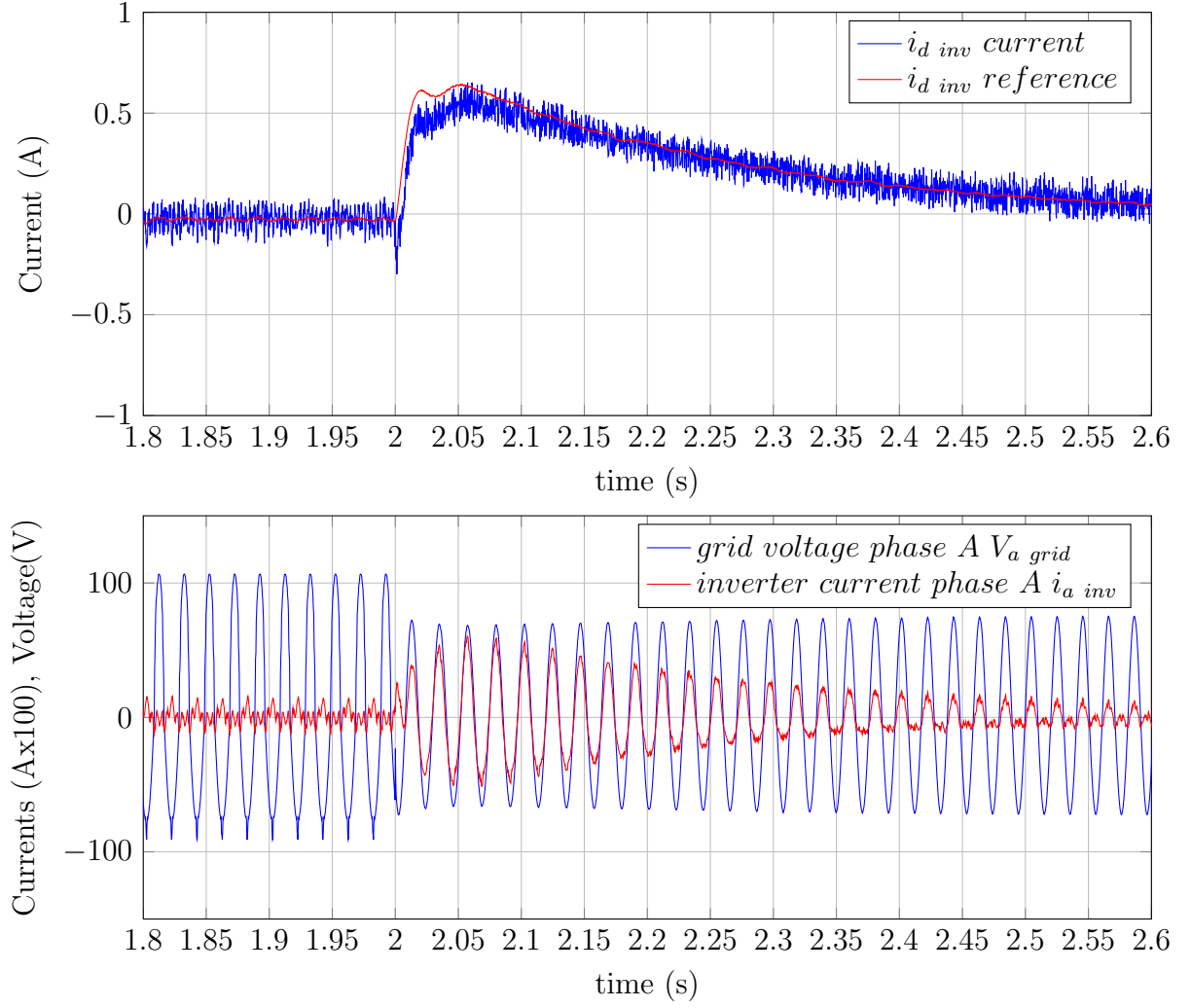
Figure 4-3: Inverter current control performance in simulation stage. Measured current and voltage.

the simplified approximated dynamic model of the generator. Thus, the performance of the controllers can be evaluated decoupling the electrical power system operation.

First, the use of PI will be discussed. Figure 4-5 shows the response given by a PI regulator under load steps. Although it presents an outstanding performance in terms of compensation, when looking at the control action, i.e. the power that the compensation system should inject, it is realized that the compensator is sharing the load consumption during steady state, being the reason for the discarding of this method.

An alternative to this is presented by the simple and classic proportional controller
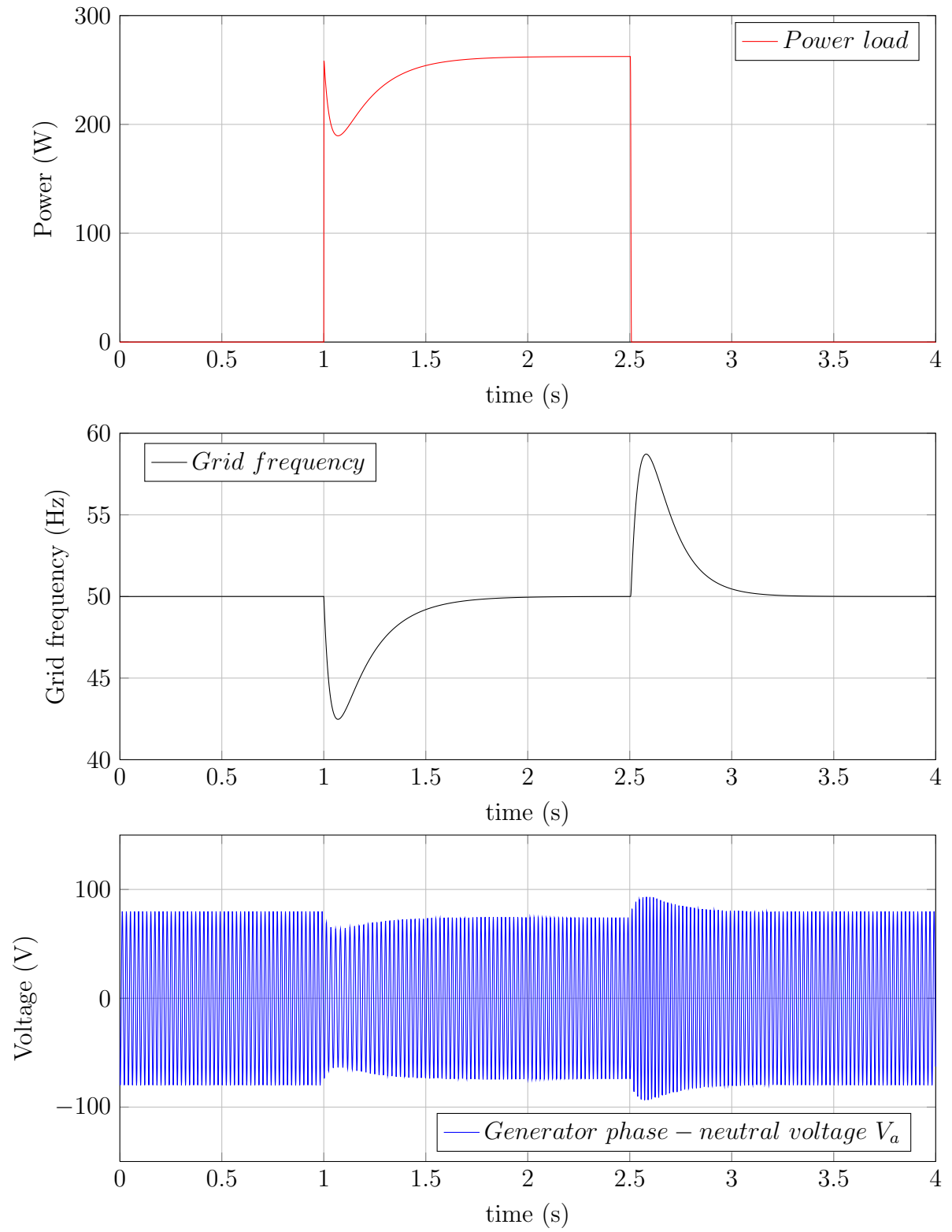
Figure 4-4: Weak-grid performance in the simulation stage.
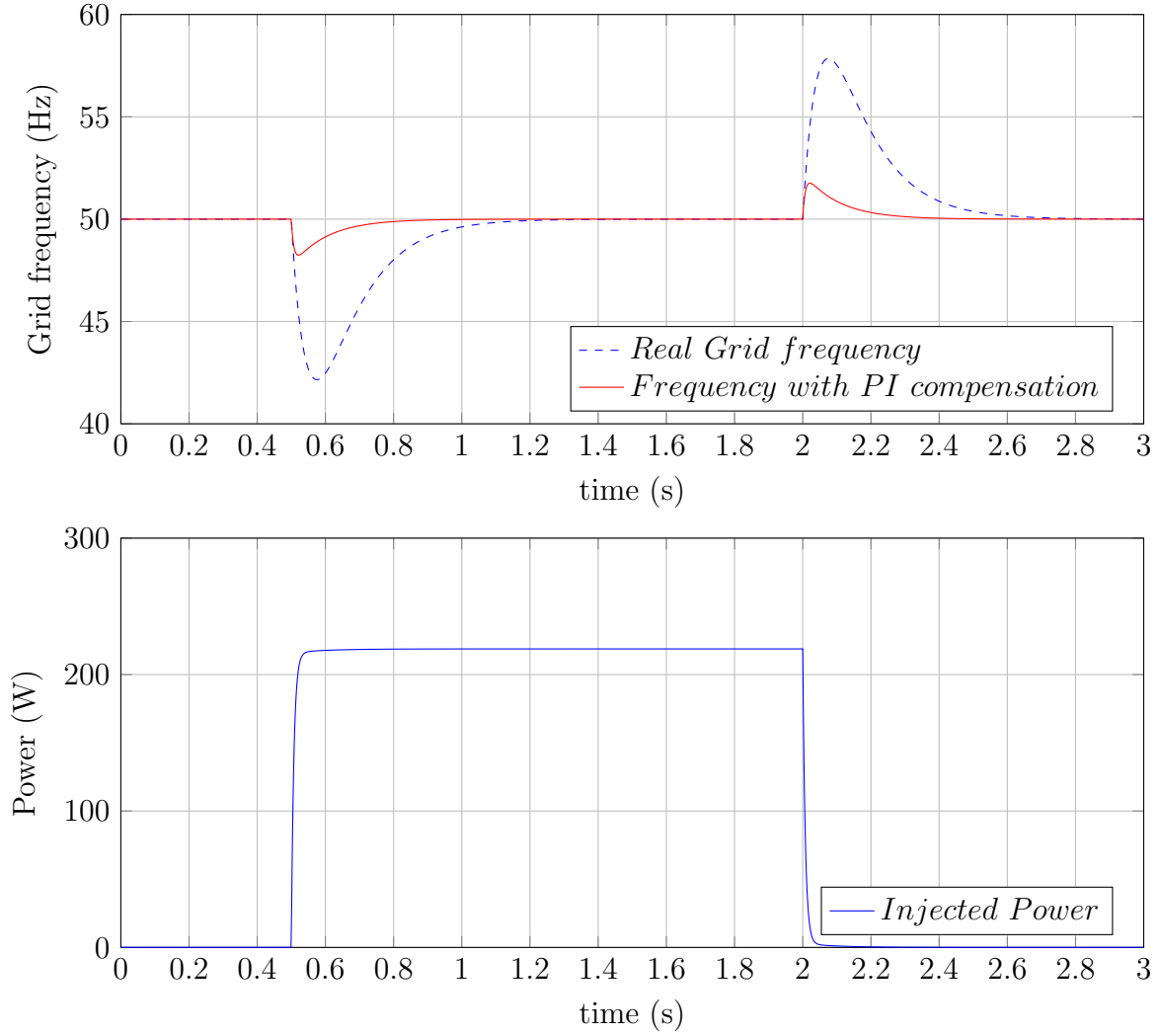
Figure 4-5: PI regulator performance used for frequency compensation.

which response is illustrated for different gain values in Figure 4-6. As expected, it smooths the transient on frequency, reducing the drop and peak as the gain is increased. However, the settling time to reach the steady state value is enlarged. Regarding the control action, unlike the PI, the P does not share apparently the load during steady state. This will be questioned when the experimental results are presented, as this kind of regulator can present steady state error.

Finally, Figure 4-7 shows the comparison of the different strategies. This will only settle an example of performance of each one, as its behaviour depends on the parameters used for its tuning. As shown, P-D method provides an improvement of
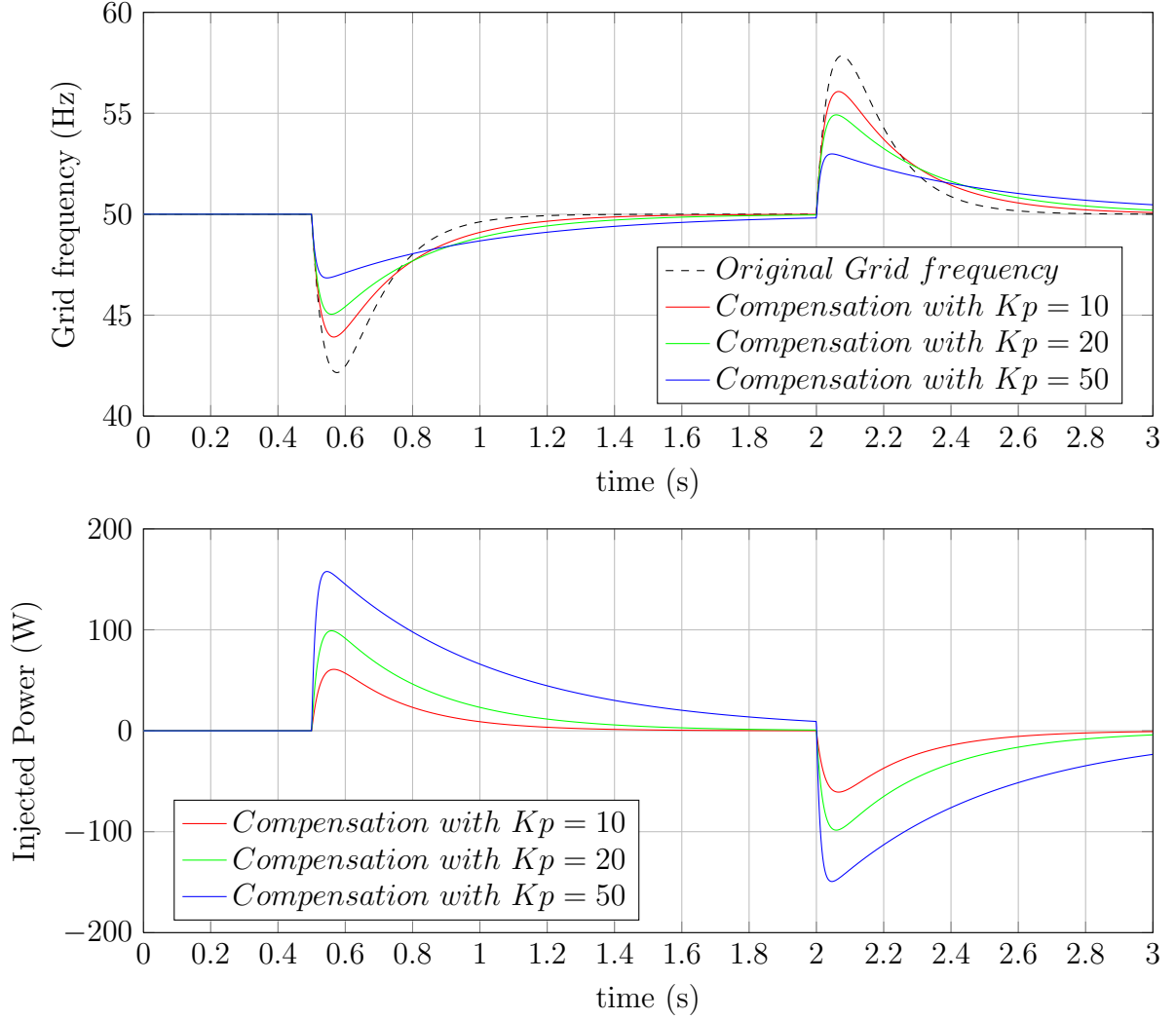
Figure 4-6: Proportional regulator performance used for frequency compensation using different gains.

P regulator performance, while the use of system information of the control with DID shows certain advantage compared to the others.

It is worth noting that the performance using DID with P or P-D control methods are pretty similar. Although the selection of the strategy depends on several factors as the tuning method of the regulator's gains, for the implementation in the simulated system the option with the P instead of the P-D will be chosen for the use with DID. By doing so, the complexity is reduced while keeping a proper performance. Moreover, the use of differentiators and derivatives in a real system could present several problems related to noise in the measured signals, that can worsen the performance of
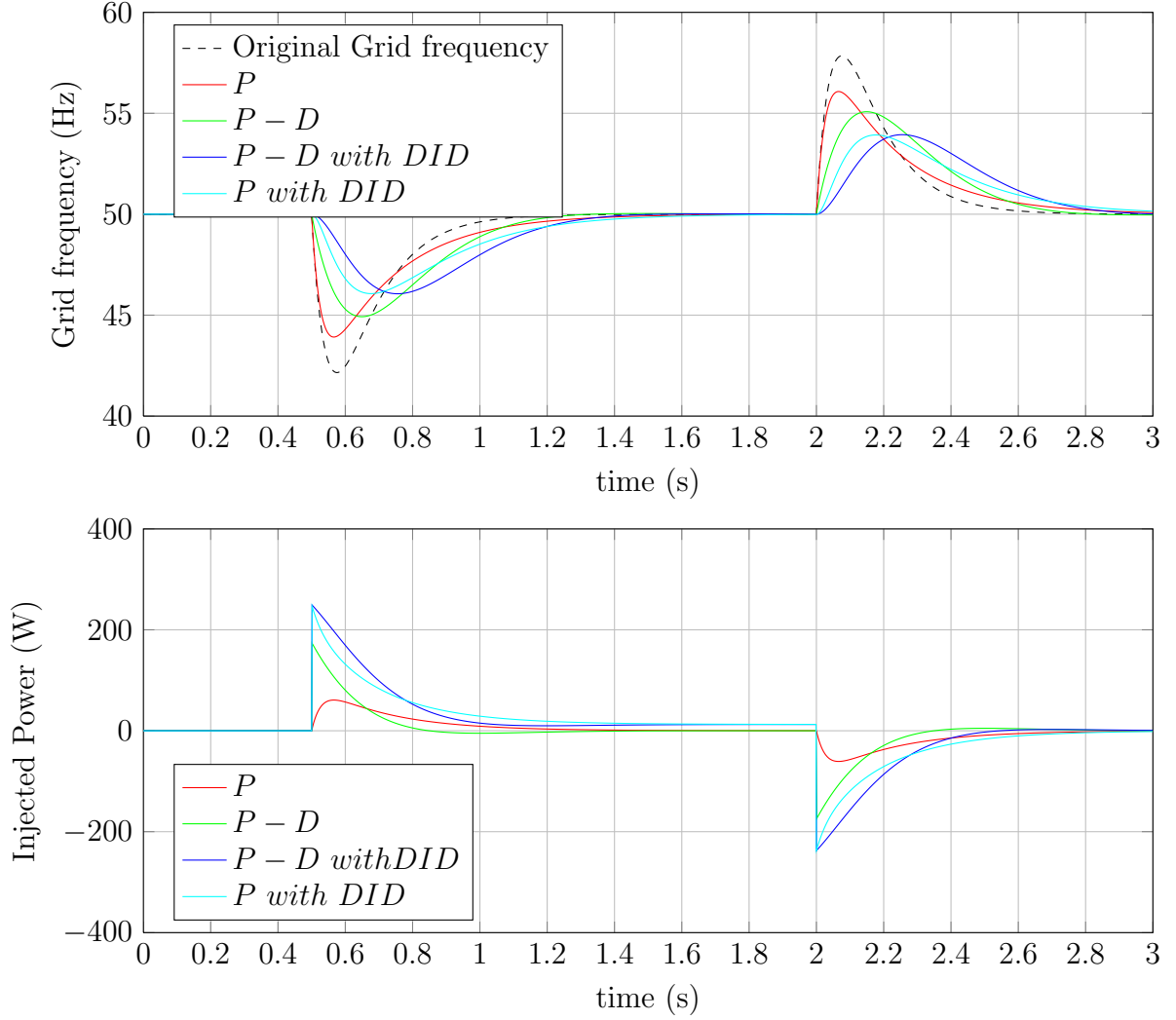
Figure 4-7: Comparison between the performance of 4 different control techniques. P with Kp=10, P-D with Kp=10 and Kd=2, P with DID, and PD with DID using a 1Hz high pass filter for both of them.

the control system, needing special care when implementing this kind of operations.

4.5 Complete system behaviour using SimPower-Systems in Simulink

Once the different points of the model performance have been covered, the operation of the inverter with the ESS is analysed, displaying the entire chain and the events that take place in the micro-grid model. Figure 4-8 collects the performance in a multi

plot figure showing the power injected by the inverter with the ESS, the changes on the battery state of charge, the DC link voltage and the grid frequency, using 3 different control methods: P regulator, P-D regulator with feedback D (PDF) and Disturbance Input Decoupling feedback combined with a P regulator. The used gains has been proportional gain equal 10, and differential gain equal 2.

As the main conclusion, the results are similar to the ones obtained using the simplified system. As shown, when a load step is introduced, the inverter with ESS injects active power during the frequency transient, returning to zero injection when steady state conditions are again reached. During the load connection transient, the battery state of charge decreases as the injected power is provided entirely by it. The effects on the DC link are also appreciated, suffering a small voltage drop which is compensated by the V_{DC} control. On the other hand, when the load is disconnected, the generator tends to accelerate, increasing the grid frequency. At that moment, the inverter with ESS will start to absorb active power, which will charge the battery, improving the transient frequency drift.
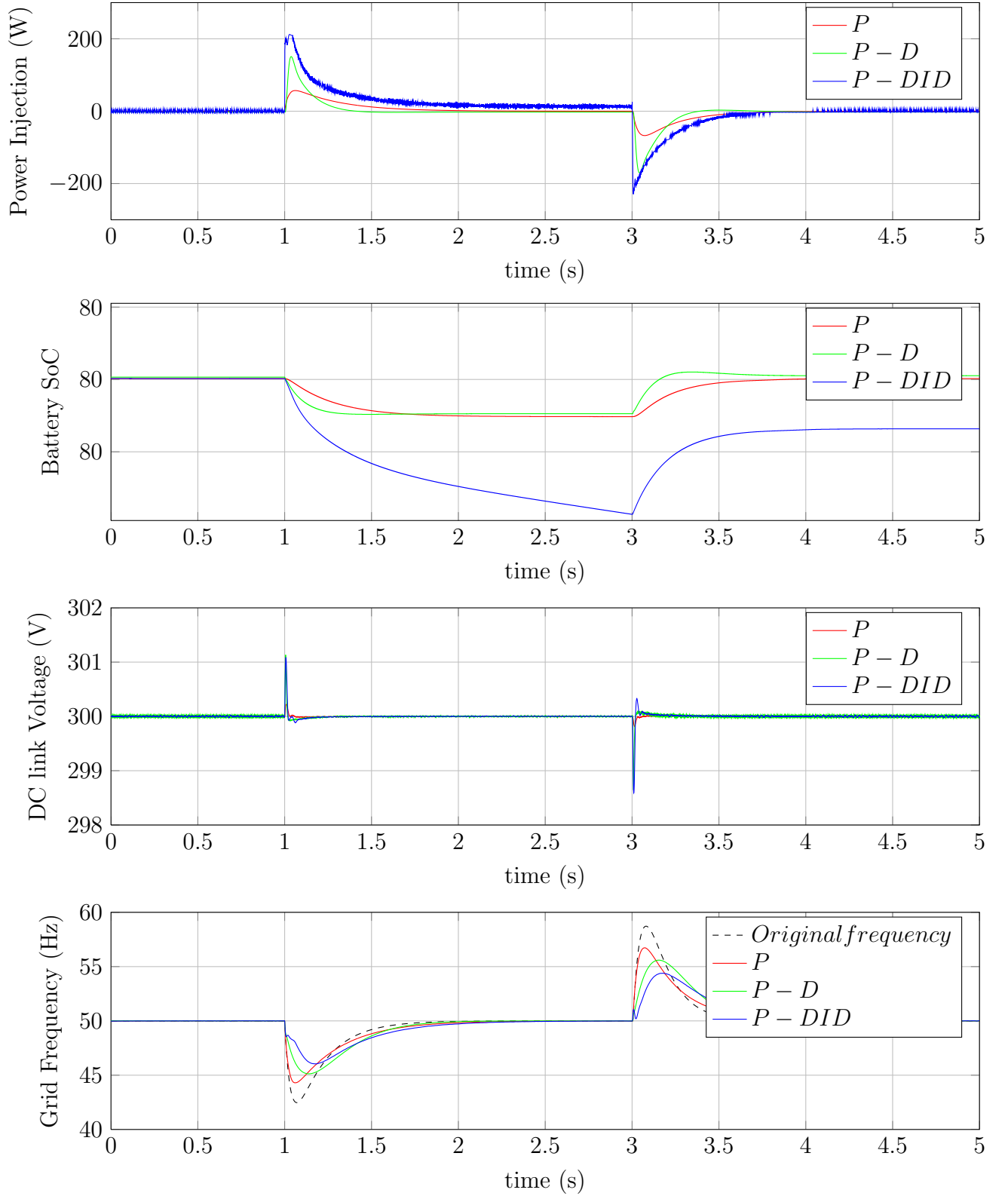
Figure 4-8: Transient frequency drift compensation using inverter with ESS in simulation stage.

Chapter 5

Experimental Implementation of the Proposed System

The experimental setup consists on the implementation of the proposed solution and its test integrated in a micro-grid similar to the one proposed in Chapter 3 Section 3.2. Some particular characteristics of the experimental scheme are worth to be mentioned:

- The experimental micro-grid will consist on two identical PM machines, coupled through their shafts, one acting as generator and the other one as the prime mover motor. Thus, the generator will provide with 3-phase sinusoidal voltage waveform that will depend on its speed of rotation and its back emf constant. The motor will be controlled through a commercial drive.

- Both the inverter and DC/DC converter will be implemented using commercial devices with embedded drivers and sensors, using extra sensors for external signals such as the grid and the battery voltages.

- The control system has been implemented using C code in the Texas Instrument Digital Signal Controller TMS320F28335, assisted by an interface card for communication and control of the commercial converters.

- Just one load exist on the system, which, as well as the other elements in the micro-grid model, can be connected and disconnected by using a 3-phase switch

controlled from the DSP.

- Due to the lack of a real battery for the experimentation stage, the need has arisen for a solution that allows to either supply or absorb active power in order to provide the system with bidirectional power flow capability. The system consists on the combined use of a 3-phase rectifier supplied by a grid connected autotransformer and a braking circuit that allows to consume energy in a resistive load.

A graphical description of the experimental setup is given in Apendix A. The system and control parameters are summarized in tables B.1, B.3, B.2 in Appendix B.

The experimental stage has covered two main objectives. The first one is the modelling of a platform useful for future development in the topic of contingencies in micro-grids. Thus, the design and implementation of the DC/DC converter and the AC/DC inverter has been carried out including the complete control scheme, which has been implemented using the first proposed control method in Chapter 3. The second objective has been the testing of one frequency control strategy in order to validate the implemented system. In this Chapter, the most relevant experimental results obtained with the developed system are shown.

5.1 Experimental results

5.1.1 Interleaved boost DC/DC converter behaviour in experimental implementation

One of the enhanced properties on the system compared to other power topologies shown before in the application of frequency drift compensation [2], is the use of an interleaved DC/DC converter as the interface in the ESS. Figure 5-1 represents the performance of such a topology in experimental setup, showing the currents through each boost inductor and the current at the input, i.e., the one seen by a battery in

case is used as ESS. Currents are illustrated in detail view, showing the ripple in each point.
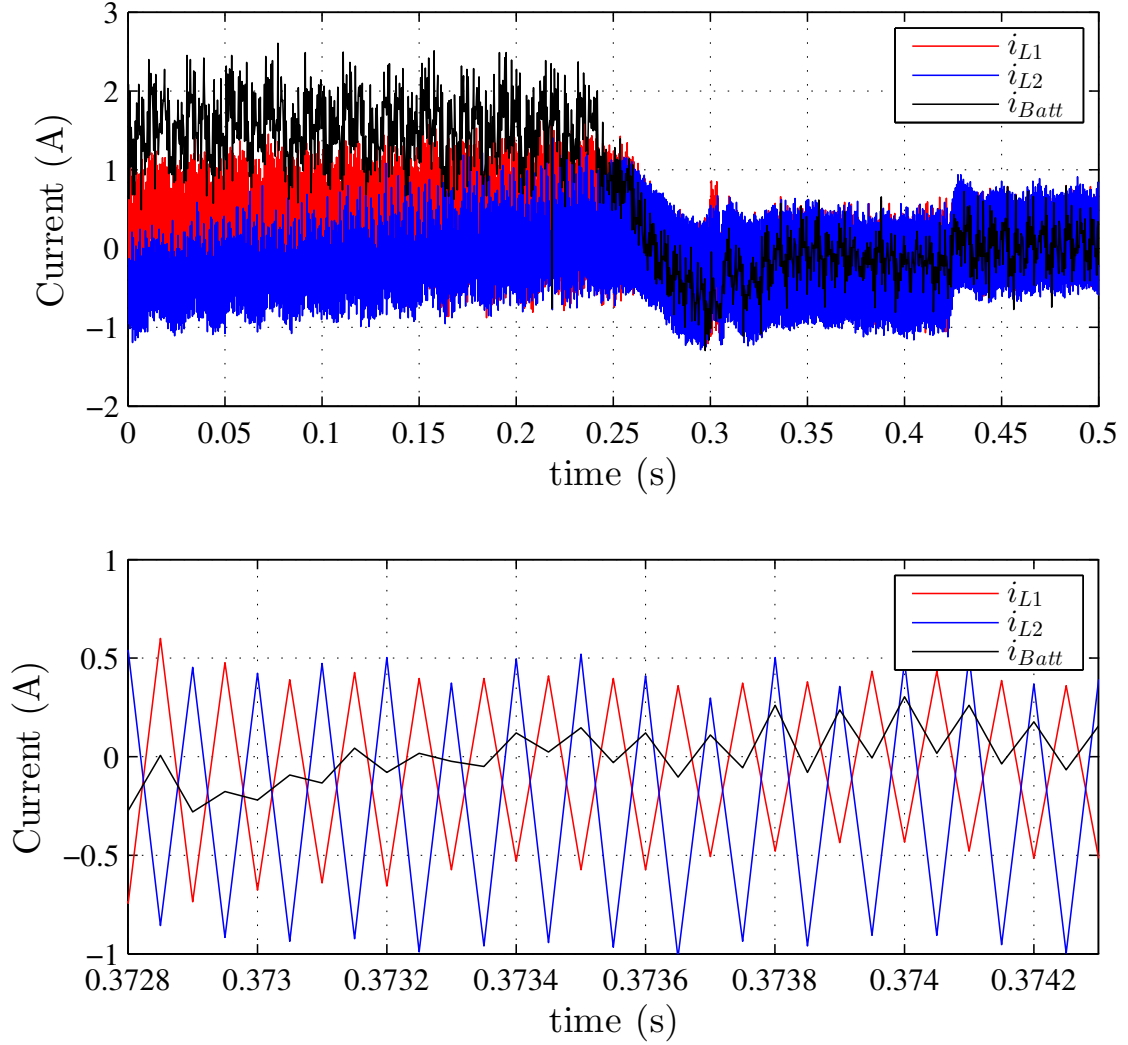
Figure 5-1: Interleaved DC/DC converter performance in experimental setup. Currents through interleaved phases and battery during a transient frequency compensation.

As shown, although the results are not as good as in simulation, it is appreciated the reduction in current ripple of the battery compare to the current ripple in the boost inductors. This differences with respect to the simulation can be due to several factors as the dead-time in the PWM that drives the IGBT gates or any unbalance

in the current sensors used for the feedback signals.

5.1.2 Experimental weak grid response and behaviour

The final results have been carried out based on the available experimental setup.

Thus, the experimental weak grid was taken as a model for the system design and simulation stage. Figure 5-2 shows the weak grid performance under a step on the active load. Then, the transient frequency drift issue is shown, having the grid similar performance to the one presented in the simulations (view Chapter 4 Section 4.2). Figure 5-3 shows a detailed view of the phase to phase grid voltages under a step on load, seen that it is near to perfect sinusoidal waveform.

5.1.3 Enhancement of grid frequency estimation: PLL vs FLL

The frequency estimation is one of the main task in the control for frequency drift compensation. One of the problems presented in the real implementation was the performance of the mechanism for the grid frequency. First, the PLL proposed in [11] was used. However, although the performance of such a method allows a perfect angle tracking, the provided estimated frequency is not suitable for using it as a frequency feedback due to the noise content. Thus, the method proposed in [35] based on Frequency Lock Loop (FLL) was implemented, obtaining a much adequate signal. A third approach can be implemented using the combination of PLL and low pass filter (LPF). Figure 5-4 shows the comparison of the three methods.

As shown, even if the frequency given by the PLL is more approximated to the real response, it is a much noisy signal than the FLL method. Such a noise, can be reduced using a low pass filter, however, it introduce a delay and not only the PLL should be tuned but also the additional filter. Moreover, even using the LPF, the signal still contains more noise than the FLL signal as shown in the detailed view in Figure 5-4. Out of the scope of this Thesis, the improvements and study in the selection of these solutions is proposed for future studies.
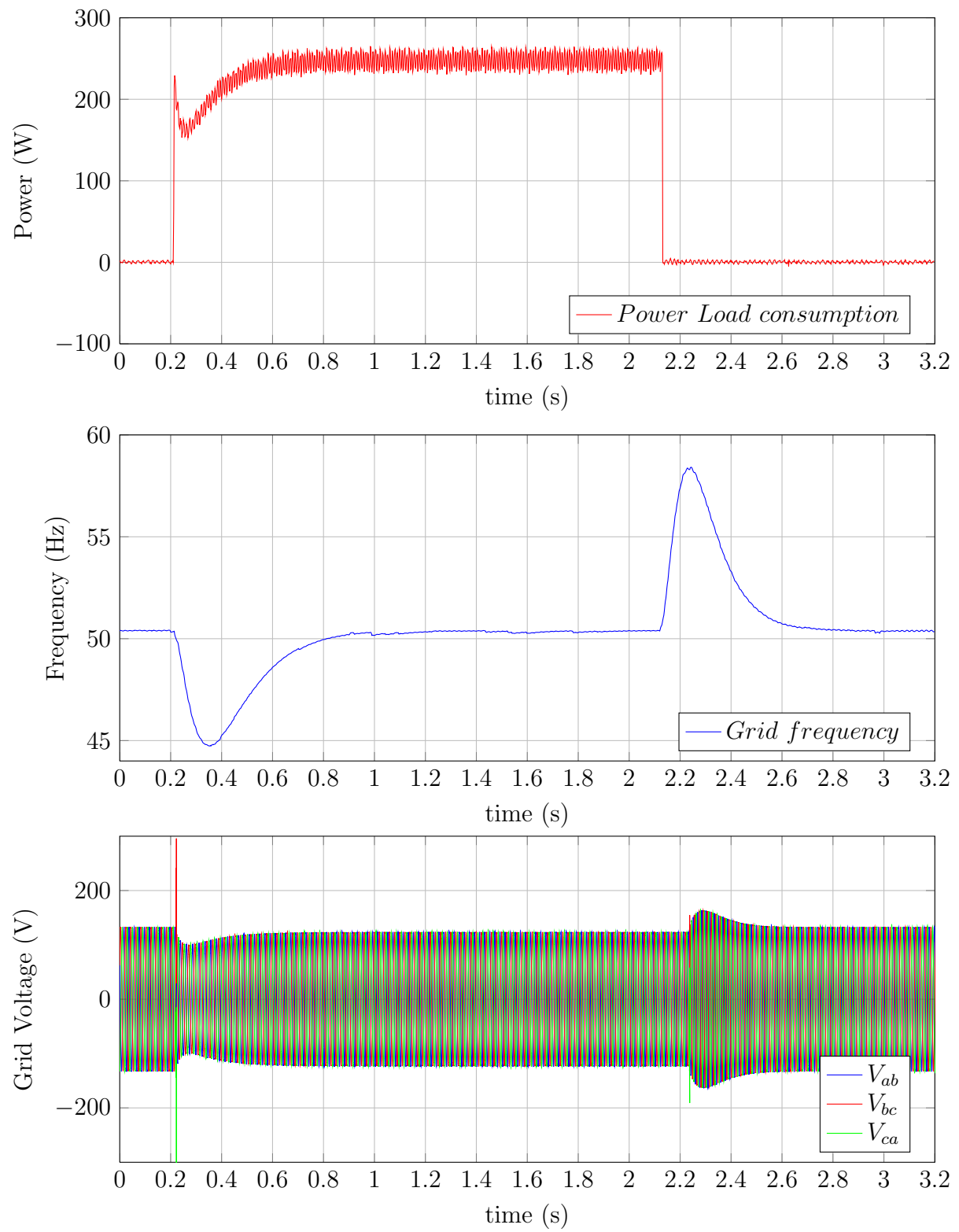
Figure 5-2: Experimental Weak-grid performance. The frequency drift during a load transient is illustrated.
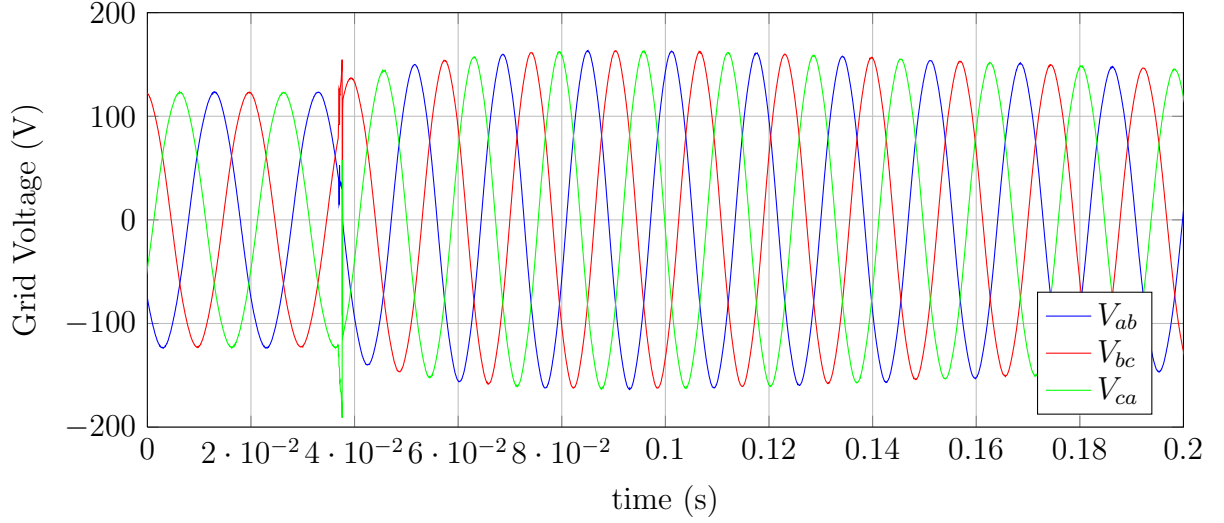
Figure 5-3: Experimental Weak-grid performance. Phase to phase grid voltages.

5.1.4 Experimental results for Frequency Disturbance Compensation

As the final experimentation, in order to evaluate the validity of the proposed inverter with ESS for its use in transient frequency drift compensation, a first approach for the compensation control strategy was implemented using the proportional P regulator method. The experimental results are shown below.

Figure 5-5 shows the interleaved DC/DC converter operation during a transient compensation injecting power when the load is connected and absorbing when it is disconnected. The DC link performance is outstanding showing inappreciable changes when power is injected.

Figure 5-6 shows the inverter side AC currents during the compensation. As shown, once the transient is detected, current is injected to compensate the frequency drift. However, it is shown that current is still present during steady state operation due to the steady state error introduced by the used P regulator.

Finally the obtained results in frequency compensation are shown in Figure 5-7, where the performance of the implemented experimental system is shown for 3 different gains in the regulator, illustrating both the control action, i.e. the power injected by the inverter with ESS, and the grid frequency compared to the original one.
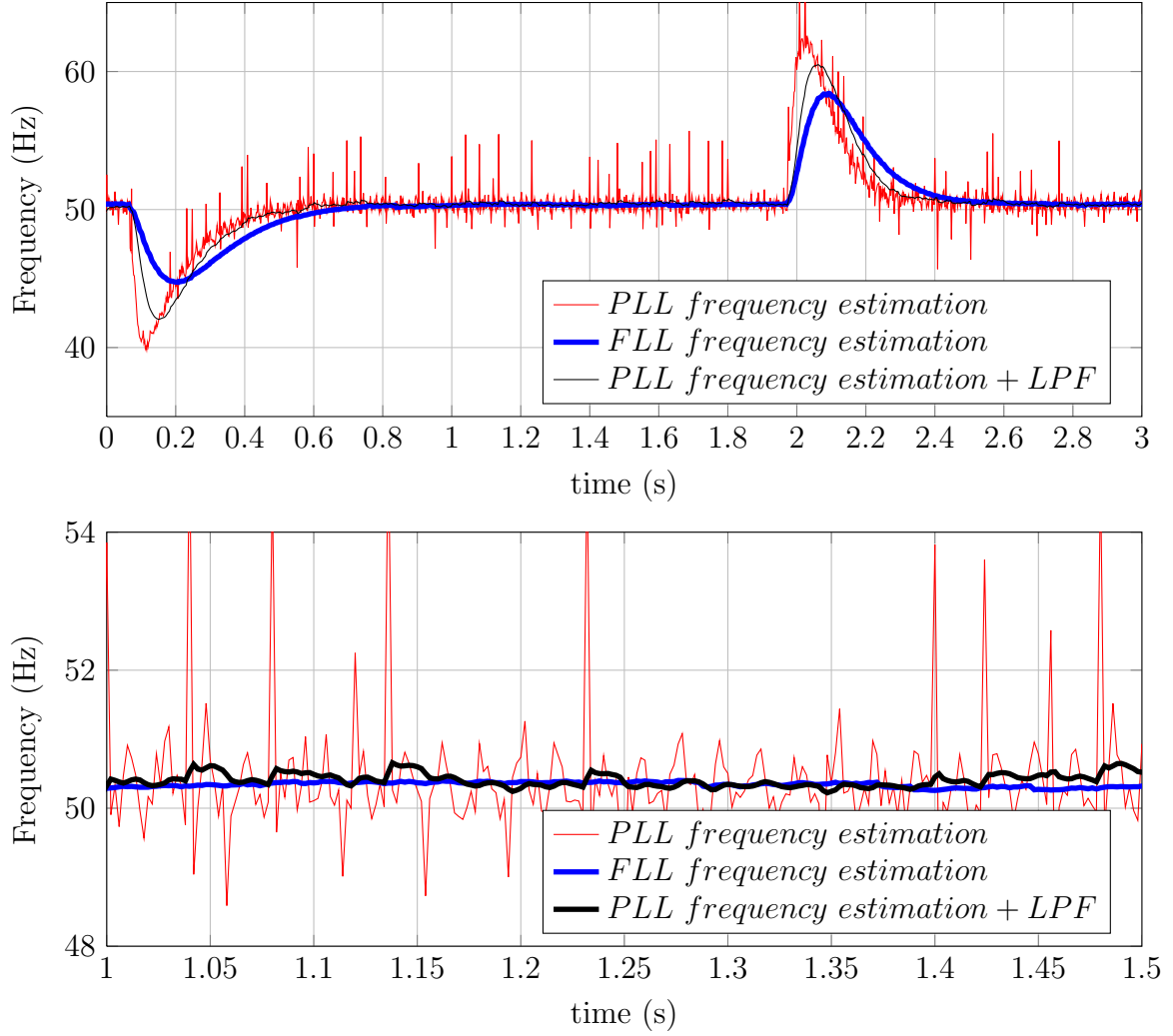
Figure 5-4: Grid frequency estimation methods. Phase Lock Loop compared to Frequency Lock Loop.

As shown in the figure, a compensation in the frequency is clearly appreciated which improves as the regulator gain is increased. These results demonstrate the capability of the implemented system for the purpose it was design for.

Nevertheless, several issues are still to be filled on the performance. Firstly, as shown in the figure, there exists a steady state error in the frequency when it is being compensated with any of the used gains. Moreover, that frequency steady state error is traduce as a constant injection of power not only in transient response but also during steady state. This last event, is not admissible for the application for which the system was designed, as it would carry a constant stress on the battery, thus
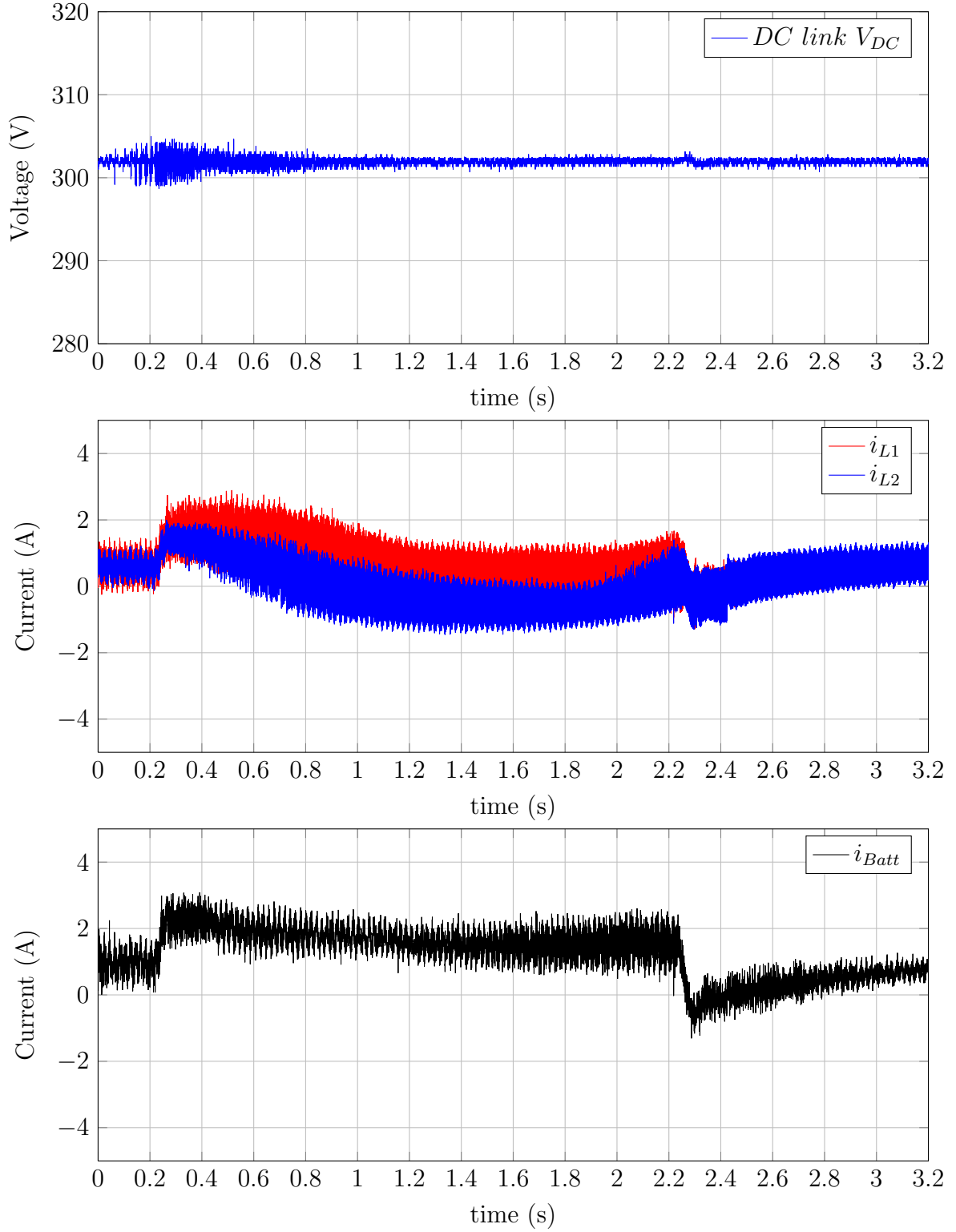
Figure 5-5: DC link and interleaved DC/DC converter currents during transient frequency drift compensation in the experimental setup.
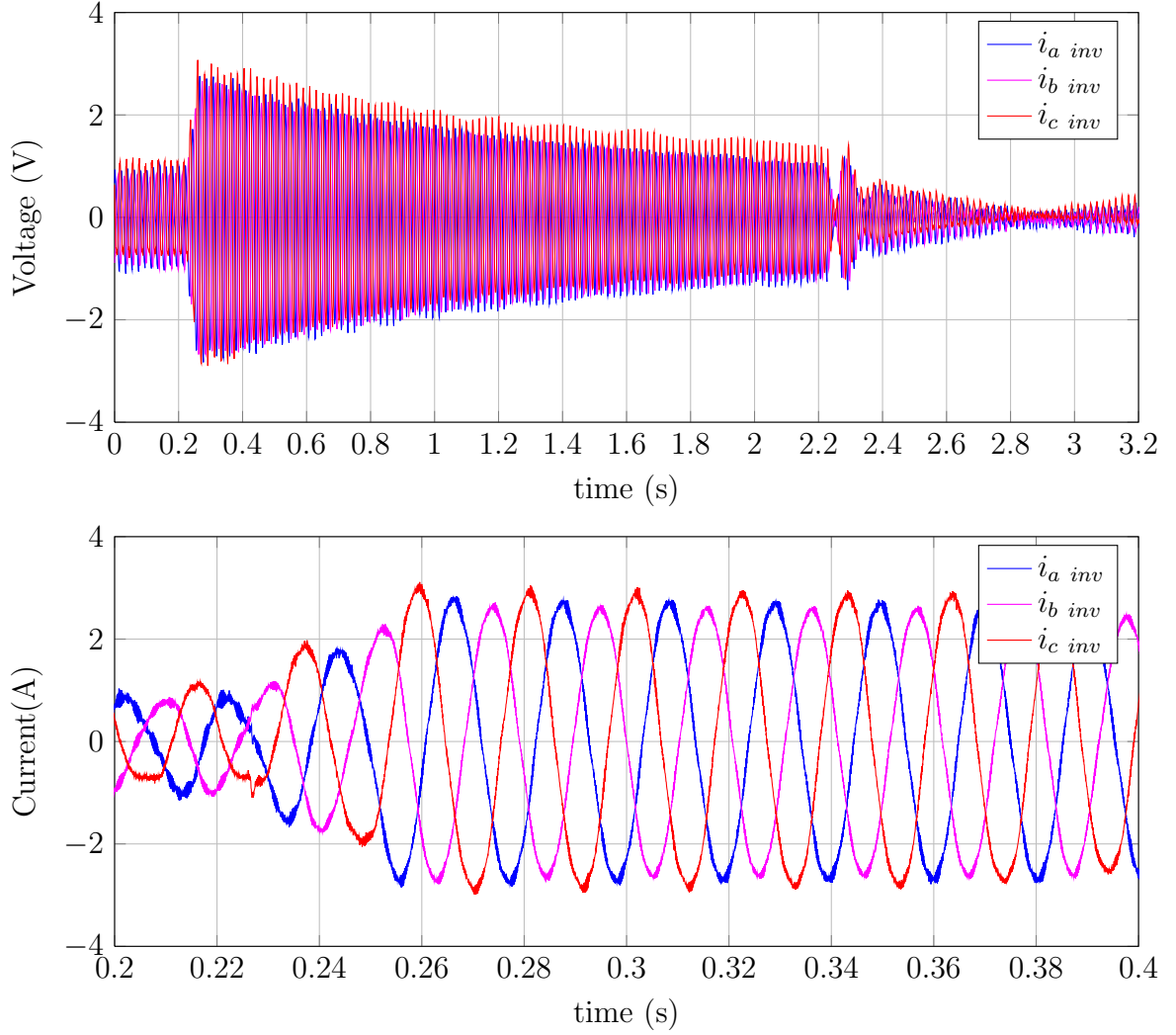
Figure 5-6: Injected 3-phase AC currents during transient frequency drift compensation in the experimental setup. Detailed view with 3-phase currents is provided.

reducing its life.

Another problem is the fact that the actual frequency command of the generator should be well known or estimated, otherwise the steady state error will be present anyway. Therefore, the control should be improved in at least two aspects that were proposed before in the document, the transient detection, in order to inject power only during transients, and the estimation of the actual grid frequency steady state command. Although they have not been implemented online in the experimental control, some methods has been already presented testing their behaviour using the experimental results in Chapter 3 as ideas to be developed in the future work.
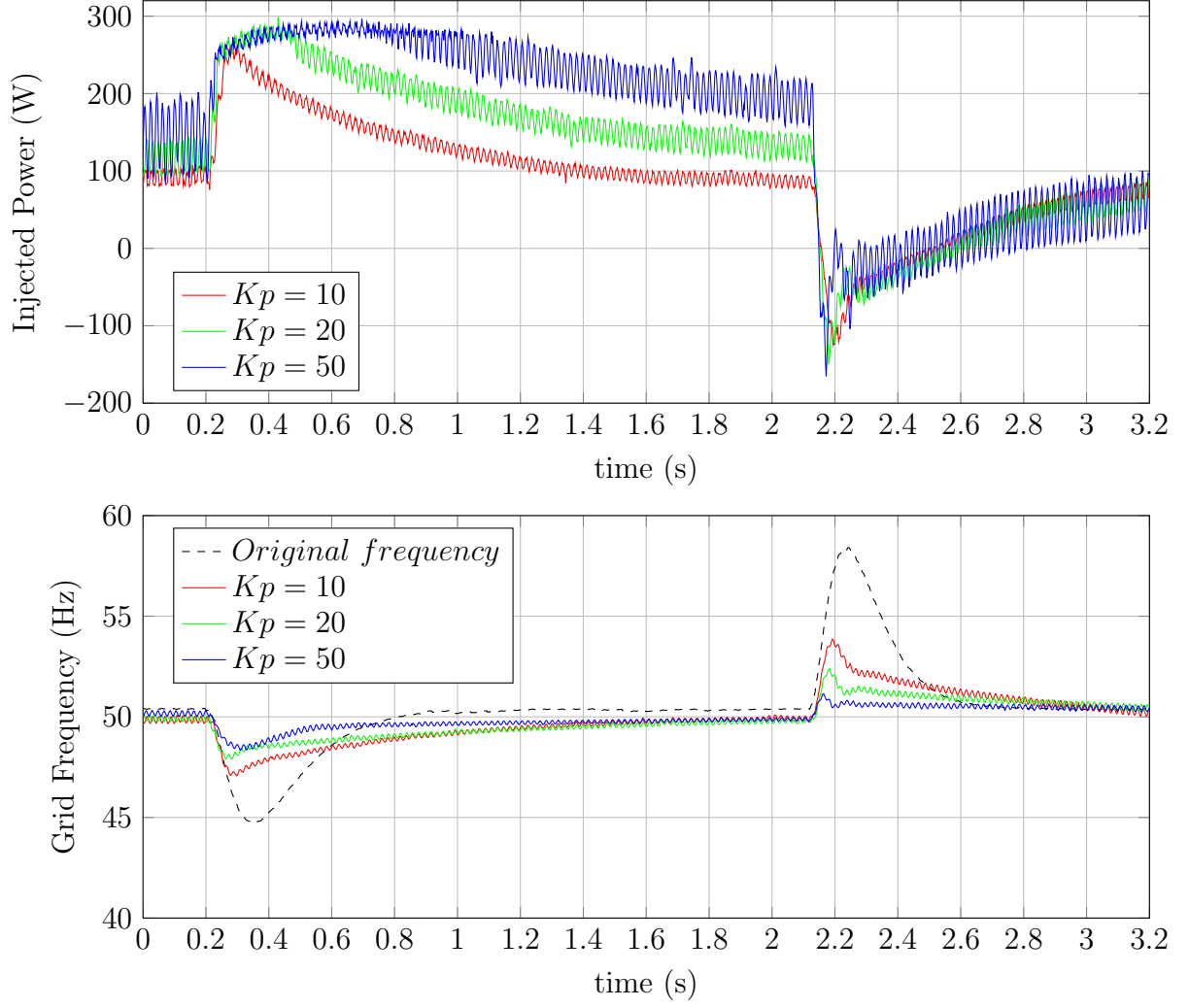
Figure 5-7: Transient frequency drift compensation using inverter with ESS in the experimental setup. Experimental results obtained for 3 different Proportional regulators using gains Kp = 10,20 and 50.

Other problem that arise concerning the grid quality is the injection of high frequency voltage in the grid due to the use of simple RL filter for coupling the inverter. This can be enhance by using a solution as LCL filter, that, even with the increased control complexity and the need of extra sensors, will allow to inject lower harmonic content currents and voltages to the grid.

Chapter 6

Conclusions and Future Work

Although micro-grids appear as the the future solution for electrical energy manage-
ment, much remains to be done for the complete proper solution of this concept, due
to the several contingencies to be solved that compromise the power quality in this
weak grids. Among that quality issues, this document has covered one of the most
important one, concerning the effect of active power transients in the network. This
Chapter conclude the carried study with the discussion of the reached results and
future work.

6.1   Conclusions

The transient frequency drift compensation has been the major concern in the scope
of this master thesis. In order to accomplish this contingency study, the problem
has been presented and a possible solution has been proposed and developed in an
experimental setup, following several steps. The covered points and conclusions are
stated below.

- First of all, the problem has been identified and the current studies and litera-
  ture related with the topic has been reviewed.

- Secondly, a possible solution for transient frequency drift compensation based
  on ESS has been proposed. Thus, both the power topology and its associated

control scheme has been defined, including the modelling of the test micro-grid and the system has been simulated using the parameters available in the experimental setup devices in order to analyse the performance under the same conditions that were given in the experimental tests

- Different control strategies for the frequency compensation has been proposed and analysed, obtaining their advantages and limitations, concluding that simple methods as P regulator offers a limited performance for this application while the methods that include differentiators could be too sensitive to noise in the real implementation. Considering that, the use of external information for controlling, as DID with load current measurements, seems to be the preferred option for future developments.

- The use of Interleaved DC/DC converter for the interface of the ESS has been proposed and analysed in simulation and experimental prototype as an enhance topology for ripple reduction in battery currents.

- The method for the grid frequency estimation has been discussed, proposing the analysis of PLL and FLL, as well as modification of those, in order to reach a proper performance in future developments.

- Some methods has been proposed for the detection of the frequency transient in order to improve the performance during steady state, including methods for the steady state frequency command estimation. This methods has been tested offline using information from experimental results.

- The designed system has been constructed and implemented in a laboratory experimental setup obtaining experimental results to verify the suitability of the proposed solution. The implemented system includes the design and building of the power converter and the developing of its associated control system in a TMS320F28335 control card.

- An alternative for the substitution of battery in the system has been design

and construct, based on a 3-phase rectifier with braking resistance, allowing the bidirectional power flow.

In this stage, all the proposed objectives of the Thesis have been covered, having a experimental prototype able to compensate transient frequency drifts.

6.2   Future work

The obtained results, both simulation and experimental, have proved the validity of the proposed system for transient frequency drift compensation. Nevertheless, several points are still to be covered in the topic.

On the one hand the most remarkable ones are the detection of the transients, in order to avoid power injection during steady state, and the estimation of the grid frequency steady state command in order to assert that the compensator control has the correct frequency reference. For this issue, although they have not been implemented online in the experimental control, some methods has been already presented testing their behaviour using the experimental results as ideas to be developed in the future work. The method for proper estimation of grid frequency for its use in the controller also presents a problem to be solve in future developments.

On the other hand, the control strategies should be further analysed in order to improved the solutions proposed in this study. Then, the look for of advanced control strategies is proposed as a future development. One of the most promising ideas is the estimation of grid parameters, that might contribute to the system performance. Such parameters, as the grid impedance or inertia could by obtained by enhance control methods based on Luenberger's observers combined with signal injection techniques. These methods not only allow to estimate the unknown parameters but also to reduce the number of sensors in the system reducing it cost and increasing its reliability. The preliminary use of that idea has already being studied in the scope of this Master's Thesis and is presented in a conference paper attached to Appendix C, in which the experimental setup designed in this Thesis has been used for obtaining the experimental results.

Appendix A

Graphic description of the experimental setup
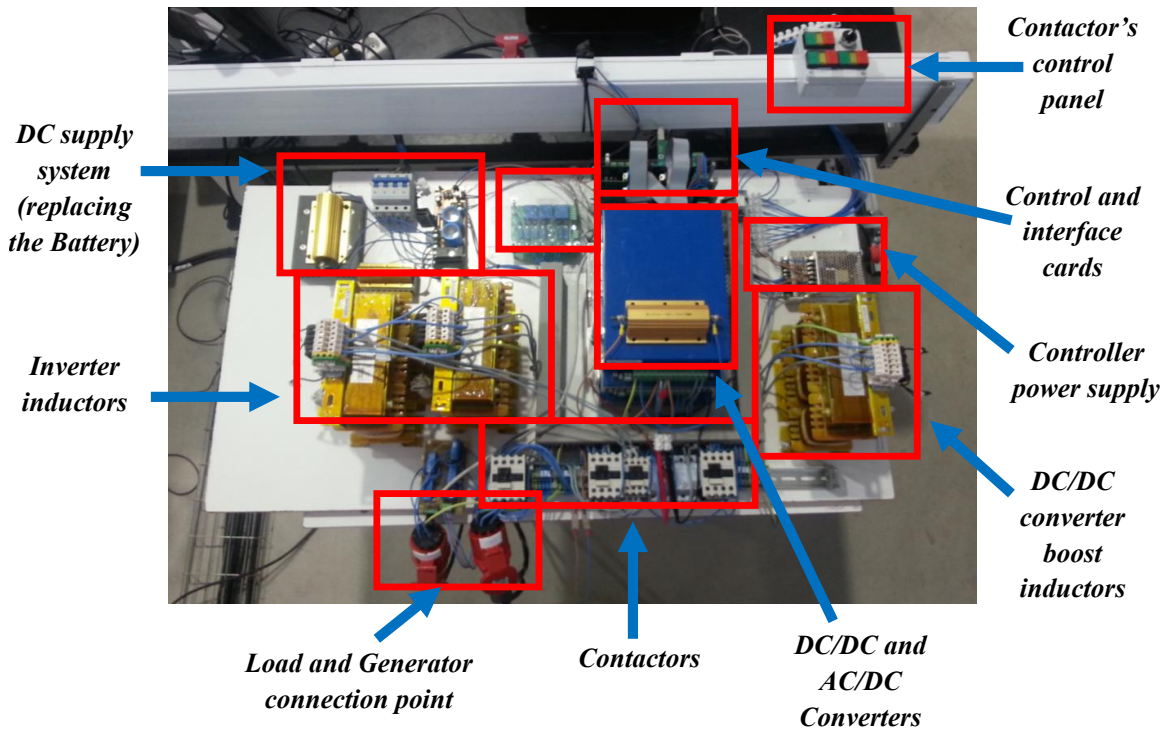
Figure A-1: Experimental setup top view.
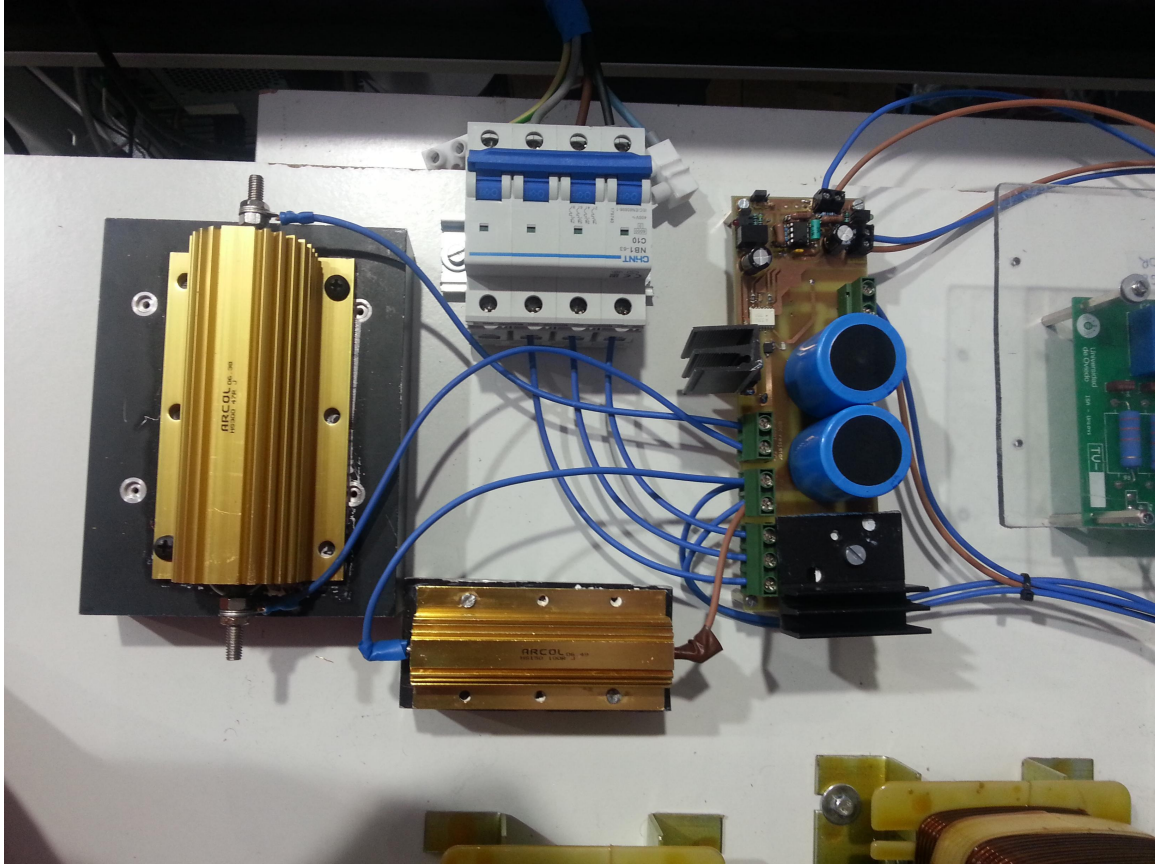
Figure A-2: DC supply system (rectifier with braking system). Replacing the battery in the system.
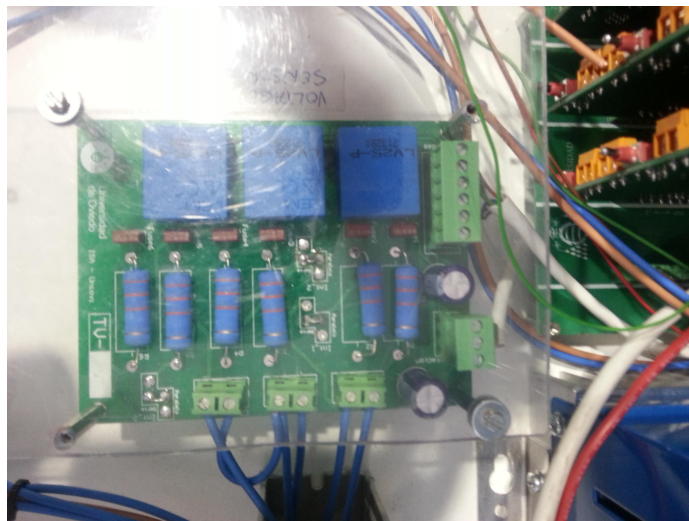
Figure A-3: External voltage sensors.

Figure A-4: External current sensors.

Figure A-5: 3-phase inverter inductors (RL fiter)
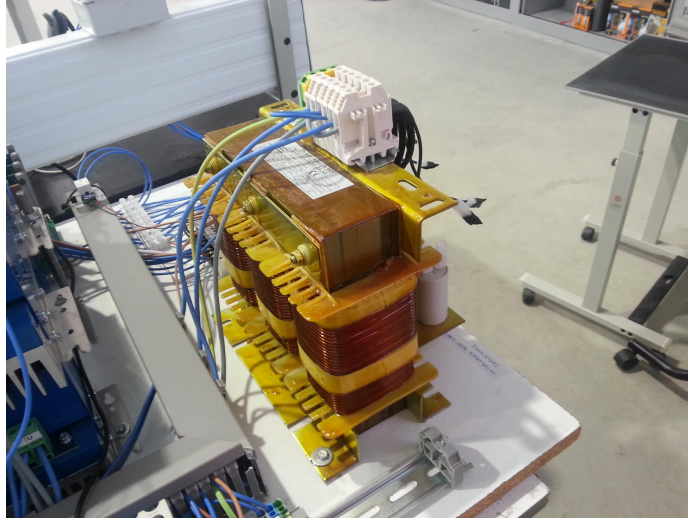
Figure A-6: Interleaved DC/DC converter boost inductors
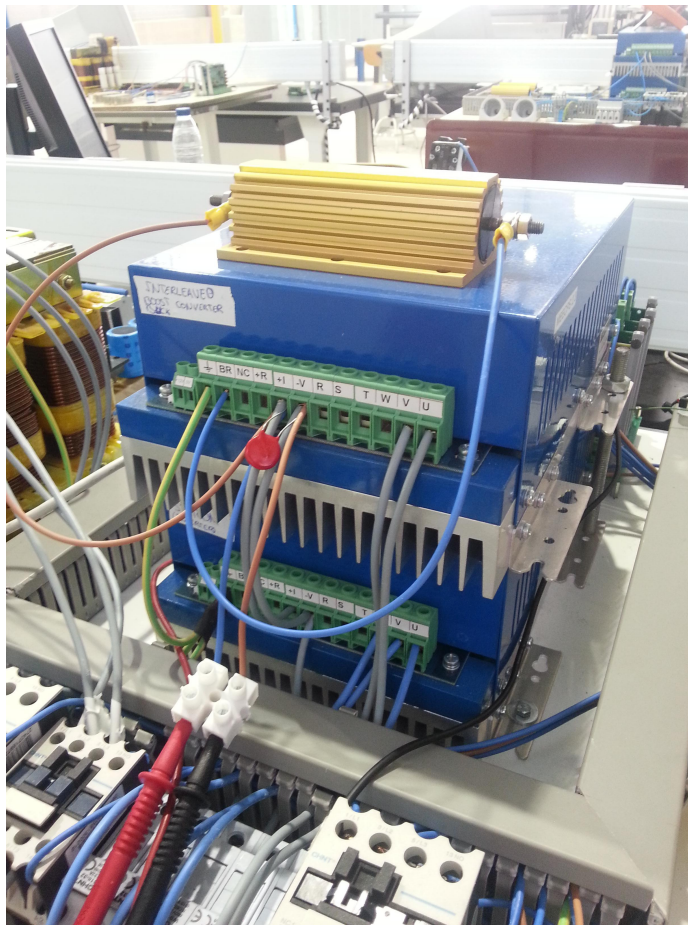
Figure A-7: Interleaved DC/DC bidirectional converter (upper) and 3-phase inverter (lower). Guasch manufacturer.
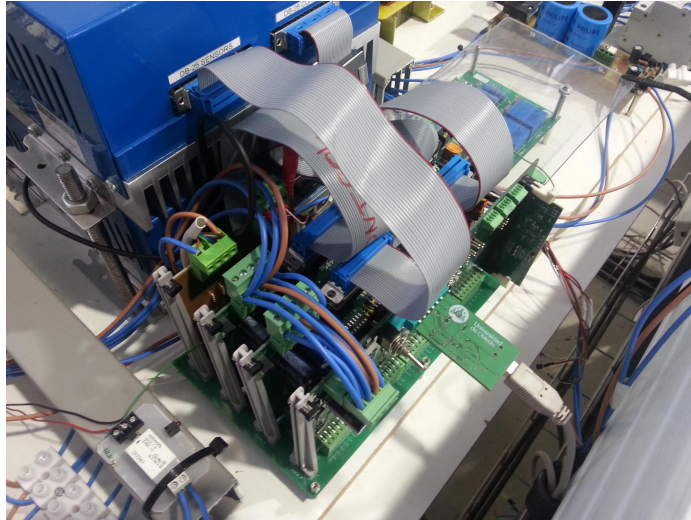
Figure A-8: Control cards and interface with the converters.
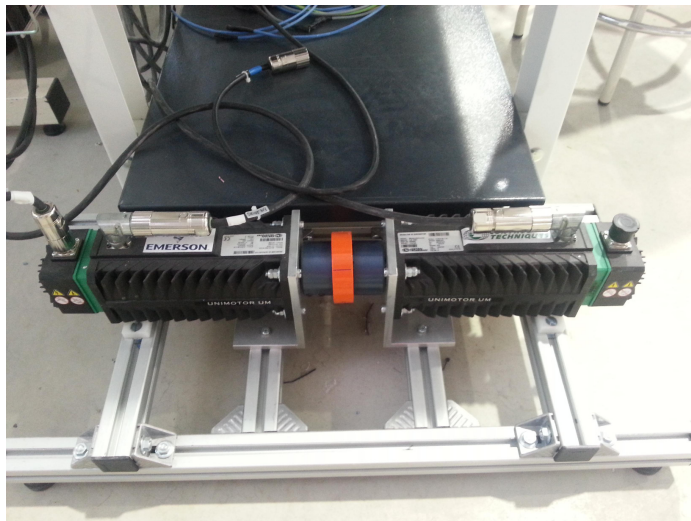
Figure A-9: PM motor-generator set, behaving as a weak grid.

Figure A-10: Commercial drive for prime mover motor speed control.

Figure A-11: 3-phase resistive load (active load).

Appendix B

Summary of Simulation and Experimental setup parameters

Table B.1: Control System Parameters

Parameter	Value	Description
BW_{Vdc}	5Hz	DC link control BW
Kp_{Vdc}	1	Proportional gain of DC link control
Ki_{Vdc}	175	Integral gain of DC link control
BW_{inv}	400Hz	Inverter current controller BW
Kp_{inv}	36.1	Proportional gain of inverter current control
Ki_{inv}	15.45	Integral gain of inverter current control
BW_{inter}	300Hz	DC/DC converter current control BW
Kp_{inter}	13.53	Proportional gain of DC/DC converter current control
Ki_{inter}	13.9276	Integral gain of DC/DC converter current control

Table B.2: Generator parameters

Parameter	Value	Description
P	3	Pole pairs
J	0.0039 $kg*m^2$	Generator inertia
b	0.02 Nms	Generator viscous friction
K_T	1.14 Nm	Torque constant
K_e	98 V/krmp	Generator back emf constant
L_{gen}	6 mH	Generator inductance
R_{gen}	2.1 Ω	Stator resistance
BW_{gen}	8 Hz	Governor speed control BW

Table B.3: Power System Parameters

Parameter	Value	Description
V_{grid}	98 V	Nominal grid phase to phase voltage in rms
f_{grid}	50 Hz	Nominal Battery voltage
V_{Batt}	140 V	Nominal Battery voltage
V_{DC}	300 V	Controlled DC link voltage
C_{DC}	2 mF	DC link equivalent capacitance
R_{inv}	0.2 Ω	Inverter RL filter resistance
L_{inv}	14.4 mH	Inverter RL filter inductance
R_{inter}	0.1 Ω	DC/DC converter resistance
L_{inter}	7.18 mH	DC/DC converter boost inductance
f_{sw}	10 KHz	switching frequency for both converters
R_{load}	32 Ω	3-phase resistor as used load (250W at nominal voltage)

Appendix C

Conference paper on future work application in the scope of this Thesis: Low Frequency Signal Injection for Grid Impedance Estimation in Three Phase Systems

Low Frequency Signal Injection for Grid Impedance Estimation in Three Phase Systems

Pablo García, Juan M. Guerrero, Jorge García,
Ángel Navarro-Rodríguez
Dept.of Elec., Computer & System Engineering
University of Oviedo
Gijón, 33204, Spain
Email: garciafpablo@uniovi.es, guerrero@uniovi.es,
garciajorge@uniovi.es, angelnr23@gmail.com

Mark Sumner
Department of Electrical and Electronic Engineering
The University of Nottingham
Nottingham, NG7 2RD, UK
Email: Mark.Sumner@nottingham.ac.uk

Abstract—This paper deals with the estimation and decoupling of grid impedance and LCL filter parameters variation using signal injection techniques and Luenberger type observer. When integrating a power converter in the AC grid as an interface for any Distributed Generation Systems (DGS) or other grid quality compensator like Active Power Filters (APF) or STATCOM, inner control loop normally requires current control. Current controller performance is greatly affected by the filter and grid impedance values. Although normally the filter impedance dominates the dynamics of the current controller, in weak networks the impedance of the grid can not be neglected. Additionally, other often required functions, as islanding detection, also rely on the estimation of the grid impedance. For this paper, a Luenberger based observer is proposed for controlling the grid current when a LCL filter is used. The proposed method will rely on measuring the converter side current and the grid voltage and will cope with parameter variation at the filter transfer function. For variations at the grid impedance, the control action deliver by the observer feedback path will be used for triggering an injection mechanism. A Low Frequency Signal Injection (LFSI) approach is proposed for online estimating the grid impedance using an RLS algorithm. The proposed estimation technique is well suited to be incorporated into an adaptive current controller scheme.

I. INTRODUCTION

Use of Voltage Source Converters (VSC) interfaced to the AC grid requires to control the current deliver to the grid. In order to accurately design the current controller, it is critical to understand the existing dynamic model between the applied converter output voltage and the resulting grid current. The dynamic model will affect in different ways the performance, depending on the used sensors and the filter used for the connection of the converter to the grid. When using a LCL filter for the interface, there exist multiple options for the placement of the current and voltage sensors, each of those with their advantages and drawbacks [1], [2]. When the control of the AC voltage at the output of the converter is needed, it is

usual to measure the voltage at the filter capacitor. However, this will make the current controller dependent on the grid side impedance. The variation is effectively decoupled by moving the voltage sensor to the Point of Common Coupling (PCC), but then the capacitor voltage/current needs to be estimated in order to damp the current controller. The issue is more critical when interfacing the power converter to weak networks having a non negligible grid impedance, thus affecting the total output impedance. In order to overcome this problem there are two different alternatives: 1) to force the known output filter to be the dominant dynamic system in any grid situation by implementing passive/active damping or virtual impedance techniques [3], [4] and, 2) to implement and adaptive current controller [5], [6] which parameters change depending on the grid impedance.

For this second option, it is needed to online estimate the grid impedance and the variations at the LCL filter parameters. Impedance estimation could be implemented using two different approaches: 1) model based techniques and, 2) signal injection based techniques. Model based techniques, use the transfer function between the applied voltage and the current for estimating the parameters. In [7], the use of the resonance of a LCL filter is proposed in order to make the estimation. As commented by the authors, the principal issue of this technique is the existence of two resonance peaks when passive reactive power compensation is added at the Point of Common Coupling (PCC).

Signal injection based methods use an additional excitation in order to track the response of the system [8]–[11]. For the signal excitation, several approaches can be followed. 1) High Frequency Signal Injection (HFSI) [10]–[13], 2) current regulator reaction [11], 3) Low Frequency Signal Injection (LFSI) [14], [15]. 1) and 2) are based on the same physical explanation. When injecting a voltage at a given high frequency, the resulting current includes a component at that frequency. By analyzing those current components, it is possible to obtain the impedance. However, there are some issues with this high frequency injection techniques: 1) selection of the high frequency must be done by asserting that the reaction of any APF connected to the same PCC is not removing the high

$$\frac{d}{dt}\mathbf{x} = \begin{pmatrix} -R_1^x/L_1^x & \omega_e & -1/L_1^x & 0 & 0 & 0 \\ -\omega_e & -R_1^y/L_1^y & 0 & -1/L_1^y & 0 & 0 \\ 1/C & 0 & 0 & \omega_e & -1/C & 0 \\ 0 & 1/C & -\omega_e & 0 & 0 & -1/C \\ 0 & 0 & 1/L_2^x & 0 & -R_2^x/L_2^x & 0 \\ 0 & 0 & 0 & 1/L_2^y & 0 & -R_2^y/L_2^y \end{pmatrix} \cdot \mathbf{x} + \begin{pmatrix} 1/L_1^x & 0 & 0 & 0 \\ 0 & 1/L_1^y & 0 & 0 \\ 0 & 0 & 0 & 0 \\ 0 & 0 & 0 & 0 \\ 0 & 0 & -1/L_2^x & 0 \\ 0 & 0 & 0 & -1/L_2^y \end{pmatrix} \cdot \mathbf{u}$$

$$(1)$$

frequency current harmonic; 2) the estimated impedance is not the transient impedance, which is the one needed for tuning the current regulator, but the impedance at the injection frequency.

In order to overcome the aforementioned problems, in this paper a mixed strategy based on an observer and LFSI is proposed. By one side, a Luenberger style observer will be used for controlling the grid current with a reduced number of sensors. By the other, the proposed LFSI, consisting on the injection of a pulse aligned with the zero crossing of each three phase voltages, will allow to detect changes at the grid impedance. The pulse is open loop injected by modifying the voltage command delivered by the current controller. In order to reduce the disturbance in the grid, injection of the pulse is restricted to those time intervals in which a change in the grid impedance is detected by the observer. Errors in the feedback path of the observer are proposed to trigger the signal injection mechanism.

When compared with HFSI, the following differences are found: 1) the estimation of the grid transient impedance could be directly obtained, whereas when using the high frequency signal injection just the impedance at a given frequency is estimated; 2) the LFSI is more rich in harmonic content. This could help in reducing the impact of any APF connected in parallel with the converter injecting the low frequency signal; 3) signal processing is more complicated with the LFSI. In the case of HFSI, the estimation could be directly estimated from the isolated components at the injection frequency. Isolating the components just require the use of band-pass or low-pass filters in the stationary or carrier signal frequency respectively. For the LFSI, a model approach estimation based on Recursive Least Square (RLS) method is used. However, there is no need for any additional filter stage; 4) HFSI is affected by the transients in the fundamental current, being quite challenging to remove the transient harmonics using digital filters. In [16], the use of a fundamental current observer is proposed in order to mitigate the effect. On the contrary, using the proposed LFSI, fundamental transient currents could also be used for the impedance estimation.

The paper is organized at follows. Section II explains the state space model of the LCL filter and grid impedance, the design of the observer and the digital implementation of the control system. Section III shows the injection mechanism, including the selection of the injection pulse and Section IV the RLS adaptive procedure used for the grid impedance estimation. Finally, simulation and experimental results are shown at Section V.

II. SYSTEM MODELING AND CONTROL

This section describes the system modeling in a generic reference frame as well as the theoretical background for the implemented control. It also includes the details for the digital implementation of the designed Luenberger observer.

A. System modeling

The state space representation of a LCL filter (Fig. 1) in an arbitrary reference frame is given by (1), where $\mathbf{x} = [\mathbf{i}_i, \mathbf{v}_c, \mathbf{i}_g]^T$ is the state vector and $\mathbf{u} = [\mathbf{v}_i, \mathbf{v}_g]^T$ the input vector. Also note that each component at the state and input vectors is a complex variable with two elements; the real and imaginary components, i.e $\mathbf{v} = (v_x, v_y)$. Equation (1) could be particularized for the stationary (α, β) or to the synchronous (d, q) references frames by making $\omega_e = 0$ or $\omega_e = \omega_{grid}$ respectively. An alternative representation of (1), separating the x and y terms, is shown at (2), (3) and in compact form at (4), (5). That form will be used for an easier digital implementation of the observer structure. Finally, the corresponding block diagram representation in compact complex notation is shown at Fig. 2.
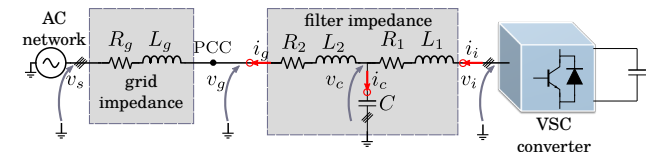

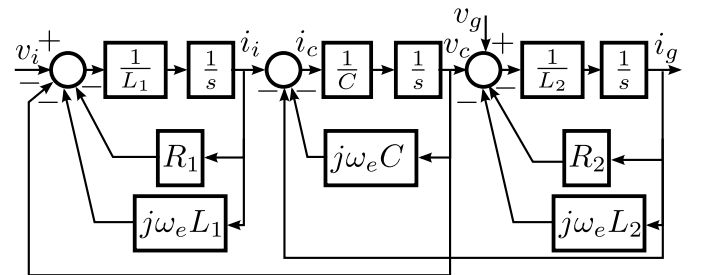Fig. 1. Connection of the LCL filter to the output of the VSC converter.

Fig. 2. LCL filter block diagram in state space form.

$$\frac{d}{dt}\mathbf{x}_x = \begin{pmatrix} -R_1/L_1 & -1/L_1 & 0 \\ 1/C & 0 & -1/C \\ 0 & 1/L_2 & -R_2/L_2 \end{pmatrix}_x \cdot \mathbf{x}_x$$
$$+ \omega_e \begin{pmatrix} 1 & 0 & 0 \\ 0 & 1 & 0 \\ 0 & 0 & 1 \end{pmatrix} \cdot \mathbf{x}_y + \begin{pmatrix} 1/L_1 & 0 \\ 0 & 0 \\ 0 & -1/L_2 \end{pmatrix}_x \cdot \mathbf{u}_x \tag{2}$$

$$\frac{d}{dt}\mathbf{x}_y = \begin{pmatrix} -R_1/L_1 & -1/L_1 & 0 \\ 1/C & 0 & -1/C \\ 0 & 1/L_2 & -R_2/L_2 \end{pmatrix}_y \cdot \mathbf{x}_y$$
$$- \omega_e \begin{pmatrix} 1 & 0 & 0 \\ 0 & 1 & 0 \\ 0 & 0 & 1 \end{pmatrix} \cdot \mathbf{x}_x + \begin{pmatrix} 1/L_1 & 0 \\ 0 & 0 \\ 0 & -1/L_2 \end{pmatrix}_y \cdot \mathbf{u}_y \tag{3}$$

$$\frac{d}{dt}\mathbf{x}_x = \mathbf{A}_x \cdot \mathbf{x}_x + \omega_e \mathbf{I} \cdot \mathbf{x}_y + \mathbf{B}_x \cdot \mathbf{u}_x \tag{4}$$
$$\frac{d}{dt}\mathbf{x}_y = \mathbf{A}_y \cdot \mathbf{x}_y - \omega_e \mathbf{I} \cdot \mathbf{x}_x + \mathbf{B}_y \cdot \mathbf{u}_y \tag{5}$$

B. Control implementation

The superior filtering performance of the LCL structure when compared to the L or LC alternatives has also important shortcomings in the design of the current controller [17]. This situation is even worsen when harmonic compensation is considered [18]. Current control for a LCL filter is a challenging task due to the resonance appearing between the capacitor and the inductances and normally an attenuation method is needed. The basic idea is to compensate or attenuate the capacitor current within the bandwidth of the current controller, but still keeping the filtering capability for frequencies at and above the switching frequency.

In the literature there are several alternatives which can be separated into passive and active damping techniques. By one side, passive damping techniques require the use of additional passive elements, such a series or parallel resistances which increase the system losses [17]. By the other, active damping methods often needs for additional current or voltage sensors. Lately, some publications have addressed the implementation of active damping methods which do not need any for extra elements [2], [19]–[24]. The methods in that group could be separated in those which require to estimate the capacitor current or the inductance voltage, thus relying on calculating derivatives which are normally noisy or require the use of complicated control algorithms. More appealing because of their simplicity are those methods relying on digital filtering of the control signal in order not to react at the resonance frequency. However, often the bandwidth of the current controller must be decreased.

For this paper, an structure based on a Luenberger type observer is proposed [25]. The proposed system will control the grid side current by using the converter side current sensors and the voltage sensors at the PCC as the solely sensing elements. This configuration has some advantages in terms of 1) costs, only the current sensors usually provided

by the power stage need to be used; 2) safety, the current sensors on the converter side are also suitable for protection of the power stage; 3) performance, PCC voltage measurement allows for measuring and decoupling the effects of a varying grid impedance but also to real power factor measurement and; 4), reliability as a reduced number of sensors reduces the fault probability.

The proposed observer and current control block diagram are shown at Fig 3. The control system works as follows. The estimated values for the converter side inductance ($\widehat{L}_1$), filter capacitor ($\widehat{C}$) and grid side inductance ($\widehat{L}_2$) are used for building the dynamic model previously shown in (1). Inputs to the observer are the commanded voltage from the converter (v_i^{ff}) and the measured converter side current (i_i). The estimated capacitor current ($\widehat{i}_c$) is obtained from the difference of the measured converter side current and the estimated grid current ($\widehat{i}_g$). $\widehat{i}_c$ is later used at the output of the current controller to implement the active damping mechanism and $\widehat{i}_g$ is used as the feedback signal for the current controller. The feedback path of the observer is generated from the estimation error of the converter side current ($e_i = i_i - \widehat{i}_i$). The error signal is the input to the observer controller (C_o) which, depending on the reference frame of the implementation, will be a PI (synchronous reference frame) or a PR for the stationary reference frame. The output of the feedback path (v_i^{fb}) is added to the feedforward value to the commanded voltage in order to compensate for any unknown in the system. The feedback voltage will also be used for triggering the low frequency pulse injection. Finally, for the current controller implementation (C_i), PI or PR structures are used depending on the selected reference frame. The active damping term and the measured PCC voltage are after added in order to damp the oscillations and to effectively reject the effects on the grid current due to any change in the grid impedance.

C. Digital control implementation

For the online implementation, the Luenberger observer and the current controller designs must be translated to the digital domain. The Luenberger observer is discretized using the Euler approximation, as shown in (6), (7), where $[k]$ corresponds to the actual sample time, $[k-1]$ to the previous one and T_s is the sample time. It is worth noting than even if here the matrix formulation is shown for the sake of simplicity, the discrete observer equations can be implemented in scalar form, more suitable for the online implementation.

$$\mathbf{x}_x[k] = (\mathbf{I} - T_s\mathbf{A}_x)^{-1} \cdot (\mathbf{x}_x[k-1] + T_s\mathbf{B}_x \cdot \mathbf{u}_x[k])$$
$$+ T_s\omega_e\mathbf{I} \cdot \mathbf{x}_y[k-1] \tag{6}$$
$$\mathbf{x}_y[k] = (\mathbf{I} - T_s\mathbf{A}_y)^{-1} \cdot (\mathbf{x}_y[k-1] + T_s\mathbf{B}_y \cdot \mathbf{u}_y[k])$$
$$- T_s\omega_e\mathbf{I} \cdot \mathbf{x}_x[k-1] \tag{7}$$

For the controller discretization, Tustin approximation is used. PI or PR structures are used depending on performing the implementation at the synchronous or the stationary reference frame respectively.
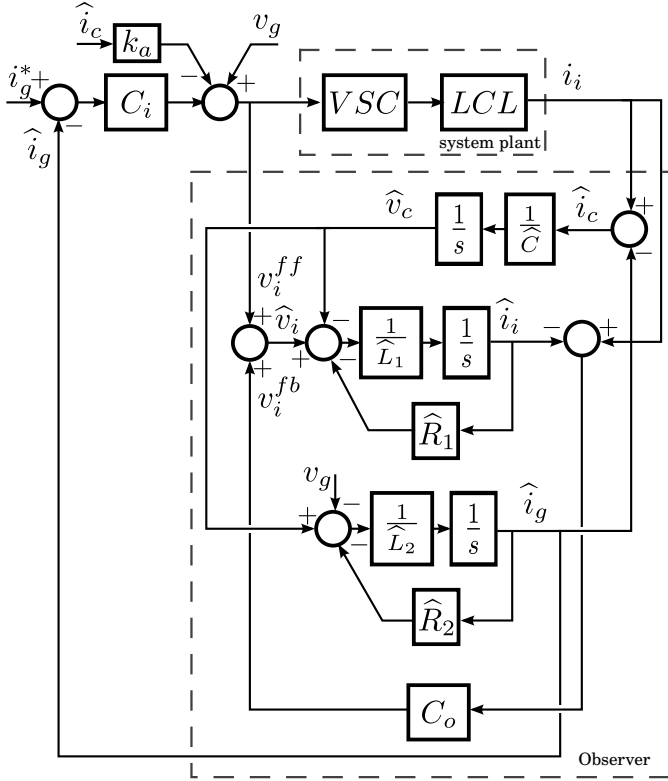
Fig. 3. Proposed observer structure in an arbitrary reference frame.

The observer performance, at the synchronous reference frame, is shown at Fig. 4 when the estimated LCL filter parameters match the real ones. As shown, the grid current is correctly tracked.
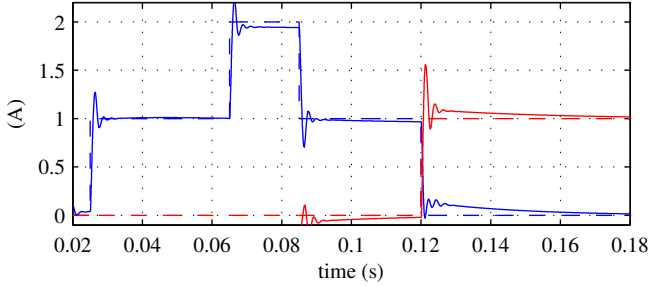

Fig. 4. Transient response for the presented observer structure in digital form.

III. LOW FREQUENCY SIGNAL INJECTION

For the LFSI, there are different alternatives and parameters which can be adjusted. As represented in Fig. 5, the signal is injected centered at the zero crossing of the phase to neutral voltages. Zero crossing is detected by using the calculated phase from the PLL used for grid synchronization. This point has been selected in order to minimize the voltage distortion, as demonstrated later in the discussion.

At this paper, three different alternatives for the pulse injection are investigated, the first two are implemented at the abc reference frame, while the third one is at the dq reference frame. The pulses are injected as a duty modifications to the output of the current controller and, during the pulse injection, the fundamental voltage command is disabled for the case of the abc injection (see Fig. 6) whereas is just an addition when implemented in the dq reference frame. This will enable both a sharper excitation but also a quite simple implementation of the signal injection. As seen in Fig. 5, both the pulse width and the magnitude can be changed. As wider is the pulse and as larger the magnitude, the bigger the disturbance delivered to the system would be. Obviously, increased disturbance values will help in the estimation procedure, but also will increase the THD of the resulting currents. For this paper, the values shown in Table I have been used. Resulting waveforms for the inverter commands and the applied voltages are shown at Fig. 7 whereas the corresponding currents at the synchronous reference frame are shown at Fig. 8. The three tested alternatives are following described:

1) **Method#1**. Pulse width is established to the desired value and the the magnitude is set to zero. Under that condition, the fundamental voltage command is clamped to zero during the pulse injection time. The implementation of this strategy is straightforward, since it is just a multiplication of the duty commands times a time window set to zero during the pulse duration. When translating to the dq reference frame, even if the pulse is mostly at the q axis, both components are modified. The pulses are transformed to a triangular shape at the q axis and the resulting current has a sinusoidal waveform.

2) **Method#2**. Fundamental command is hold at the corresponding value at the beginning of the pulse injection and when the phase crosses the zero is changed to the opposite value. Transformed to the dq reference frame, d component is also modified, although in a less noticeable way than for Method#1. The pulses at the q axis are also transformed to a triangular shape, but the resulting current has a triangular waveform of opposite phase when compared to previous method.

3) **Method#3**. When looking at the pulse result in the dq reference frame for both Method#1 and Method#2, the resulting excitation is affecting the d and q axis and, even if the pulse is an stepwise in the abc reference frame, is having a triangular form on the dq reference frame. Because the RLS algorithm will be implemented in the synchronous reference frame, it is desirable to have an step shape in that reference. This could be easily achieved by using the same strategy than for Method#2 but injecting the pulses directly in the synchronous reference frame at the q axis.

It must be remarked that all pulse injection strategies share the fact that the applied distortion to the voltage command is symmetrical, thus resulting in the voltage average error being zero. Selecting one or the other is based on the sensitivity of the current response and on the implementation burden. For this paper, Method#3 is considered because of the advantages

enumerated before.

Previous simulation results were showing the injection mechanism with the system in open loop, however the power converter will operate under current control and the pulses injection will be seen as a disturbance for the current controller. In the case the current regulator reaction is too fast, the pulses will be removed from the excitation and the estimation could not be implemented. Experimental results of the system operating under close loop with a $200Hz$ bandwidth are shown at Fig. 9. It is clear that even under close loop operation the pulses appear on the grid voltage and thus could potentially be used for the RLS estimation.
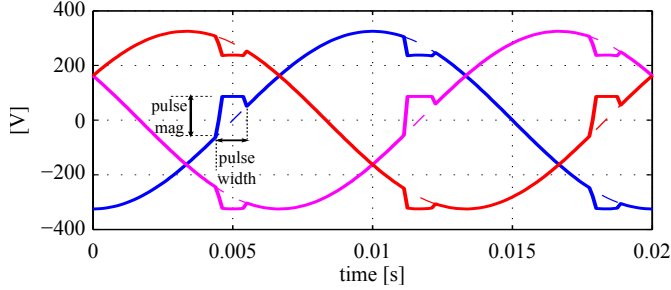

Fig. 5. LFSI pulse generation. Both magnitude and phase can be independently changed. The magnitude has been deliberately increased for illustration purposes.
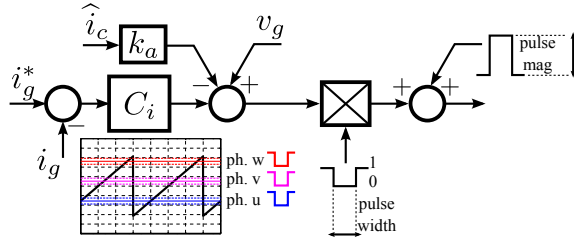

Fig. 6. LFSI implementation. The injection is synchronized and centered with respect to the grid voltage zero crossing and the fundamental voltage command is blanked during the injection time. Dashed lines show the starting and end of each phase pulse and bold ones the zero crossing of the respective phase.

IV. RLS ALGORITHM IMPLEMENTATION

In order to obtain the grid impedance parameters, an estimation procedure needs to be implemented. In the literature there are mainly two approaches. To calculate the impedance as the quotient of the injected voltage and the resulting current [10] or to use an observer or an estimator [13]. In this paper, the estimation of the system parameters is done by using a RLS approach [26]. For that, the dynamic equation of the grid impedance in the synchronous reference frame as seen from the converter is first discretized using Euler method.

The matrix equation of a three phase RL load in the synchronous reference frame, after decoupling the cross coupling terms, is given by (8). Where $\mathbf{v}_{RL}$ is the vector voltage drop across the impedance, $\mathbf{v}_g$ the PCC voltage vector, $\mathbf{v}_s$ the grid voltage vector, and $\mathbf{i}_g$ the grid current vector. $\mathbf{L}$ and $\mathbf{R}$ are, respectively, the inductance and resistance matrices.
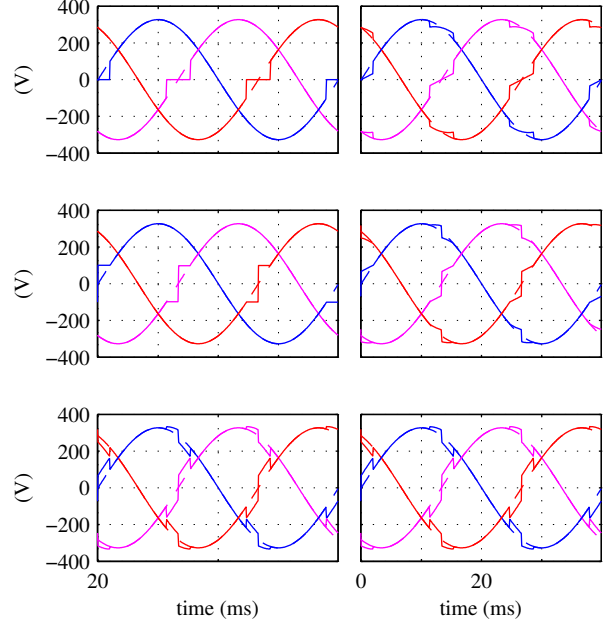
Fig. 7. LFSI waveforms for the three proposed methods in the abc reference frame. From top to bottom, Method#1, Method#2 and Method#3. Left column shows the generated phase voltage command and right column the phase to neutral voltages. Dashed lines show the signals when the pulse injection is disabled.

$$\mathbf{v}_{RL} = \mathbf{v}_g - \mathbf{v}_s = \mathbf{R}\mathbf{i}_g + \mathbf{L}\frac{d\mathbf{i}_g}{dt}. \quad (8)$$

When calculating the discrete approximation using Euler method with a sampling period T_s, equation (9) is obtained.

$$\mathbf{i}_g[k] = \mathbf{a_1}\mathbf{i}_g[k-1] + \mathbf{b_0}\left(\mathbf{v}_c[k] - \mathbf{v}_g[k]\right) \quad (9)$$

Where $\mathbf{a_1}$ and $\mathbf{b_0}$ are given by expression (10)

$$\mathbf{a_1} = \frac{\mathbf{L}}{\mathbf{R}T_s + \mathbf{L}}, \qquad \mathbf{b_0} = \frac{T_s}{\mathbf{R}T_s + \mathbf{L}} \quad (10)$$

From (10), the values for the resistance and inductance matrices can be obtained as (11) respectively.

$$\mathbf{R} = \frac{1 - \mathbf{a_1}}{\mathbf{b_0}}, \qquad \mathbf{L} = \frac{\mathbf{a_1}T_s}{\mathbf{b_0}} \quad (11)$$

It is worth noting that the above proposed model is valid for any balanced or unbalanced RL load. When the load is balanced, $\mathbf{a_1} = [a_{1d}, a_{1q}]$ components and $\mathbf{b_0} = [b_{0d}, b_{0q}]$ components will have the same value. For unbalanced loads, the resulting components will be different.

For the RLS implementation, the error between the measured and estimated current (12) is used to update the estimation. In order to decouple the effect of the unknown grid voltage, v_s, only the current generated by the pulses is used. This is done by subtracting from the overall current the reference of the fundamental current. It then assumed that the grid voltage at the pulse frequency is zero and
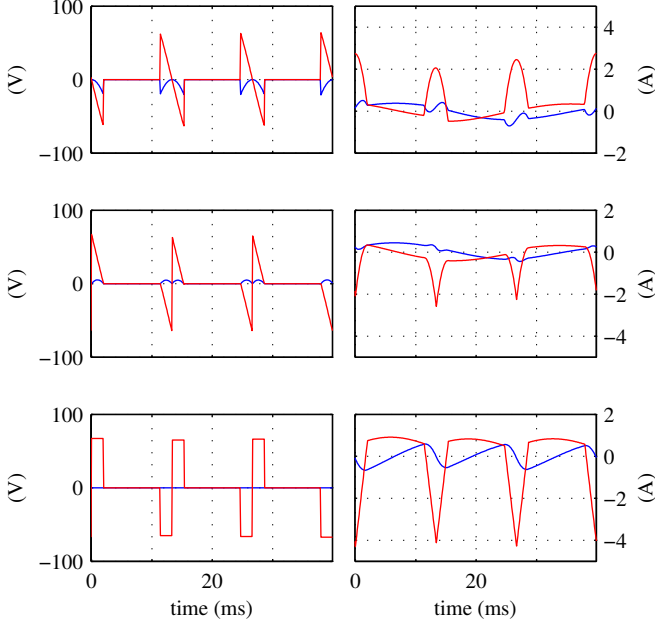
Fig. 8. LFSI waveforms for the three proposed methods in the dq reference frame. Fundamental component is removed in order to zoom on the high frequency components. From top to bottom, Method#1, Method#2 and Method#3.
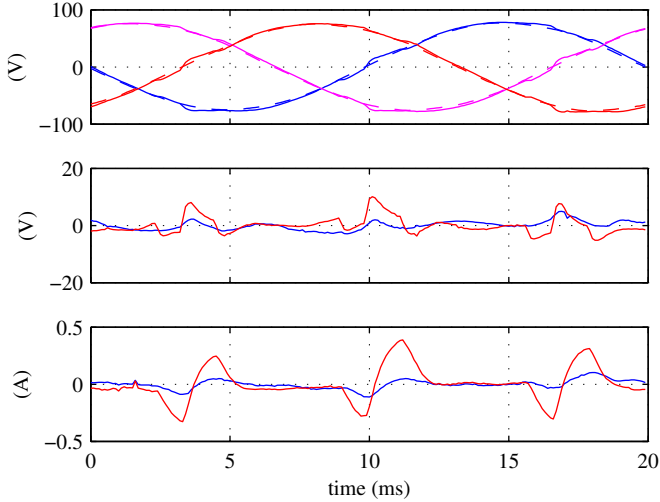

Fig. 9. Experimental results for Method#3. The system is operated in close loop with a bandwidth of $200Hz$. Filter capacitor is removed and current commands were set to zero. From top to bottom it is shown the phase to neutral voltages at the PCC, the voltage commands, and the grid currents at the synchronous reference frame. Blue color is used for the d component and red for the q.

thus could be removed from the estimation. The system equations are represented in state-space form by defining the state vector $\mathbf{X}_{[k]} = \left[\mathbf{i}_{g[k-1]}, \mathbf{v}_{g[k]}\right]^T$ and coefficients vector $\mathbf{W}_{[k]} = \left[\mathbf{a_1}_{[k]}, \mathbf{b_0}_{[k]}\right]$.

Nominal parameters	Value (Setup#1/Setup#2)
$r_1\ [\Omega]$	0.2/0.2
$r_2\ [\Omega]$	0.2/0.2
$L_1\ [mH]$	2.3/7
$L_2\ [mH]$	0.93/7
$C\ [\mu F]$	10/6
pulse mag. $[p.u]$	0.1/0
pulse width. $[ms]$	1/2
λ	0.998/0.8

$$\mathbf{e}_{[k]} = \mathbf{i}_{g[k]} - \widehat{\mathbf{i}}_{g[k]} \tag{12}$$

The least square problem is formulated in recursive form using the equations (13) - (16). $P_{(2x2)}$ is the covariance matrix and it is initialized to $P = 0.01 \begin{pmatrix} 1 & 0 \\ 0 & 1 \end{pmatrix}$, $g_{(2x1)}$ the adaptation gain and $\lambda = [0,1]$ is the forgetting factor, which need to be selected as a tradeoff of the expected estimation bandwidth and the signal to noise ratio. Frequently, values between 0.95 and 1 are selected. For this paper, the value shown in Table I has been selected. At each sample time, the estimation of the parameters $\mathbf{b_0}, \mathbf{a_1}$ is updated and a new estimation for $\mathbf{R}$ and $\mathbf{L}$ is obtained.

$$\alpha_{[k]} = \mathbf{i}_{[k]} - \mathbf{W}_{[k-1]} \cdot \mathbf{X}_{[k]} \tag{13}$$

$$g_{[k]} = P_{[k-1]} \cdot \mathbf{X}_{[k]} \cdot \left[\lambda + \mathbf{X}_{[k]}^T \cdot P_{[k-1]} \cdot \mathbf{X}_{[k]}\right]^{-1} \tag{14}$$

$$P_{[k]} = \lambda^{-1} \cdot P_{[k-1]} - g_{[k]} \cdot \mathbf{X}_{[k]}^T \lambda^{-1} \cdot P_{[k-1]} \tag{15}$$

$$\mathbf{W}_{[k]} = \mathbf{W}_{[k-1]} + \left(\alpha_{[k]} \cdot g_{[k]}\right)^T \tag{16}$$

V. SIMULATION AND EXPERIMENTAL RESULTS

For the simulation results, Simulink has been used for the implementation and Matlab for the analysis. All the simulation results were obtained using real time signal processing. The parameters' estimation and adaptation is continuously calculated at each simulation step. Fig. 10 shows a transient in the grid inductance from $7mH$ to $14mH$ and on the grid resistance from 0.2 to 0.25Ω. The figure shows the estimation of the inductance and resistance for a balanced grid, the modified voltages with the pulse injection and the estimated and real currents. As it can be seen, the parameter estimation converges in a fraction of a fundamental cycle. It is also shown that the resistance estimation drops before reaching the final value. Explanation for that behavior is related with a peak in the estimation of the a_1 coefficient. Still the problem is not too important due to the high convergence speed.

Initial experimental results were obtained using a PM15F42C power module from Triphase. The power modules is directly programmed from Simulink environment, thus allowing for easily test the simulation results. The power module is interfaced to the AC grid trough a LCL filter, which parameters are listed in Table I under Setup#1. In that table, the
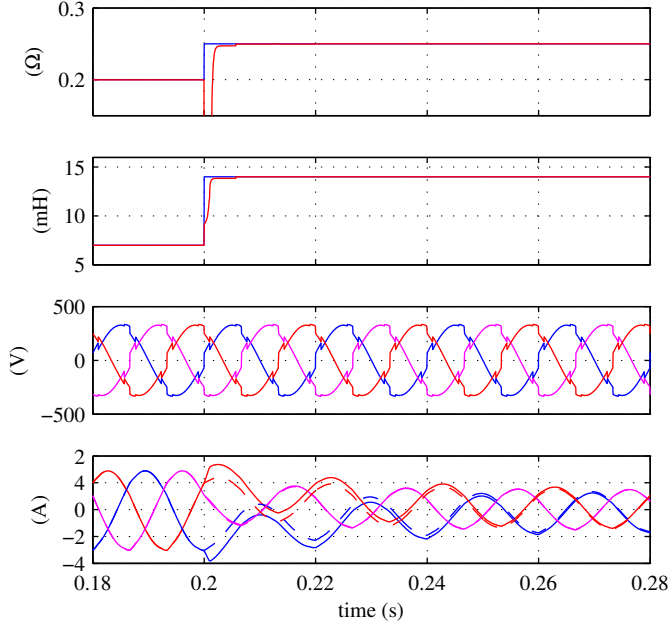
Fig. 10. Simulation results. Transient response. From top to bottom: a) resistance estimation, b) inductance estimation, c) applied voltages, d) resulting grid currents. Measured currents are shown in dashed lines, whereas estimated are in bold.

converter side inductance is L_1 and the grid side inductance L_2. An additional inductance of $L_l = 5mH$ has been placed in series after L_2 in order to simulate a weak network. During these experiments, grid impedance estimation using Method#1 were tested.

Fig. 11 shows the obtained waveforms and the corresponding currents during the experiments. By looking at the phase voltages it is clear that the pulse injection is working as expected.

Fig. 12 shows the estimated resistance and inductance during the experimental tests. By looking at the results, the inductance value is really well estimated (the sum of $L_1 + L_2 + L_l = 8.4mH$). The value of the obtained resistance seems to be too high when compared to the measured one (around 0.5Ω). A possible explanation could be the effect of the filter capacitance, which is reducing the amount of pulsating current reaching the grid side current sensor.

Additional experiments, including the online implementation of the observer, the development and testing of Method#3 and the RLS implementation in the synchronous reference frame have been taken using a MTL-CBI0010N12IXFE power stage from Rectificadores Guash and the control being implemented in a TMS320F28335 DSC from Texas Instruments. The details about the grid filter and pulse injection parameters are shown at Table I under Setup#2.

Experimental results for the the observer reference tracking capability are shown at Fig. 13. Fig. 14 shows the estimated and real currents using Method#3 for the pulse injection and RLS at the synchronous reference frame at steady state con-
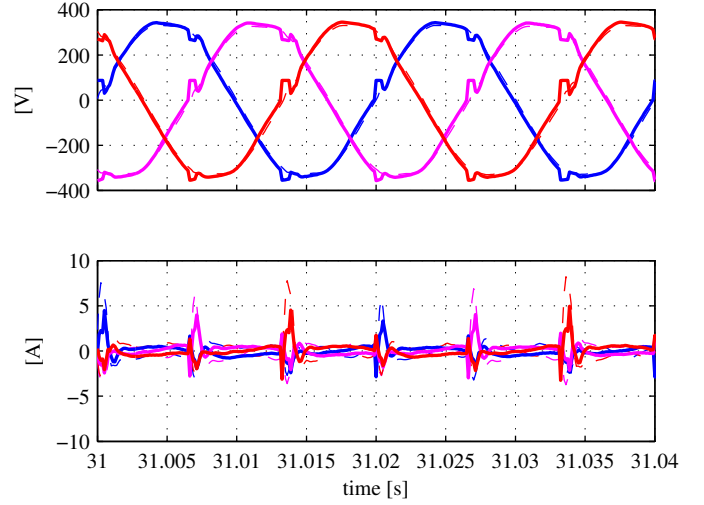
Fig. 11. Experimental results. a) LFSI and b) current response. Measured currents are shown in dashed lines and estimated in bold.
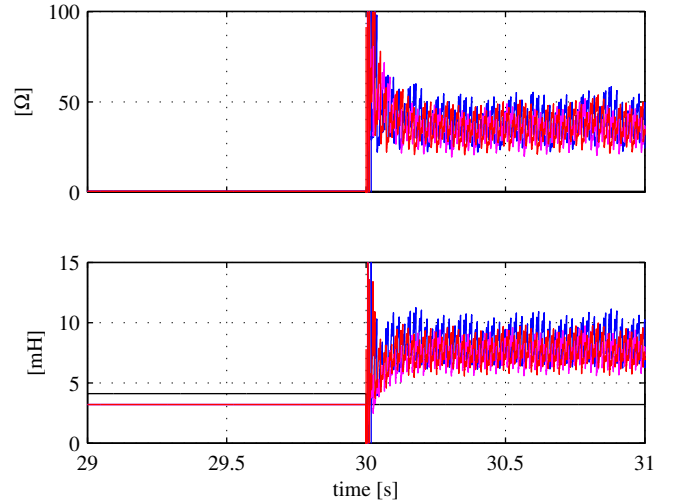
Fig. 12. Experimental results. Parameter estimation during a transient in the grid impedance. RLS estimation is enabled at $t = 30s$. a) Resistance estimation. b) Inductance estimation.

ditions. A good match between both components is obtained.

VI. CONCLUSION

Estimation of the grid impedance is a key factor for improving the performance in weak networks. This paper has proposed the use of a LFSI technique to online estimate the impedance with a moderate computational burden for online implementation. The proposed system is triggered from the error signal coming from a Luenberger observer used for the control of the grid current in a LCL filter. The proposed observer and the estimation method have been tested through simulation and experimental results. Different methods for the LFSI have been compared and an the injection in the
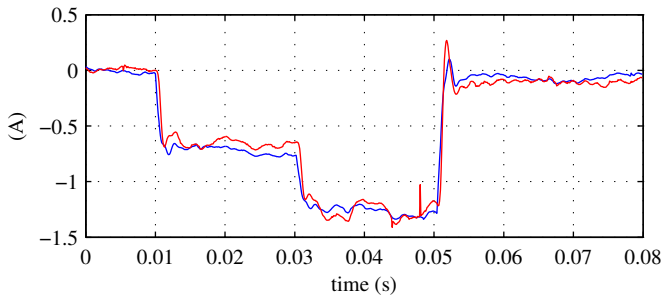
Fig. 13. Experimental results. Proposed observer working under different steps at the i_q component. Active damping gain $K_a = 10$.

Fig. 14. Experimental results. Estimation of i_d and i_q currents using RLS at the synchronous reference frame and pulse injection based on Method#3. The system was operated in close loop with both components having reference 0.

synchronous reference frame has been selected based on an increased sensitivity and reduced cross-coupling.

REFERENCES

[1] H. Xiao, X. Qu, S. Xie, and J. Xu, "Synthesis of active damping for grid-connected inverters with an LCL filter," in *2012 IEEE Energy Conversion Congress and Exposition (ECCE)*, Sep. 2012, pp. 550–556.

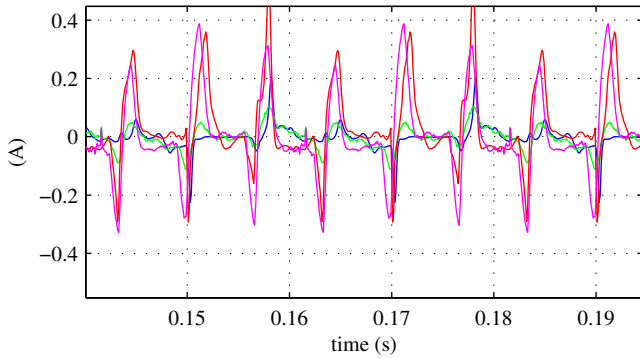[2] J. Xu, S. Xie, and T. Tang, "Active Damping-Based Control for Grid-Connected -Filtered Inverter With Injected Grid Current Feedback Only," *IEEE Transactions on Industrial Electronics*, vol. 61, no. 9, pp. 4746–4758, Sep. 2014.

[3] W. Yao, M. Chen, J. Matas, J. Guerrero, and Z.-m. Qian, "Design and Analysis of the Droop Control Method for Parallel Inverters Considering the Impact of the Complex Impedance on the Power Sharing," *IEEE Transactions on Industrial Electronics*, vol. 58, no. 2, pp. 576–588, 2011.

[4] J. He, Y. W. Li, J. Guerrero, F. Blaabjerg, and J. Vasquez, "An Islanding Microgrid Power Sharing Approach Using Enhanced Virtual Impedance Control Scheme," *IEEE Transactions on Power Electronics*, vol. 28, no. 11, pp. 5272–5282, 2013.

[5] M. Sumner, B. Palethorpe, and D. Thomas, "Impedance measurement for improved power quality-Part 2: a new technique for stand-alone active shunt filter control," *IEEE Transactions on Power Delivery*, vol. 19, no. 3, pp. 1457–1463, 2004.

[6] J. Massing, M. Stefanello, H. Grundling, and H. Pinheiro, "Adaptive Current Control for Grid-Connected Converters With LCL Filter," *IEEE Transactions on Industrial Electronics*, vol. 59, no. 12, pp. 4681–4693, 2012.

[7] M. Liserre, F. Blaabjerg, and R. Teodorescu, "Grid Impedance Estimation via Excitation of LCL -Filter Resonance," *IEEE Transactions on Industry Applications*, vol. 43, no. 5, pp. 1401–1407, 2007.

[8] D. Martin and E. Santi, "Auto tuning of digital deadbeat current controller for grid tied inverters using wide bandwidth impedance identification," in *2012 Twenty-Seventh Annual IEEE Applied Power Electronics Conference and Exposition (APEC)*, 2012, pp. 277–284.

[9] L. Asiminoaei, R. Teodorescu, F. Blaabjerg, and U. Borup, "A digital controlled PV-inverter with grid impedance estimation for ENS detection," *IEEE Transactions on Power Electronics*, vol. 20, no. 6, pp. 1480–1490, 2005.

[10] D. Reigosa, F. Briz, C. Charro, P. Garcia, and J. Guerrero, "Active Islanding Detection Using High-Frequency Signal Injection," *IEEE Transactions on Industry Applications*, vol. 48, no. 5, pp. 1588–1597, 2012.

[11] D. Reigosa, F. Briz, C. Blanco, P. Garcia, and J. Manuel Guerrero, "Active Islanding Detection for Multiple Parallel-Connected Inverter-Based Distributed Generators Using High-Frequency Signal Injection," *IEEE Transactions on Power Electronics*, vol. 29, no. 3, pp. 1192–1199, 2014.

[12] M. Sumner, B. Palethorpe, and D. Thomas, "Impedance measurement for improved power quality-Part 1: the measurement technique," *IEEE Transactions on Power Delivery*, vol. 19, no. 3, pp. 1442–1448, 2004.

[13] N. Hoffmann and F. Fuchs, "Minimal Invasive Equivalent Grid Impedance Estimation in Inductive #x2013;Resistive Power Networks Using Extended Kalman Filter," *IEEE Transactions on Power Electronics*, vol. 29, no. 2, pp. 631–641, 2014.

[14] L. Asiminoaei, R. Teodorescu, F. Blaabjerg, and U. Borup, "Implementation and Test of an Online Embedded Grid Impedance Estimation Technique for PV Inverters," *IEEE Transactions on Industrial Electronics*, vol. 52, no. 4, pp. 1136–1144, 2005.

[15] A. Timbus, P. Rodriguez, R. Teodorescu, and M. Ciobotaru, "Line Impedance Estimation Using Active and Reactive Power Variations," in *IEEE Power Electronics Specialists Conference, 2007. PESC 2007*, 2007, pp. 1273–1279.

[16] F. Briz, A. Diez, and M. W. Degner, "Dynamic operation of carrier-signal-injection-based sensorless direct field-oriented AC drives," *IEEE Transactions on Industry Applications*, vol. 36, no. 5, pp. 1360–1368, Oct. 2000.

[17] M. Liserre, F. Blaabjerg, and S. Hansen, "Design and control of an LCL-filter-based three-phase active rectifier," *IEEE Transactions on Industry Applications*, vol. 41, no. 5, pp. 1281–1291, Sep. 2005.

[18] D. Wojciechowski, "Novel predictive control of 3-phase LCL-based active power filter," in *Compatibility and Power Electronics, 2009. CPE '09.*, May 2009, pp. 298–305.

[19] J. Dannehl, M. Liserre, and F. Fuchs, "Filter-Based Active Damping of Voltage Source Converters With Filter," *IEEE Transactions on Industrial Electronics*, vol. 58, no. 8, pp. 3623–3633, Aug. 2011.

[20] M. Liserre, A. Aquila, and F. Blaabjerg, "Genetic algorithm-based design of the active damping for an LCL-filter three-phase active rectifier," *IEEE Transactions on Power Electronics*, vol. 19, no. 1, pp. 76–86, Jan. 2004.

[21] S. Zhang, S. Jiang, X. Lu, B. Ge, and F. Z. Peng, "Resonance Issues and Damping Techniques for Grid-Connected Inverters With Long Transmission Cable," *IEEE Transactions on Power Electronics*, vol. 29, no. 1, pp. 110–120, Jan. 2014.

[22] R. Pena-Alzola, M. Liserre, F. Blaabjerg, R. Sebastian, J. Dannehl, and F. Fuchs, "Systematic Design of the Lead-Lag Network Method for Active Damping in LCL-Filter Based Three Phase Converters," *IEEE Transactions on Industrial Informatics*, vol. 10, no. 1, pp. 43–52, Feb. 2014.

[23] F. Huerta, E. Bueno, S. Cobreces, F. Rodriguez, and C. Giron, "Control of grid-connected voltage source converters with LCL filter using a Linear Quadratic servocontroller with state estimator," in *IEEE Power Electronics Specialists Conference, 2008. PESC 2008*, Jun. 2008, pp. 3794–3800.

[24] M. Malinowski and S. Bernet, "A Simple Voltage Sensorless Active Damping Scheme for Three-Phase PWM Converters With an Filter," *IEEE Transactions on Industrial Electronics*, vol. 55, no. 4, pp. 1876–1880, Apr. 2008.

[25] D. Luenberger, "Observing the State of a Linear System," *IEEE Transactions on Military Electronics*, vol. 8, no. 2, pp. 74–80, Apr. 1964.

[26] A. Arriagada, J. Espinoza, J. Rodriguez, and L. Moran, "On-line filtering reactance identification in voltage-source three-phase active-front-end rectifiers," in *The 29th Annual Conference of the IEEE Industrial Electronics Society, 2003. IECON '03*, vol. 1, Nov. 2003, pp. 192–197 vol.1.

Bibliography

[1] A Agbedahunsi, M. Sumner, E. Christopher, A Watson, A Costabeber, and R. Parashar. Frequency control improvement within a microgrid, using enhanced statcom with energy storage. In *Power Electronics, Machines and Drives (PEMD 2012), 6th IET International Conference on*, pages 1–6, March 2012.

[2] Alex Taiwo Agbedahunsi. *Frequency Control for Microgrids using Enhanced STATCOM and Supercapacitor Energy Storage*. PhD thesis, The University of Nottingham, May 2013.

[3] A Arulampalam, M. Barnes, N. Jenkins, and J.B. Ekanayake. Power quality and stability improvement of a wind farm using statcom supported with hybrid battery energy storage. *Generation, Transmission and Distribution, IEE Proceedings-*, 153(6):701–710, November 2006.

[4] A Arulampalam, J.B. Ekanayake, and N. Jenkins. Application study of a statcom with energy storage. *Generation, Transmission and Distribution, IEE Proceedings-*, 150(3):373–384, May 2003.

[5] Hua Bai and C. Mi. The impact of bidirectional dc-dc converter on the inverter operations and battery current in hybrid electric vehicles. In *IEEE International Conference on Power electronics and ECCE Asia*, pages 1013–1015, 2011.

[6] S.K. Balibani, G. Gurrala, and I Sen. Power system stability enhancement using a statcom with ess. In *India Conference (INDICON), 2013 Annual IEEE*, pages 1–6, Dec 2013.

[7] M.E. Baran, S. Teleke, L. Anderson, A Huang, S. Bhattacharya, and S. Atcitty. Statcom with energy storage for smoothing intermittent wind farm power. In *Power and Energy Society General Meeting - Conversion and Delivery of Electrical Energy in the 21st Century, 2008 IEEE*, pages 1–6, July 2008.

[8] J.A Barrado, R. Grino, and H. Valderrama-Blavi. Power-quality improvement of a stand-alone induction generator using a statcom with battery energy storage system. *Power Delivery, IEEE Transactions on*, 25(4):2734–2741, Oct 2010.

[9] F. Caricchi, F. Crescimbini, G. Noia, and D. Pirolo. Experimental study of a bidirectional dc-dc converter for the dc link voltage control and the regenerative braking in pm motor drives devoted to electrical vehicles. In *Ninth Annual*

Conference Proceedings Applied Power Electronics Conference and Exposition, APEC, volume 1, pages 381–386, 1994.

[10] Ying Cheng, Chang Qian, M.L. Crow, S. Pekarek, and Stan Atcitty. A comparison of diode-clamped and cascaded multilevel converters for a statcom with energy storage. *Industrial Electronics, IEEE Transactions on*, 53(5):1512–1521, Oct 2006.

[11] Se-Kyo Chung. A phase tracking system for three phase utility interface inverters. *Power Electronics, IEEE Transactions on*, 15(3):431–438, May 2000.

[12] George Ellis. *OObserver in Control Systems: A practical guide*. Academic Press, an imprint of Elsevier Science, 2002.

[13] M.C. Falvo, L. Martirano, and D. Sbordone. D-statcom with energy storage system for application in smart micro-grids. In *Clean Electrical Power (ICCEP), 2013 International Conference on*, pages 571–576, June 2013.

[14] J. M. Guerrero. Editorial special issue on power electronics for microgrids 2014;part ii. *Power Electronics, IEEE Transactions on*, 26(3):659–663, March 2011.

[15] J.M. Guerrero, Poh Chiang Loh, Tzung-Lin Lee, and M. Chandorkar. Advanced control architectures for intelligent microgrids 2014;part ii: Power quality, energy storage, and ac/dc microgrids. *Industrial Electronics, IEEE Transactions on*, 60(4):1263–1270, April 2013.

[16] Xin Guo, Xuhui Wen, and Ermin Qiao. A dsp based controller for high power dual-phase dc-dc converters. In *Power Electronics and Motion Control Conference, 2006. IPEMC 2006. CES/IEEE 5th International*, volume 1, pages 1–5, Aug 2006.

[17] Dong-Hyun Ha, Nam ju Park, Kui-Jun Lee, Dong-Gyu Lee, and Dong-Seok Hyun. Interleaved bidirectional dc-dc converter for automotive electric systems. In *Industry Applications Society Annual Meeting, 2008. IAS '08. IEEE*, pages 1–5, Oct 2008.

[18] P.J. Hart, P.J. Kollmeyer, L.W. Juang, R.H. Lasseter, and T.M. Jahns. Modeling of second-life batteries for use in a certs microgrid. In *Power and Energy Conference at Illinois (PECI), 2014*, pages 1–8, Feb 2014.

[19] M.T. Holmberg, M. Lahtinen, J. McDowall, and T. Larsson. Svc light with energy storage for frequency regulation. In *Innovative Technologies for an Efficient and Reliable Electricity Supply (CITRES), 2010 IEEE Conference on*, pages 317–324, Sept 2010.

[20] R. Kuiava, R.A Ramos, and N.G. Bretas. Control design of a statcom with energy storage system for stability and power quality improvements. In *Industrial*

Technology, 2009. ICIT 2009. IEEE International Conference on, pages 1–6, Feb 2009.

[21] Duck-Su Lee, Soo-Nam Kim, Young-Chan Choi, Byung-San Baek, and Jong-Sung Hur. Development of wind power stabilization system using bess and statcom. In *Innovative Smart Grid Technologies (ISGT Europe), 2012 3rd IEEE PES International Conference and Exhibition on*, pages 1–5, Oct 2012.

[22] Sanghoey Lee, Jeong-Hoon Lee, and Hanju Cha. Grid synchronization pll robust to frequency variation, unbalanced and distorted voltage. In *Energy Conversion Congress and Exposition (ECCE), 2011 IEEE*, pages 1150–1155, Sept 2011.

[23] C.M. Liaw, Y. K. Chen, K.H. Chao, and H.C. Chen. Quantitative design and implementation of pi-d controller with model-following response for motor drive. *Electric Power Applications, IEE Proceedings -*, 145(2):98–104, Mar 1998.

[24] Du Limin, Zhang Ke, and Jin Guang. Linear auto disturbance rejection controller for vector-controlled pmsm drive system. In *Transportation, Mechanical, and Electrical Engineering (TMEE), 2011 International Conference on*, pages 879–882, Dec 2011.

[25] R. Majumder. Some aspects of stability in microgrids. *Power Systems, IEEE Transactions on*, 28(3):3243–3252, Aug 2013.

[26] C. Marinescu and I Serban. About the main frequency control issues in microgrids with renewable energy sources. In *Clean Electrical Power (ICCEP), 2013 International Conference on*, pages 145–150, June 2013.

[27] M.G. Molina, P.E. Mercado, and E.H. Watanabe. Analysis of using facts controllers with superconducting magnetic energy storage in the primary frequency control of power systems. In *Transmission Distribution Conference and Exposition: Latin America, 2006. TDC '06. IEEE/PES*, pages 1–7, Aug 2006.

[28] N. Mukherjee and D. Strickland. Modular ess with second life batteries operating in grid independent mode. In *Power Electronics for Distributed Generation Systems (PEDG), 2012 3rd IEEE International Symposium on*, pages 653–660, June 2012.

[29] J. Mundackal, AC. Varghese, P. Sreekala, and V. Reshmi. Grid power quality improvement and battery energy storage in wind energy systems. In *Emerging Research Areas and 2013 International Conference on Microelectronics, Communications and Renewable Energy (AICERA/ICMiCR), 2013 Annual International Conference on*, pages 1–6, June 2013.

[30] D.Y. Ohm. Analysis of pid and pdf compensators for motion control systems. In *Industry Applications Society Annual Meeting, 1994., Conference Record of the 1994 IEEE*, pages 1923–1929 vol.3, Oct 1994.

[31] Sukin Park and Yujin Song. An interleaved half-bridge bidirectional dc-dc converter for energy storage system applications. In *Power Electronics and ECCE Asia (ICPE ECCE), 2011 IEEE 8th International Conference on*, pages 2029–2034, May 2011.

[32] Thao Tran Phuong, R. Furusawa, C. Mitsantisuk, and K. Ohishi. Force sensing considering periodic disturbance suppression based on high order disturbance observer and kalman-filter. In *Human System Interactions (HSI), 2011 4th International Conference on*, pages 336–341, May 2011.

[33] T. Piraisoodi and S. Sadhu. Characteristic analysis of high order disturbance observer. In *INDICON, 2005 Annual IEEE*, pages 431–436, Dec 2005.

[34] P.F. Ribeiro, B.K. Johnson, M.L. Crow, A Arsoy, and Y. Liu. Energy storage systems for advanced power applications. *Proceedings of the IEEE*, 89(12):1744–1756, Dec 2001.

[35] P. Rodriguez, A Luna, M. Ciobotaru, R. Teodorescu, and F. Blaabjerg. Advanced grid synchronization system for power converters under unbalanced and distorted operating conditions. In *IEEE Industrial Electronics, IECON 2006 - 32nd Annual Conference on*, pages 5173–5178, Nov 2006.

[36] P. Roncero-Sanchez, X. del Toro Garcia, AP. Torres, and V. Feliu. Fundamental positive- and negative-sequence estimator for grid synchronization under highly disturbed operating conditions. *Power Electronics, IEEE Transactions on*, 28(8):3733–3746, Aug 2013.

[37] E. Saito and S. Katsura. A filter design method in disturbance observer for improvement of robustness against disturbance in time delay system. In *Industrial Electronics (ISIE), 2012 IEEE International Symposium on*, pages 1650–1655, May 2012.

[38] A Sattar, A Al Durra, C. Caruana, S.M. Muyeen, and J. Tamura. Real time implementation of the bess to smoothen the output power fluctuation of the variable speed wind turbine generator. In *Electrical Machines and Systems (ICEMS), 2012 15th International Conference on*, pages 1–6, Oct 2012.

[39] I Serban and C. Marinescu. Control strategy of three-phase battery energy storage systems for frequency support in microgrids and with uninterrupted supply of local loads. *Power Electronics, IEEE Transactions on*, 29(9):5010–5020, Sept 2014.

[40] I Serban, R. Teodorescu, and C. Marinescu. Energy storage systems impact on the short-term frequency stability of distributed autonomous microgrids, an analysis using aggregate models. *Renewable Power Generation, IET*, 7(5):531–539, Sept 2013.

[41] M. R I Sheikh, F. Eva, M. A Motin, and M. A Hossain. Wind generator output power smoothing and terminal voltage regulation by using statcom/smes. In *Developments in Renewable Energy Technology (ICDRET), 2012 2nd International Conference on the*, pages 1–5, Jan 2012.

[42] D. Siemaszko. Grid synchronization of power converters to weak unbalanced networks with disturbances. In *Electrical Systems for Aircraft, Railway and Ship Propulsion (ESARS), 2012*, pages 1–6, Oct 2012.

[43] Bhim Singh, K. Al-Haddad, and A Chandra. A review of active filters for power quality improvement. *Industrial Electronics, IEEE Transactions on*, 46(5):960–971, Oct 1999.

[44] P. Srithorn, M. Sumner, L. Yao, and R. Parashar. A statcom with supercapacitors for enhanced power system stability. In *Power Electronics, Machines and Drives, 2008. PEMD 2008. 4th IET Conference on*, pages 96–100, April 2008.

[45] Seung-Ki Sul. *Control of Electric Machine Drive Systems*. Wiley IEEE press, 2011.

[46] Zhengping Xi, B. Parkhideh, and S. Bhattacharya. Improving distribution system performance with integrated statcom and supercapacitor energy storage system. In *Power Electronics Specialists Conference, 2008. PESC 2008. IEEE*, pages 1390–1395, June 2008.

[47] Zhang Xuhui, Xuhui Wen, Zhao Feng, and Guo Xinhua. A new control strategy for bi-directional dc-dc converter in electric vehicle. In *International Conference on Electrical Machines and Systems (ICEMS)*, pages 1–4, 2011.

[48] Z. Yang, C. Shen, L. Zhang, M.L. Crow, and S. Atcitty. Integration of a statcom and battery energy storage. *Power Systems, IEEE Transactions on*, 16(2):254–260, May 2001.

[49] A. Yazdani and R. Iravani. *Voltage-Sourced Converters in Power Systems:Modelling ,Control and Applications*. John Wiley & Sons, Inc., 2010.

[50] Lirong Zhang, Yi Wang, Heming Li, and Pin Sun. Hybrid power control of cascaded statcom/bess for wind farm integration. In *Industrial Electronics Society, IECON 2013 - 39th Annual Conference of the IEEE*, pages 5288–5293, Nov 2013.